Predicting maternal-fetal cannabinoid exposure during pregnancy using physiologically-based pharmacokinetic modeling and simulation

Gabriela Patilea-Vrana

A dissertation

submitted in partial fulfillment of the

requirements for the degree of

Doctor of Philosophy

University of Washington

2019

Reading Committee:

Jashvant Unadkat, Chair

Bhagwat Prasad

Qingcheng Mao

Program Authorized to Offer Degree:

Pharmaceutics

University of Washington

ABSTRACT

Predicting maternal-fetal cannabinoid exposure during pregnancy using physiologically-based pharmacokinetic modeling and simulation

Gabriela Patilea-Vrana

Chair of the Supervisory Committee:

Professor Jashvant D. Unadkat

Department of Pharmaceutics

Maternal marijuana (cannabis) use during pregnancy is associated with reduced fetal growth and subtle but persistent neurodevelopmental effects. It is not possible to establish the independent risk associated with maternal cannabis use via prospective clinical studies due to ethical considerations. In vitro and animal studies identified (-)-Δ^9-tetrahydrocannabinol (THC), the psychotropic component of cannabis, and its active hydroxy metabolite, 11-OH-THC, as potential perpetrators of fetal developmental risk. The observed toxicity to THC and 11-OH-THC may not be translated from preclinical studies to humans without knowing the exposure of these cannabinoids during pregnancy. As such, maternal-fetal cannabinoid (hereafter cannabinoid refers to THC and 11-OH-THC) exposure needs to be determined. However, sampling maternal and fetal cannabinoid plasma concentrations during pregnancy is logistically difficult or unethical. Physiological-based pharmacokinetic (PBPK) modeling and simulation can be used to predict drug exposure in silico. PBPK modeling incorporates physiological data, such as tissue composition and blood flows, with drug specific pharmacokinetic (PK) parameters, such as metabolism and transport, to mechanistically predict in vivo PK of a drug. We hypothesize that we can predict maternal and fetal THC and 11-OH-THC exposure using maternal-fetal-PBPK (m-f-PBPK) modeling and simulation. To do so, we first quantified the pertinent mechanistic drug parameters in vitro, which included

the identification of enzymes, their contribution, and kinetics relevant to maternal THC/11-OH-THC hepatic disposition. Next, we extrapolated the in vitro mechanistic information to in vivo and built a THC/11-OH-THC PBPK model in nonpregnant women using PBPK software Simcyp®, and verified using observed data. Lastly, we incorporated the gestational-age dependent physiological changes via the m-f-PBPK model to predict THC and 11-OH-THC exposure in the maternal-fetal pair. By bridging cannabinoid disposition data with m-f-PBPK modeling, this project translated in vitro PK mechanistic information into predictions of maternal and fetal pharmacologically relevant cannabinoid exposure following THC consumption. The predicted THC and 11-OH-THC concentrations during pregnancy can then be used in preclinical studies to establish the toxicity of THC exposure during pregnancy.

DEDICATION

To my parents, Mihaela and Romeo Patilea, whose sacrifices allowed me to pursue my dream.

To my husband, Marc Vrana, whose encouragement and jokes helped me maintain my dream.

ACKNOWLEDGEMENTS

I would like to express my sincere gratitude to my advisor, Dr. Jashvant Unadkat. His patience, guidance, and knowledge made it possible for me to navigate through my thesis successfully. In addition, Dr. Unadkat has helped me grow as a scientist by providing endless opportunities for training, presenting, writing, and teaching. His ability to detect my strengths and weaknesses and carefully build around them make him an exceptional mentor. Lastly, I appreciate the confidence and independence he has given me. I made the transition from caterpillar to butterfly through my graduate studies because of Dr. Unadkat.

To my thesis reading and doctoral supervisory committee members, Drs. Bhagwat Prasad, Qingcheng Mao, Nina Isoherranen, Nephi Stella, and Gail Anderson, I wish to express my sincere gratitude for their encouragement, support, and guidance. Each committee member's expertise helped ensure that I looked at my project from multiple angles while the challenging questions asked helped elevate my project. I also appreciate the intellectually stimulating conversations that helped me think of creative solutions.

To the faculty of the Pharmaceutics and Medicinal Chemistry departments, I thank you for creating a high-quality learning and research environment. I built my theoretical PK foundation through the various classes, seminars, journal clubs, and interactions with the faculty.

To the staff of the Pharmaceutics and Medicinal Chemistry departments, I wish to thank you for helping me succeed in aspects outside of research.

My sincere thanks also goes to Drs. Baiteng Zhao and Maurice Emery, who provided me with a snapshot of research and life in industry during my internship at Seattle Genetics. From my experience there, I learned how to translate my research skills learned in academia to the biopharmaceutical field.

I would like to thank the current and former members of the Unadkat lab. Specifically, Faye Zhang, who established the maternal-fetal PBPK model and Lena Anoshchenko, who helped with the 11-OH-THC reaction phenotyping studies. The supportive, fun, and sometimes silly folk in the lab helped me get through tough days, celebrate small and large successes, and create an environment that I enjoyed going to everyday.

Finally, I would like to thank my family and friends. My deepest gratitude goes to my parents, who individually sacrificed aspects of their former lives when they moved our family from Romania to the United States in 2001. They helped me develop a strong personal foundation that enabled me to get through my thesis. I would like to thank my husband, Marc, who started his own thesis journey not too long after I started mine. While dinner conversations sometimes turned into heated scientific debates, he also helped me keep myself grounded and take much-needed breaks. To my friends, who often whisked me away to go salsa dancing, go hiking, or go for a drink, and take a break from being a scientist. Thank you for the encouragement, support, and understanding when I had to cancel plans. Lastly, the many animals in my life who always provide love, a tail wag, or a purr, no matter the time of day.

TABLE OF CONTENTS

LIST OF TABLES

LIST OF FIGURES

LIST OF SUPPLEMENTARY TABLES

LIST OF SUPPLEMENTARY FIGURES

Chapter 1. Introduction

1.1. Rational and Specific Aims

The prevalence of marijuana (cannabis) use among pregnant women is rising, with current prevalence as high as 7.1% of pregnant women in the United States (Brown et al., 2017; SAMHSA, 2017). A comprehensive review from the National Academies of Science, Engineering and Medicine identified substantial evidence that low birth weight is associated with maternal cannabis use (National Academies of Sciences Engineering and Medicine (U.S.). Committee on the Health Effects of Marijuana, 2017). Furthermore, a meta-analysis showed that neonatal morbidity (specifically neonatal infection and neurological morbidity) is associated with maternal cannabis use when controlling for tobacco use, clinical, and socioeconomic factors (Metz et al., 2017). Subtle but persistent neurodevelopmental effects are associated with maternal cannabis use, including impaired neurocognitive and executive functions, increased hyperactivity and attention deficit, and deficits in academic achievement (Day et al., 1994; Fried et al., 2003; El Marroun et al., 2011; Goldschmidt et al., 2012; Huizink, 2014). However, establishing the independent risk factors of maternal cannabis use using observational studies is difficult because of confounding factors, such as reliance on self-reporting, concurrent tobacco and alcohol use, socioeconomic background, and types and modes of cannabis products consumed. Nevertheless, emergent data identifies that reduced fetal growth and neurotoxicity is associated with maternal cannabis use during pregnancy.

Preclinical studies identified (-)-Δ^9-tetrahydrocannabinold (THC), the psychotropic component in cannabis, as a perpetrator of the developmental adverse outcomes in the offspring associated with maternal cannabis use. Evidence from in vitro and animal studies demonstrate that dysregulation of the endocannabinoid system by THC and its active metabolite, 11-OH-THC, can impact early pregnancy advancement (Paria et al., 1995; Wang et al., 2006), fetal axon growth (Tortoriello et al., 2014; de Oliveira et al., 2019), and placentation (Costa, 2016). While the preclinical studies identify the biological mechanism of toxicity associated with THC and 11-OH-THC exposure, it is difficult to translate the magnitude of toxicity to humans since it is unknown how the doses/concentrations of THC used in preclinical studies relate to those observed in-utero in humans.

Given the confounding factors associated with observational clinical studies and difficulty in translating toxicity observed in preclinical studies, it is unclear how THC exposure during pregnancy will ultimately impact the development of the fetus and child. Conducting prospective studies to explore the safety and toxicity of THC during pregnancy is ethically not possible. As such, in order to anticipate the risk associate with maternal cannabis use, a THC and 11-OH-THC exposure-risk relationship must be built. To build such a relationship, as a first step, the maternal and fetal THC and 11-OH-THC concentrations must be known. As such, to further the knowledge on the risk of cannabis consumption during pregnancy, we hypothesize that we can predict cannabinoid (hereafter cannabinoid refers to THC and its active metabolite, 11-OH-THC) exposure in pregnant women and the fetus using maternal-fetal-physiologically based pharmacokinetic (m-f-PBPK) modeling and simulation (M & S). PBPK incorporates physiological data, such as tissue composition and blood flows, with xenobiotic specific pharmacokinetic parameters, such as metabolism and transport, to mechanistically predict a xenobiotic's disposition profile in vivo. We focused our studies to identify and quantify the necessary PK parameters required to build the m-f-PBPM model. In **Aim 1,** we identified and quantified the individual contribution (fm) of hepatic drug-metabolizing enzymes (DMEs) to the maternal disposition of THC and 11-OH-THC in vitro. In **Aim 2,** we quantified the metabolic kinetics (CL_{int}, K_m, V_{max}) of DMEs identified in **Aim 1**. In **Aim 3**, we built and verified a THC/11-OH-THC PBPK model in nonpregnant population using mechanistic xenobiotic parameters from **Aims 1-2** and verified using observed clinical data after intravenous (IV) administration and inhalation of THC. Finally, in **Aim 4**, we extrapolated THC/11-OH-THC nonpregnant disposition model from **Aim 3** to pregnancy by accounting for gestational-age dependent changes that impact drug PK (e.g. induction of DME's and increase in body fat) and simulated THC/11-OH-THC maternal and fetal exposure using maternal-fetal PBPK M & S. Utilizing PBPK M & S, maternal and fetal cannabinoid concentrations can be predicted at various gestational ages in silico. The results from this project will inform in vitro and animal studies on the pharmacologically relevant cannabinoid concentrations to be used when assessing the effects of fetal cannabinoid (THC and 11-OH-THC) exposure, and thus ultimately help further knowledge on the safety and toxicity of cannabis use during pregnancy.

1.2. Cannabis use during pregnancy

Cannabis is the most used illicit drug among pregnant women in the United States. In the most recent National Survey on Drug Use and Health (NSDUH) survey, 7.1% of pregnant women reported cannabis use in the past-month while 3.1% of pregnant women reported daily or almost daily use of cannabis during pregnancy (SAMHSA, 2017). The overall prevalence of cannabis use during pregnancy has been steadily increasing (Brown et al., 2017). The prevalence of cannabis use is the highest and lowest during the first and third trimester, respectively (Ko et al., 2015; Volkow et al., 2017). Interestingly, the 2017 NSDUH reported a change in these trends, namely 11%, 3.9%, and 6.4% prevalence of past-month cannabis use during the first, second, and third trimester, respectively (SAMHSA, 2017).

Reasons for using cannabis during pregnancy include to treat nausea, stimulate appetite, manage stress, and improve mood (Chang et al., 2019). For example, up to 96% of women reported nausea as the reason for continued use of cannabis during pregnancy (Mark et al., 2017). Indeed, prevalence of cannabis use is higher in pregnant women suffering from nausea and vomiting in pregnancy compared with women who do not (11.1% versus 5.8%) (Young-Wolff et al., 2018). The use of cannabis to combat nausea reflects the higher prevalence of cannabis use during the first trimester.

One reason for the increased use of cannabis during pregnancy is a lowered risk perception (Bayrampour et al., 2019). In one study, 78% of pregnant women perceived slight to no risk of cannabis when used one-to-two times per week (Ko et al., 2015). The trend in risk perception can also be somewhat attributed to the increase in cannabis legalization and uncertainty about the perinatal adverse outcomes (Bayrampour et al., 2019). Furthermore, there is a perception that cannabis is not a “drug” but instead is viewed as “natural”, an “herb”, and “vegan”, and thus perceived safe to use during pregnancy (Holland et al., 2016; Cook and Blake, 2018; Bayrampour et al., 2019; Chang et al., 2019).

1.3. Fetal, child, and maternal health-outcomes associated with cannabis use during pregnancy

As outlined by the National Academies of Science, Engineering and Medicine review, the strongest association with maternal cannabis uses is low birth weight (National Academies of Sciences

Engineering and Medicine (U.S.). Committee on the Health Effects of Marijuana, 2017). A meta-analysis study found that while statistically significant, difference in the birth weight of infants that were exposed to cannabis during pregnancy versus those that were not was roughly 3% (Gunn et al., 2016). To note, the metrics of neonatal risk, namely low birth weight (< 2500 gram) and preterm birth (gestational age < 37 weeks or < 32 weeks for very preterm), are associated with motor and cognitive developmental delays, and while infants eventually catch up during childhood and adolescence, there is large variability in the overall developmental trajectories (Oudgenoeg-Paz et al., 2017). As such, the observed birth weight difference is unlikely to be a major contributor to longitudinal adverse outcomes (see discussion below). The meta-analysis by Gunn et al. cannot delineate the impact of cannabis alone since studies where both alcohol and tobacco were consumed were included. Interestingly, a different meta-analysis study showed the observed neonatal risk disappeared when adjustments were made for tobacco use (Conner et al., 2016). In another study, neonatal morbidity (specifically neonatal infection and neurological morbidity) were significantly associated with maternal cannabis use (Metz et al., 2017). The study by Metz et al. controlled for tobacco use, clinical, and socioeconomic factors as well as assessed cannabis exposure via toxicology tests, thus providing better evidence of direct impact of prenatal cannabis use on neonatal outcomes. Lastly, one study found that birth weight was lower for infants whose mothers used cannabis throughout pregnancy compared to mothers who used only during early pregnancy (El Marroun et al., 2009). Furthermore, the meta-analysis by Conner et al. showed that infants whose mothers used cannabis weekly or more during pregnancy were at higher risk for low birth weight and preterm birth when compared to mothers that used cannabis less than weekly (Conner et al., 2016). These data elude to the cannabis exposure-risk relationship, in that, early pregnancy and sustained in utero exposure to cannabis is associated with higher neonatal risk.

Several longitudinal studies assessed the long-term impact of prenatal cannabis exposure on child development, however the conclusions are inconsistent (Huizink, 2014; Stickrath, 2019). The three most extensive studies (OPPS – started in 1978, MHPCD – started in 1982, and Generation R – started in 2001), while mixed in the pattern of their findings, generally showed subtle neurodevelopmental effects (Huizink, 2014). This includes impaired executive functions (Fried et al., 2003), decreased memory and

verbal skills (Day et al., 1994), increased hyperactivity and attention deficit (El Marroun et al., 2011), and lower academic achievement (Goldschmidt et al., 2012). One set of studies observed that cognitive effects were more pronounced in children that were exposed to cannabis in the first trimester (Goldschmidt et al., 2012).

Maternal outcomes associated with cannabis use during pregnancy are also inconsistent. For example, a meta-analysis found an increased odds ratio of anemia for women that used cannabis during pregnancy versus those that did not (Gunn et al., 2016), however the association went away after adjusting for tobacco use, clinical, and socioeconomic factors (Metz et al., 2017). There are several case-reports of cannabinoid hyperemesis syndrome (CHS) during pregnancy (Alaniz et al., 2015; Andrews and Bracero, 2015; Lambert TE, 2016; Kim et al., 2018). CHS, a rare condition that can occur in heavy and long-term cannabis users, presents as severe nausea and episodic cyclic vomiting that can be temporarily relieved by hot showers and topical capsaicin (Pergolizzi, 2018). Discontinuation of cannabis use stops CHS symptoms. CHS can become problematic in the extreme cannabis users since cannabis is typically used as an antiemetic during pregnancy yet continued use will exacerbate CHS symptoms. The impact of CHS on fetal outcomes has not been studied.

As outlined thus far, there is ambiguity on the independent risk factor of cannabis exposure during pregnancy. There are several reasons that likely confound the results:

- **Self-report versus toxicological testing.** Majority of studies rely on self-reports of cannabis use, however, self-reporting severely underestimates cannabis exposure during pregnancy (Young-Wolff et al., 2017). For example, Metz et al. used both self-reporting and toxicological testing to assess cannabis exposure and found that of women with positive cord homogenate, 7% self-reported cannabis use, and among women that self-reported cannabis use, 8% tested positive (Metz et al., 2017). This demonstrates the unreliability of self-reports.
- **Poly-drug use.** There is variation in the exclusion criteria regarding use of alcohol, tobacco, and other illicit substances in the various clinical studies, making interpretation of the independent risk factor of cannabis use difficult. For example, between 2005 and 2014, 3.3% of women reported past-month use of tobacco and cannabis but only 1.0% of women reported past-month cannabis use only

(Coleman-Cowger et al., 2017). Based on this data and the NSDUH prevalence of pregnant women that self-report cannabis use, roughly 2.2% of women use only cannabis during pregnancy. The meta-analysis by Conner et al. found that the neonatal adverse outcomes associated with cannabis exposure are no longer significant when adjusting for tobacco use (Conner et al., 2016). However, when adjusting for tobacco use and utilizing both self-report and toxicological testing, maternal cannabis use remains associated with neonatal morbidity (Metz et al., 2017).

- **Socioeconomic differences.** Pregnant women that use cannabis are more likely to be of younger age (<25 years), non-Hispanic black, earn less than $20,000 annually, have lower education levels, smoke tobacco, and use alcohol and other illicit drugs (El Marroun et al., 2009; Ko et al., 2015; Metz et al., 2017; Volkow et al., 2017). As such, these factors may contribute to the adverse outcomes observed, independent of cannabis use. However, several studies still obverse neonatal adverse outcomes associated with maternal cannabis use when adjusting for clinical and socioeconomic factors (Metz et al., 2017).
- **Changing composition of cannabis.** The results of longitudinal studies may vary depending on the year when the studies were conducted because the composition of cannabis has changed (e.g. OPPS started in 1978 versus Generation R which started in 2001). Specifically, the concentrations of (-)-Δ^9-tetrahydrocannabinold (THC), the psychotropic component in cannabis, have increased (**Figure 1.1**). For example, the average THC concentrations in confiscated cannabis specimens were 1.3% in 1980 and 11.8% in 2014 (ElSohly et al., 2000; ElSohly et al., 2016). Furthermore, commercially available cannabis strains vary widely in their THC content. For example, the median THC levels ranged 18%-23% in Washington state (depending on the lab where testing was conducted) and was 18%, 19%, and 21% for popular strains Blue Dream, Girl Scout Cookies, and Gorilla Glue #4, respectively (Jikomes and Zoorob, 2018). THC and its active metabolite, 11-OH-THC (**Figure 1.2**) are partial agonists of cannabinoid receptor 1 (CB_1) and this interaction has been highlighted as a potential mechanism responsible for neurodevelopmental outcomes in children exposed to cannabis in utero (explained more in **Section 1.4**) (Alpár et al., 2016).

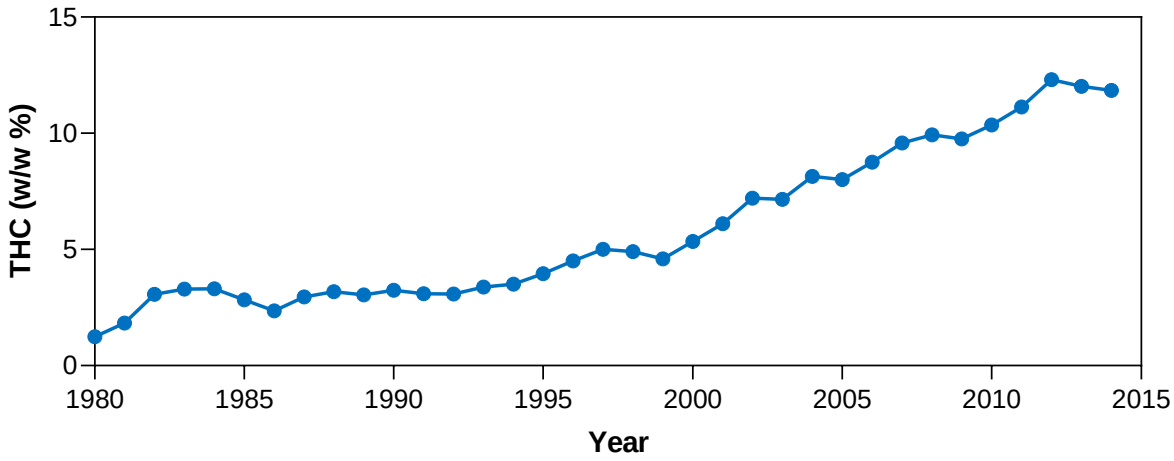

Figure 1.1. Concentrations (% weight/weight) of THC in confiscated cannabis (plants). Figure adapted from ElSohly et al., and 2000; ElSohly et al., 2016.

- **Route of administration.** None of the clinical studies controlled for the cannabis administration mode. For example, the most popular administration modes are smoking (e.g. using joints – 89% of users, bong/waterpipe/hookah – 49% of users, bowl/pipe – 48% of users), oral administration (edibles and drinks – 30% of users), and vaporization (typically using an electronic device – 6% of users) (Schauer et al., 2016). The modes of cannabis administration among pregnant women are unknown. The route of administration may be important in the observed adverse outcomes since, for example, smoking cannabis will generate carcinogenic polycyclic aromatic hydrocarbons (PAHs) whereas ingesting cannabis infused edibles will not. Indeed, in utero exposure to PAHs are associated with negative fetal outcomes, both for women that smoke tobacco and non-smokers during pregnancy (Machado et al., 2014; Polanska et al., 2014; Banderali et al., 2015). Interestingly, in a survey of cannabis dispensaries in Colorado, the use of cannabis infused edibles was more frequently recommended compared to inhalation (51% versus 38%) for pregnant women in the first trimester (Dickson et al., 2018).

It is difficult to decipher the independent risk factor of in utero exposure to cannabis from the observational clinical studies given the reasons listed above. Nevertheless, there is a consensus that maternal cannabis use leads to lower birth weight and subtle neurodevelopmental impacts in the offspring. Prospective clinical studies are ideal to establish the fetal risk associated with maternal

cannabis use; however, these are virtually impossible due to ethical and logistical reasons. An alternative is to establish the fetal exposure-risk relationship of the perpetrators within cannabis that lead to developmental deficits at different stages throughout pregnancy. Insults to the endocannabinoid system during fetal development by THC and its active hydroxy metabolite, 11-hydroxy-THC (11-OH-THC) (**Figure 1.2**) have been hypothesized to mediate fetal risk (Alpár et al., 2016; Grant et al., 2017). There is preclinical evidence (described in **Section 1.4**) that demonstrates the negative impact of THC on embryonic developmental, placental integrity, and fetal neurodevelopment. However, it is difficult to translate the toxicity observed in the preclinical studies to humans since the in-utero exposure to THC is unknown. As such, prospective predictions of fetal THC and 11-OH-THC exposure at different gestational-ages using PBPK M & S is a crucial step in determining the pharmacologically relevant cannabinoid concentrations that are needed to be used in in vitro and animal studies in order to establish the fetal safety and toxicity of maternal cannabis use (described further in **Section 1.5**).

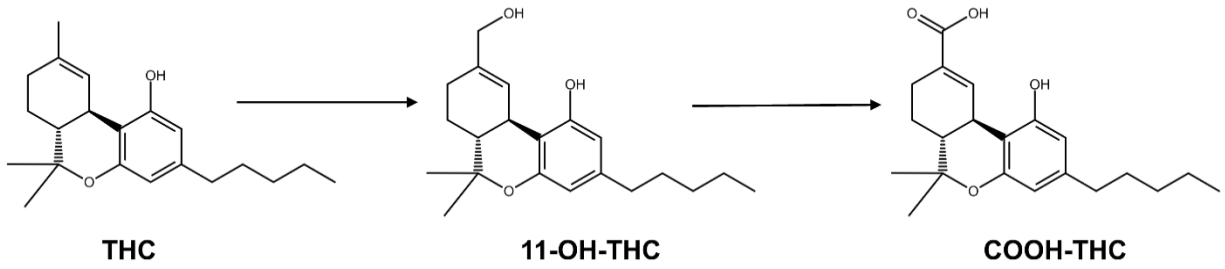

Figure 1.2. THC metabolic scheme.
In vivo, THC is hydroxylated to 11-OH-THC, the primary and psychoactive metabolite. 11-OH-THC is oxidized to COOH-THC, a nonactive metabolite that is the major circulating cannabinoid metabolite found (as the glucuronide conjugate) in blood and urine.

1.4. Preclinical evidence of THC and 11-OH-THC mediated fetal toxicity

The endocannabinoid system is comprised of endogenous lipid-based ligands (e.g. anandamide and 2-arachidonoylglycerol) that bind to G protein-coupled receptors, mainly cannabinoid receptor 1 and 2 (CB_1 and CB_2, respectively). The endocannabinoid system is expressed ubiquitously and plays a role in central and peripheral nervous system signaling, including mediating brain reward systems and stress response, maintaining metabolic/energy homeostasis, and regulating the immune system response

(Chanda et al., 2019). The phototropic effects of cannabis is due THC and 11-OH-THC engaging with CB_1 in the brain (Grotenhermen, 2003; Huestis, 2007). During pregnancy, the endocannabinoid system plays an important regulatory role during implantation, decidualization, placentation, and parturition (Sun and Dey, 2012; Correa et al., 2016). As such, dysregulation of the endocannabinoid system at any stage during pregnancy may lead to deleterious fetal outcomes.

THC is a partial agonist of CB_1 and CB_2 with K_i values (affinities) in the low nM range and a higher affinity for CB_1 compared to CB_2 (Pertwee, 2008). THC but not CBD (a CB_1/CB_2 antagonist) inhibited the development of blastocysts in mice in a concentration and CB_1 dependent manner (THC concentrations: 6.4 – 160 nM) (Paria et al., 1995). Continuous infusion of THC (5 mg/kg per day) resulted in oviductal retention in mice. This effect was reversed with a CB_1 antagonist and did not occur with administration of CBD (Wang et al., 2006). These results demonstrate THC can mediate fetal toxicity during early pregnancy via dysregulation of CB_1. While animal studies have not been conducted with 11-OH-THC, the toxicity via CB_1 interaction is likely to be like that of THC when tested at comparable concentrations. This is because 11-OH-THC exerts similar psychoactive effects as THC when administered at the same dose in humans (Perez-Reyes et al., 1972) thus demonstrating similar CB_1 affinity. As such, fetal toxicity is driven by the combined exposure of THC and 11-OH-THC.

In primary human trophoblast cells, ≤ 25 μM THC prevented cell death, increased cell metabolic activity, and impaired syncytialization, whereas ≥ 50 μM THC led to decrease in cell viability (Costa et al., 2015). The proliferation of BeWo cells, a cytotrophoblast cell model, was inhibited by ≥ 15 μM THC (Khare et al., 2006). Furthermore, 15 μM THC modulated the expression of several genes relevant to placental integrity, including increase and decrease in histone deacetylase 3 (HDAC3) and thyroid hormone receptor β1 (TRβ1) expression, respectively (Khare et al., 2006). Folic acid uptake by human cytotrophoblast cells was inhibited 38% by 0.1 μM THC (Keating et al., 2009), and uptake of α-aminoisobutyric acid and valine by human placental slices was inhibited by ≥ 10 μM THC (Fisher et al., 1987). Lastly, 40 μM THC increased anandamide levels in human placental villous explants (Maia et al., 2019). These data demonstrate that THC exposure can interfere with proper placental development by impacting trophoblast viability and differentiation, nutrient transport, and endocannabinoid homeostasis. It

should be noted that the concentration of THC utilized in the above experiments are much higher than observed total (bound and unbound) concentrations in plasma (in vitro experiments used THC in the μM range while in vivo (bound and unbound) concentrations are in the nM range, see **Table 1.1**), and as such, may not translate to placental toxicity in vivo, as long as plasma THC concentrations are reflective of placental concentrations. This limitation yet again highlights the necessity of THC and 11-OH-THC exposure predictions during pregnancy via m-f-PBPK M & S.

Animal studies that assessed the neurodevelopment toxicity due to fetal exposure to THC mirror the results observed in human clinical studies, mainly negative impacts on learning and memory, reduction in skilled motor activity and increased prevalence of seizure, inhibited social behavior, anxiety-like symptoms, and altered physical activity levels (Grant et al., 2017). One of the molecular mechanisms for fetal neurotoxicity is alterations to the endocannabinoid system in the fetal brain. For example, regulation of microtubule turnover by SCG10/stathmin 2 in the mouse fetal neuron is impacted by THC (3 mg/kg) activation of CB_1 in utero (Tortoriello et al., 2014). The maternal-fetal PBPK model previously developed in our lab includes fetal brain (Zhang et al., 2017a; Zhang and Unadkat, 2017), and as such, prospective predictions of THC and 11-OH-THC fetal brain concentrations may be made.

As evidenced by the preclinical studies, dysregulation of the endocannabinoid system is a biological mechanism that may explain some of the adverse fetal outcomes observed in humans. Since the concentrations of the perpetrators drive the magnitude of fetal toxicity, the fetal concentrations of THC and 11-OH-THC need to be elucidated.

1.5. Maternal-fetal PBPK modeling and simulation

Due to ethical and logistical constraints that make measuring in utero drug concentrations impossible, in silico tools, such as PBPK M & S, offer a non-invasive alternative. PBPK modeling incorporates physiological data, such as tissue composition and blood flows, with drug specific PK parameters, such as metabolism and transport kinetics data, to mechanistically predict xenobiotic disposition profile in vivo. The backbone of PBPK M & S is making in vitro to in vivo extrapolation (IVIVE) of drug enzyme and transporter clearance based off in vivo enzyme and transporter tissue expression.

Particularly for pregnancy, where animal models are inadequate due to high interspecies differences, in vitro tools are critical. In vitro clearance is typically measured in microsomal, cytosolic, and S9 fractions (for metabolism) and transfected cell lines and vesicles (for transporters), which is then scaled up to in vivo activity based off in vitro enzyme and transporter expression. This approach is well verified for metabolism IVIVE (Rostami-Hodjegan and Tucker, 2007) and is in the process of being verified for transporters (Kumar et al., 2015; Ishida and Unadkat, 2016; Kumar et al., 2016). The challenge with this approach is that all enzymes and transporters that determine a xenobiotic's disposition as well as the expression of these enzymes and transporters in vivo must be known for proper in vitro to in vivo extrapolation (IVIVE) (see **Aim 1-2** in **Section 1.7** and **Chapters 2-3**). The next steps during PBPK model development is to refine the initial PBPK model using a training clinical dataset, verify using an independent clinical dataset, then extrapolate the PBPK model to different populations or scenarios (Kuepfer et al., 2016). As outlined in **Section 1.7**, in **Aim 3** and **Chapter 4**, the THC/11-OH-THC PBPK model was built and verified in a nonpregnant population using observed clinical data after IV administration and inhalation of THC, and in **Aim 4** and **Chapter 5**, the PBPK model was extrapolated to pregnancy.

Our lab, in collaboration with Certara (Simcyp®), has developed and verified a pregnancy PBPK model that includes time-dependent physiological and DME changes (Ke et al., 2012; Ke et al., 2014b). The latter is important to include because several hepatic cytochrome P450 (CYPs) are induced or repressed during pregnancy (Anderson, 2005; Ke et al., 2014b). Utilizing this PBPK model, the exposure of drugs such as midazolam, indinavir, and glyburide have been successfully predicted for pregnant women in their third trimester (Ke et al., 2012; Ke et al., 2014a). This PBPK model has been further expanded to simulate placental and fetal drug exposure via the addition of placental and fetal time-dependent physiological and drug-dependent information (Zhang et al., 2016). The maternal and fetal concentrations at term were successfully predicted for drugs that passively diffuse across the placenta: midazolam, theophylline, and zidovudine (Zhang and Unadkat, 2017).

Maternal drug concentrations drive fetal drug exposure. The maternal THC and 11-OH-THC exposure is determined by the PK of these cannabinoids, namely absorption, distribution, metabolism,

excretion, and transport (ADMET) processes (described in **Section 1.6**). Since the PK of THC and 11-OH-THC in pregnant women is unknown, the disposition of these cannabinoids needs to be extrapolated from a nonpregnant population. Absorption, distribution, and excretion patterns in nonpregnant population is collected from observed clinical PK studies (summarized in **Section 1.6**) or determined using in silico prediction tools, such as the Rowland and Rodgers method for predicting tissue distribution. Since metabolism and transport clearance may be different between nonpregnant and pregnant women due to changes to enzymes expression during pregnancy, detailed mechanistic information is necessary. Such mechanistic information includes theidentification and contribution of relevant enzymes (described in **Chapter 2**) and their nonlinear kinetics (CL_{int}, V_{max}, K_m) (described in **Chapter 3**). In **Chapter 4**, the disposition of THC and 11-OH-THC in nonpregnant population was predicted by PBPK M & S using the mechanistic PK information presented in **Chapters 2** and **3**. The predicted concentrations of THC and 11-OH-THC were verified by comparing the predicted concentrations and PK parameters (such as clearance (CL), volume of distribution at steady state (V_{ss}) and area under the curve (AUC)) with those from cannabinoid clinical PK studies. Lastly, in **Chapter 5**, using the data in nonpregnant population from **Chapter 4**, maternal-fetal exposure to cannabinoids was extrapolated using the m-f-PBPK model established in our laboratory.

1.6. THC and 11-OH-THC PK

1.6.1. Absorption and distribution

The concentration – time profiles of THC and its metabolites, 11-OH-THC and COOH-THC (non-psychoactive metabolite) are similar between intravenous (IV) and inhalation but differ after oral administration of THC (**Figure 1.3**, **Table 1.1**). Of note, **Table 1.1** shows information pooled from clinical studies for metabolites 11-OH-THC and COOH-THC (**Figure 1.2**) but only the 11-OH-THC information will be described in text since COOH-THC is not a psychoactive metabolite or CB_1 agonist and thus not the focus of this project.

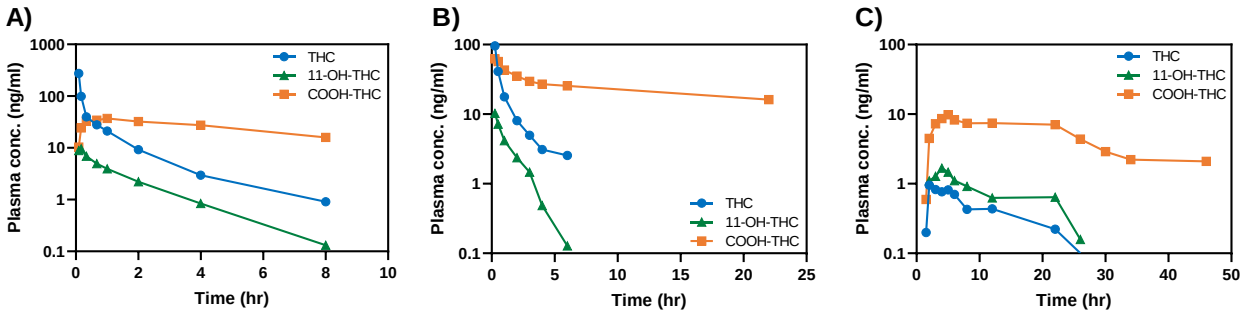

Figure 1.3. Representative concentration-time profiles of THC and its metabolites in vivo. Profiles of THC and its metabolites after A) IV administration of 0.053 mg/kg THC – figure adapted from Naef et al. 2004; B) smoking a cannabis cigarette containing 54 mg THC – figure adapted from Schwope et al. 2011; C) ingestion of 50 mg THC brownie – figure adapted from Vandrey et al. 2017.

On average, time to peak plasma concentrations (t_{max} and C_{max} respectively) for THC is 8 minutes versus 1.9 hours following inhalation and oral administration of THC, respectively (**Table 1.1**). Similar patterns for t_{max} are observed for 11-OH-THC. Due to the differences in t_{max}, onset of psychoactive effect is much longer after oral administration compared to inhalation of THC (Lemberger et al., 1972b).

The average dose-normalized THC C_{max} and AUC are 6.6 – and 2.0 – fold lower after oral administration when compared to inhalation, respectively (**Table 1.1**). Furthermore, THC bioavailability after inhalation and oral administration ranges from 2-56% (Ohlsson et al., 1980; Agurell et al., 1986) and 4-20% (Ohlsson et al., 1980; Wall et al., 1983), respectively. During inhalation, about 23-30% THC is lost via pyrolysis (measured using a cigarette-smoking machine and water-pipe smoking) and 40-50% by side-stream smoke (smoke that is produced but not inhaled – measured using a cigarette-smoking machine) and so approximately only about 20-37% of the original THC dose in the cannabis cigarette is inhaled (Perez-Reyes, 1990). Furthermore, depth of inhalation, puff duration, breathhold, and interval between breathhold influence inhalation bioavailability (Azorlosa et al., 1995; McClure et al., 2012), and thus gives rise to large interindividual variability of smoking topography. The above data suggest that incomplete absorption from the cannabis cigarette and significant hepatic first-pass metabolism are likely the reasons for the low bioavailability following inhalation and oral administration of THC, respectively.

Table 1.1. Pooled analysis of cannabinoid PK properties after various routes of administration

Route of administration	PK Parameter	Cannabinoid		
		THC	11-OH-THC	COOH-THC
Intravenous	Dose range (mg)	0.5 – 5	—	—
	C_{max}/Dose (nM/mg)	133 [90.0 – 197]	4.68 [2.71 – 8.08]	23.4 [15.5 – 35.4]
	t_{max} (hours)	—	—	—
	AUC/Dose (min/L)	1.47 [0.90 – 2.41]	0.147 – 0.496[b]	N/A
	$t_{1/2}$ (hours)	29.5 [19.4 – 44.8]	15 – 33[b]	25 – 55[b]
Inhalation	Dose range (mg)	8.9 – 70	—	—
	C_{max}/Dose (nM/mg)	9.93 [7.00 – 14.1]	0.65 [0.50 – 1.05]	3.73 [2.31 – 6.00]
	t_{max} (hours)	0.13 [0.10 – 0.16]	0.25 [0.19 – 0.34]	0.55 [0.41 – 0.74]
	AUC/Dose (min/L)	0.14 [0.10 – 0.21]	0.03 [0.02 – 0.05]	0.33 [0.20 – 0.55]
	$t_{1/2}$ (hours)	98.4[a]	N.R.	N.R.
Oral	Dose range (mg)	2.5 – 90	—	—
	C_{max}/Dose (nM/mg)	1.50 [1.32 – 1.71]	1.10 [0.90 – 1.34]	13.3 [9.74 – 18.0]
	t_{max} (hours)	1.93 [1.59 – 2.34]	2.36 [1.95 – 2.87]	3.10 [2.53 – 3.79]
	AUC/Dose (min/L)	0.07 [0.05 – 0.10]	0.14 [0.12 – 0.16]	3.73 [2.19 – 6.34]
	$t_{1/2}$ (hours)	8.67 [5.42 – 16.6]	12.4 [10.7 – 14.5]	25 – 37[b]

Data shown is geometric mean and 95% confidence interval of the average PK parameters from individual PK clinical studies (detailed in **Supplementary Tables 1-3**). C_{max} and AUC of 11-OH-THC and COOH-THC are normalized to the administered THC dose. Only studies with > 8 hour sampling time were used for calculating average $t_{1/2}$. N.R. – not reporting because studies had sampling time was < 8 hours [a] Average $t_{1/2}$ from Johansson et al. 1988 that had 360 hour sampling time [b] Range of average PK parameters from one or two studies.

After inhalation of THC, the average dose-normalized 11-OH-THC C_{max} and AUC are 15 – and 4.7 – fold lower than THC. However, after oral administration of THC, 11-OH-THC C_{max} is approximately that of THC whereas 11-OH-THC AUC is 1.9 – fold larger. Furthermore, 11-OH-THC AUC is 0.21 – fold of THC AUC after inhalation but 2-fold larger than THC AUC after oral administration. This indicates that much more 11-OH-THC is formed upon hepatic compared to pulmonary first – pass metabolism. Furthermore, these data exemplify the importance of 11-OH-THC, particularly after oral administration of THC, when considering the cannabis exposure – risk relationship during pregnancy.

Table 1.1 shows pharmacologically relevant plasma concentrations of THC and 11-OH-THC after administration of contemporary doses of THC and thus this information was used to guide in vitro studies outlined in **Chapter 2-3**. The average THC concentrations in cannabis plants are 12% (weight/weight) (ElSohly et al., 2016) and the average joint weight is 660 mg (Mariani et al., 2011). Based on **Table 1.1**, the average C_{max} for THC and 11-OH-THC after smoking a joint of contemporary THC concentration (~79

mg THC per joint) are 786 nM and 52 nM, respectively. The standard serving of a cannabis edible is 10 mg THC but THC content in cannabis edible products range from 2 – 1000 mg (Vandrey et al., 2015; Barrus et al., 2016). Based on **Table 1.1**, the average C_{max} for THC and 11-OH-THC after ingesting a standard serving of cannabis edible are 15 nM and 11 nM, respectively. To note, the selected THC doses varies widely among individuals and is driven by factors such as the experience of the users (Grotenhermen, 2003).

THC has a large steady-state volume of distribution (V_{ss}) of 3.4 - 10 L/kg (Hunt and Jones, 1980; Wall et al., 1983). The V_{ss} of 11-OH-THC has not been reported, but it is likely large, like THC V_{ss}, due to similar physicochemical properties. THC and 11-OH-THC are highly lipophilic compounds with logP of 6.97 and 5.99, respectively (Thomas et al., 1990). This leads to extensive protein binding in plasma - measured fu_p range <1% – 5% (Garrett and Hunt, 1974; Widman et al., 1974; Klausner et al., 1975; Fanali et al., 2011). Majority of THC is bound to lipoproteins, primarily to low density lipoprotein (LDL) (Wahlqvist et al., 1970; Klausner et al., 1975). Both THC and 11-OH-THC have little distribution to red blood cells (9%) (Widman et al., 1974). As such, the blood to plasma ratio (B:P) of THC and 11-OH-THC has been measured to be 0.39 – 0.67 and 0.53 – 0.63, respectively (Widman et al., 1974; Giroud et al., 2001; Schwilke et al., 2009). Due to their lipophilic nature, THC and 11-OH-THC sequester into fatty tissues, particularly in adipose, liver, and lung, as shown in human (Kudo et al., 1995; Gronewold and Skopp, 2011; Kemp et al., 2015; Saenz et al., 2017) and animal (Kreuz and Axelrod, 1973; Brunet et al., 2006) studies, thus leading to large volume of distribution. In humans, 11-OH-THC is found in in the greatest amounts in bile, urine, and liver (Gronewold and Skopp, 2011; Saenz et al., 2017).

In regards to distribution during pregnancy, one human clinical study observed that the THC concentrations in umbilical cord blood were 0.16 – 0.38 – fold the concentrations in maternal blood (Blackard and Tennes, 1984). This trend is observed in rhesus macaques where the fetal-to-maternal (F/M) AUC ratio was 0.3 (Bailey et al., 1987). Since the F/M ratio is less than one, this suggests impediment of THC transfer from the mother to the fetus, either due to activity of placental efflux transporters or placental and/or fetal metabolism. No information on 11-OH-THC distribution during pregnancy is available.

1.6.2. Metabolism and elimination

THC is hydroxylated at the C11 position to produce 11-OH-THC (**Figure 1.2**), at the C8 position on the alicyclic ring and at all positions of the pentyl chain, resulting in biotransformation to multiple metabolites (Dinis-Oliveira, 2016). 11-OH-THC is the predominate primary metabolite formed in vitro using human liver microsomes (HLMs) as well as the major primary circulating metabolite in vivo (Agurell et al., 1986). Cytochrome P450 2C9 (CYP2C9) catalyzes the metabolism of THC to 11-OH-THC, as evidenced by studies with recombinant enzymes and HLMs (Bornheim et al., 1992; Watanabe et al., 1995; Bland et al., 2005; Watanabe et al., 2007). Supporting this conclusion, CYP2C9 deficient carriers (*CYP2C9*3/*3*) have a 3-fold higher THC plasma $AUC_{0\text{-}inf}$ when administered a single oral dose of 15 mg THC (Sachse-Seeboth et al., 2009). Recombinant CYP3A4, CYP2C19, and CYP2D6 also metabolize THC (Stout and Cimino, 2014). Other THC metabolites are 8α/β-OH-THC, which have been observed to form at significant amounts in HLMs and be mediated by CYP3A4 (Bornheim et al., 1992; Watanabe et al., 2007). Therefore, CYP2C9, 2C19, 2D6, and 3A4 are the DMEs that account for the depletion of THC, while all of the listed DMEs except for CYP3A form 11-OH-THC.

42-50% of the radiolabeled THC dose is excreted in the first three days after IV administration of THC, mainly as metabolites (Wall et al., 1983). Detection of THC and its metabolites persists for >30 days (Karschner et al., 2016). Less than 5% of THC is excreted unchanged in the urine or feces. Roughly 20% of the radiolabeled THC IV dose is excreted in the urine, mostly as conjugated COOH-THC. The remaining 80% of THC IV dose is excreted in the feces, as COOH-THC (28%), polar acids (26%), unchanged 11-OH-THC (20%), and 8α/β-OH-THC, 8β-11-di-OH-THC (26%) (Wall and Perez-Reyes, 1981).

Besides biotransformation of 11-OH-THC to COOH-THC (**Figure 1.2**), further hydroxylation of 11-OH-THC yields 8β-11-di-OH-THC or other dihydroxylated THC metabolites (Dinis-Oliveira, 2016). A thorough investigation on the P450 enzymes that metabolize 11-OH-THC has not been conducted in vitro, however in vivo evidence suggests that CYP2C9 and CYP3A4 metabolize 11-OH-THC (Stout and Cimino, 2014). In recombinant enzymes studies, UGT1A9 and UGT1A10 conjugate 11-OH-THC (Mazur

et al., 2009a). To note, the study by Mazur et al. did not observe THC conjugation by any of the tested UGT enzymes, however, a THC glucuronide was detected in human urine (Desrosiers et al., 2014).

70-80% of radiolabeled 11-OH-THC IV dose is excreted within the first seven days after IV administration of 11-OH-THC< with 20-25% of the 11-OH-THC dose recovered in the urine, mainly as acid metabolites, and 70-75% of the dose is recovered in the feces (Lemberger et al., 1973). Less than 5% of the 11-OH-THC dose is excreted unchanged in urine. Of the 11-OH-THC dose excreted in the feces, ~42% is unchanged 11-OH-THC, ~37% is 8β-11-di-OH-THC, and ~21% is conjugated 11-OH-THC (Lemberger et al., 1972a). The large fraction of 11-OH-THC in the feces may be due to deconjugation of the 11-OH-THC glucuronide in the intestines or significant transport of these 11-OH-THC into the bile by the canalicular transporters (e.g. P-gp, BCRP or MRP2) (see below for further discussion).

The plasma concentration-time profiles of THC and 11-OH-THC can be described by two- (Wall et al., 1983; Awasthi et al., 2018) or three-compartment kinetics (THC only) (Hunt and Jones, 1980; Heuberger et al., 2015) (also see **Figure 1.3**). The initial half-life of THC after inhalation has been estimated between 1.4 – 12.8 min (Hunt and Jones, 1980; Chiang and Barnett, 1984; Strougo et al., 2008) while the terminal half-life has been estimated between 20-36 hours (Huestis, 2007; Heuberger et al., 2015). The initial half-life is indicative of the fast metabolism of THC whereas the long terminal half-life is due to slow redistribution of THC and 11-OH-THC from fatty tissues. Indeed, measured THC plasma clearance after IV administration is 11.2 ± 5.7 ml/min/kg (Naef et al., 2004), indicating THC is a fast clearance compound. After IV administration of 11-OH-THC, the 11-OH-THC plasma profile and half-life is like that of THC – about 22 hours (Lemberger et al., 1972a; Lemberger et al., 1973). The terminal half-life of THC appears to differ with administration route (**Table 1.1**). For example, THC $t_{1/2}$ was 20 hours (48 hour sampling time) (Ohlsson et al., 1982) after IV administration, 98 hours (360 hour sampling time) after inhalation (Johansson et al., 1988), and 7.5 hours (72 hour sampling time) after oral administration (Sachse-Seeboth et al., 2009). Given the long absorption time of THC after oral administration (t_{max} of 1.9 hours -**Table 1.1**), the difference in half-lives after inhalation versus oral administration might be a distributional phenomenon and severely impacted by sampling time.

After IV and inhalation of administration of THC, the terminal half-life of 11-OH-THC is similar or slightly larger compared THC, suggesting formation limited kinetics (Naef et al., 2004; Kauert et al., 2007; Toennes et al., 2008; Toennes et al., 2011). However, after oral administration, 11-OH-THC half-life is larger than of THC (8.67 hours versus 12.4 hours –**Table 1.1**). This data would suggest 11-OH-THC is elimination rate-limited. Again, distributional kinetics as well as sampling time may mask the true half-life of THC and 11-OH-THC between the different administration routes. Further discussion of 11-OH-THC elimination kinetics can be found in **Chapter 4**.

1.6.3. Transport

Based on animal studies, THC is a substrate of efflux transporters, P-gp and BCRP. *Abcb1a/b* and *Abcg2* knock-out mice had up to 4.2- and 6.1-fold increase in the brain/blood THC ratio compared to wild-type mice, respectively (3 mg/kg THC administered intraperitoneally) (Spiro et al., 2012b). After oral administration of 25 mg/kg THC to CF1 mice, which lack P-gp, the AUC of THC in CF1 mice was 2.2-fold higher than in wild-type mice (Bonhomme-Faivre et al., 2008). There is no information on the transport of 11-OH-THC. Therefore in vitro studies are need to confirm THC and establish 11-OH-THC P-gp- or BCRP-mediated transport, using transporter membrane vesicles or transporter transfected cells.

THC has been observed to impact in vitro and in vivo P-gp transporter activity. THC (50 μM) weakly inhibited P-gp mediated calcein-AM transport and BCRP mediated mitoxantrone in HEK293-MDR1 and HEK293-BCRP cells, respectively (Tournier et al., 2010). Acute exposure of 10 μM THC for 4 hours but not 1, 8, or 48 hours caused an increase in *MDR1* mRNA and decrease in Rhodamine 123 (P-gp substrate) intracellular accumulation in the T lymphoblastoid leukemia cell line CEM/VLB_{100} (Holland et al., 2006; Arnold et al., 2012). In mice treated with 1 mg/kg THC daily for 14 days followed by a 14-day wash-out, there was an increase of P-gp expression (assessed using immunofluorescence) in brain microvessels and 25-50% decrease in brain accumulation of risperidone, a schizophrenic drug (Brzozowska et al., 2017). However, in vitro incubation of >1 μM THC for 72 hours decreased P-gp expression up to 50% in a dose-dependent manner in CEM/VLB_{100} cells (Holland et al., 2006). Pooled together, acute and chronic exposure of THC appears to enhance and decrease P-gp activity, respectively. The mechanisms of the observed P-gp induction by THC are not known.

Limited in vitro evidence shows THC may inhibit BCRP and MRP1. THC (2 μM) increased intracellular accumulation of the BCRP probe substrate mitoxantrone in the MEF3.8/Bcrp1 cell line and inhibited basal and substrate-stimulated ATPase activity of wild-type human ABCG2 (Holland et al., 2007). Furthermore, THC increased the intracellular accumulation of MRP1 substrates Fluo3 and vincristine in the cell line 2008/MRP1 with IC_{50} = 107 – 161 μM (Holland et al., 2008)..

Collectively, these data suggest that THC can inhibit the efflux activity of P-gp, BCRP, and MRP1, and on chronic administration decreases protein expression of P-gp. Conversely, acute exposure of cannabinoids may enhance P-gp expression. However, the THC concentrations/doses used in these studies (μM range) were much higher than those likely to be observed in vivo in humans (nM range – **Table 1.1**). As such, these data demonstrate that THC is a substrate of P-gp and BCRP, which are both efflux transporters expressed at the placental barrier, and unlikely to inhibit efflux activity of these transporters at the plasma concentrations observed in vivo.

1.7. Executive summary

Prospective clinical studies to assess the maternal and fetal safety and toxicity of cannabis are difficult due to ethical and logistical constraints. Furthermore, confounding factors, such as self-reporting, polydrug use, socioeconomic background, changing composition of cannabis, and mode of cannabis administration make it difficult to investigate the independent risk factor associated with maternal cannabis use using observations studies. Cannabinoids THC and 11-OH-THC are perpetrators of fetal risk due to their interaction with the endocannabinoid system which leads to adverse fetal outcomes. In vitro and animal studies are useful in interrogating the effects of THC and 11-OH-THC exposure during different stages of pregnancy. However, the magnitude to effect/risk cannot be translated from preclinical studies to humans without knowledge of the maternal and fetal drug concentrations in humans. Due to the limitations, the independent risk of maternal cannabis use can be established through the maternal and fetal THC/11-OH-THC exposure-toxicity relationship. However, assessing the maternal and fetal concentrations of THC/11-OH-THC in vivo is not possible due to logistical and ethical considerations. An alternative is to make in silico predictions using PBPK M & S. PBPK models incorporates physiological data, such as tissue composition and blood flows, with mechanistic drug PK parameters, such as

metabolism and transport, to mechanistically predict in vivo disposition of a xenobiotic. Utilizing PBPK M & S, the objective of this dissertation project is to prospectively predict cannabinoid (THC and its active metabolite, 11-OH-THC) exposure in pregnant women and the fetus. This non-invasive approach was able to simulate maternal-fetal cannabinoid exposure for varying THC doses, administration routes, at different gestational ages, as well as different populations (e.g. nonpregnant versus pregnant). Maternal-fetal cannabinoid exposure predictions in vivo can inform preclinical and animal studies on which pharmacologically relevant cannabinoid concentrations to use when establishing cannabinoid exposure – fetal risk relationship in preclinical studies. Additionally, this information will help design better clinical trials, predict drug-cannabinoid interaction in both pregnant and nonpregnant populations, and predict impact of genetic polymorphism on cannabinoid exposure.

The aims and results of this project were as follows:

1. **Identify the drug metabolizing enzymes (DMEs) and the fraction metabolized (fm) by these enzymes at THC/11-OH-THC plasma concentrations observed in vivo.**
   1.1. *Use recombinant P450 and UGT enzymes to identify the enzymes important in disposition of THC/11-OH-THC.* The identity of maternal, placental, and fetal enzymes that are involved in the biotransformation of THC and 11-OH-THC need to be established for inclusion in the PBPK model. A reaction phenotyping study using recombinant P450 and UGT enzymes was conducted and the depletion of THC/11-OH-THC and formation of 11-OH-THC was monitored. Maternal DMEs involved in THC and 11-OH-THC metabolism identified from the reaction phenotyping studies were CYP2C9, 3A, 2C19, 2D6, 1A1/2, UGT1A9 and 2B7. Placental/fetal DMEs identified from the reaction phenotyping studies that may be of importance were CYP1A1, 3A7 and UGT1A9 and 2B7.
   1.2. *Quantify fm using pooled HLMs at THC and 11-OH-THC concentrations observed after smoking cannabis of contemporary concentrations*. Since maternal drug exposure drives fetal exposure, it is important to identify contributions of the relevant DMEs to maternal cannabinoid disposition. Using pharmacologically relevant concentrations of THC and 11-OH-THC, fm values were estimated in pooled HLMs using chemical inhibitors and adjusting for enzyme cross-inhibition.

CYP2C9 was identified as the major enzyme responsible for the depletion of THC and formation of 11-OH-THC. The remaining THC depletion was via CYP2D6. 11-OH-THC was depleted mainly by UGTs (UGT1A9 and UGT2B7), CYP3A, and CYP2C9.

Studies described above in Aims 1.1-1.2 are described in detail in **Chapter 2**.

2. Quantify metabolic kinetics of THC/11-OH-THC in HLMs

2.1. *Quantify kinetic parameters (V_{max}, K_m, CL_{int}) of THC depletion and 11-OH-THC depletion and formation in pooled HLMs.* Identifying the depletion and formation kinetics (V_{max}, K_m, CL_{int}) of THC and 11-OH-THC disposition is necessary to predict cannabinoid exposure at different doses, different administration routes, as well as for extrapolating metabolic clearance from nonpregnant to pregnant population based on enzyme abundance. The kinetics of P450 depletion of THC/11-OH-THC, formation of 11-OH-THC/COOH-THC, and UGT depletion of 11-OH-THC was quantified in pooled HLMs.

2.2. *Estimate kinetic parameters of relevant enzymatic pathways involved in the sequential metabolism of THC/11-OH-THC using in vitro modelin*g. Since multiple metabolites of THC and 11-OH-THC are formed, the kinetic parameters in **Aim 2.1** are of multiple enzymatic pathways, and as such represent aggregated kinetics. For PBPK M&S, information via a particular enzymatic pathway is necessary. Using information about the relevant DMEs from Aim 1, depletion and formation kinetics of THC/11-OH-THC was monitored in the presence of chemical inhibitors of CYP2C9 and CYP3A4, then a sequential P450 and UGT kinetic model was fitted to the in vitro concentration-time curves to estimate kinetic parameters via individual enzymatic pathways. V_{max}, K_m, CL_{int}, and fm estimates for CYP2C9, 3A4, 2D6 and UGT enzymes are presented.

Studies described above in Aims 2.1-2.2 are described in detail in **Chapter 3**.

3. Build and verify a THC/11-OH-THC PBPK in nonpregnant population using mechanistic drug parameters from Aim 1-2.

3.1. *The mechanistic drug information generated in Aims 1-2 (fm, V_{max}, K_m, CL_{int}, fu_p) was extrapolated to in vivo and incorporated into a linked THC/11-OH-THC PBPK model using nonpregnant population.* Additional drug information, such as physicochemical properties (summarized in **Section 1.6**), from published studies was incorporated to establish the cannabinoid nonpregnant PBPKmodel. The THC/11-OH-THC PBPK model was verified using clinical PK studies after IV THC administration (for THC disposition) and inhalation of THC (for 11-OH-THC disposition).

Studies described above in Aim 3 are described in detail in **Chapter 4**.

4. Simulate THC/11-OH-THC exposure during pregnancy using maternal-fetal PBPK M&S

4.1. *Identify and quantify placental metabolism of THC/11-OH-THC.* Studies in **Aim 1.1** identified several DMEs that may metabolize THC and 11-OH-THC in the placenta. Disposition of THC and 11-OH-THC was monitored in placental microsomes from first, second, and third trimesters. Limited depletion was observed, and thus it was concluded that there is negligible placental metabolism of THC and 11-OH-THC.

4.2. *Extrapolate THC/11-OH-THC exposure from Aim 3 at various gestational-ages using maternal-fetal PBPK modeling and simulation.* Using an established maternal-fetal PBPK model (Zhang et al., 2017a; Zhang and Unadkat, 2017), the disposition of THC in nonpregnant population (established in **Aim 3**) was extrapolated based on pregnancy-induced physiological changes, such an induction of CYP3A4 and 2C9. Since the observed F/M THC ratio is <1 in humans, the activity of placental efflux transporters (as characterized using total fraction transported via P-gp and BCRP) was simulated in order to recapitulate the observed distribution in vivo.

Studies described above in Aims 4.1 – 4.2 are described in detail in **Chapter 5**.

The final results from this project are a linked THC/11-OH-THC PBPK model in nonpregnant and pregnant populations. The nonpregnant PBPK model can be advanced by including mechanistic information on extrahepatic metabolism (e.g., lung and intestines) to simulate THC and 11-OH-THC concentrations after inhalation and oral administration of THC. Mechanistic studies on the transport of

THC and 11-OH-THC at the placental barrier are needed for inclusion in the m-f-PBPK model. Lastly, the maternal-fetal PBPK predictions need to be verified using in vivo data of paired maternal and umbilical (fetal) concentrations at term. A summary of general conclusions and future directions are detailed in **Chapter 6**.

Supplementary Table 1.1. Mean PK endpoints for THC and its metabolites following intravenous administration of THC.

Dose (mg)	Sampling duration (hr)	THC				11-OH-THC				COOH-THC				Reference
		C_{max} (nM)	T_{max} (hr)	AUC (ng*min/ml)	$T_{1/2}$ (hr)	C_{max} (nM)	T_{max} (hr)	AUC (ng*min/ml)	$T_{1/2}$ (hr)	C_{max} (nM)	T_{max} (hr)	AUC (ng*min/ml)	$T_{1/2}$ (hr)	
0.5	72	—	—	—	57	—	—	—	—	—	—	—	—	(Lemberger et al., 1970)
0.5	72	—	—	—	28	—	—	—	—	—	—	—	—	(Lemberger et al., 1971)
2	24	334	—	—	20	—	—	—	—	—	—	—	—	(Hunt and Jones, 1980)
5	48	228	—	5460	—	—	—	—	—	—	—	—	—	(Ohlsson et al., 1982)
2.2	48	270	—	12100	29	11.5	—	—	33	69.7	—	—	24	(Wall et al., 1983)
4	48	226	—	16800	36	11.2	—	—	15	110	—	—	55	(Wall et al., 1983)
5	48	193	—	5180	20	—	—	—	—	—	—	—	—	(Ohlsson et al., 1982)
2.5	2	562	—	2047	—	13.3	—	—	—	—	—	—	—	(Morrison et al., 2009)
2.5	2	480	—	1753	—	—	—	—	—	—	—	—	—	(Barkus et al., 2011)
0.053 mg/kg	8	864	—	9951	1.22	27.5	—	1508	—	107	—	—	—	(Naef et al., 2004)
0.053 mg/kg	8	864	—	4103	1.22	27.5	—	622	—	107	—	—	—	(Naef et al., 2004)
4.5	72	197	—	—	—	10.3	—	—	—	41	—	—	—	(Wall and Perez-Reyes, 1981)
5	3	696	—	4330	1.42	—	—	—	—	—	—	—	—	(Ohlsson et al., 1980)
5	2	916	—	4300	—	—	—	—	—	—	—	—	—	(Lindgren et al., 1981)
5	2	960	—	6040		—	—	—	—		—	—	—	(Lindgren et al., 1981)
5	8	1228	—	7094	1.56	—	—	—	—	126	—	—	149	(Kelly and Jones, 1992)
5	8	1392	—	9908	1.95	—	—	—	—	110	—	—	125	(Kelly and Jones, 1992)

Supplementary Table 1.2. Mean PK endpoints for THC and its metabolites following administration of THC by smoking (inhalation)

Dose (mg)	Dose % (w/w)	Sampling duration (hr)	THC				11-OH-THC				COOH-THC				Reference
			C_{max} (nM)	T_{max} (hr)	AUC (ng*min/ml)	$T_{1/2}$ (hr)	C_{max} (nM)	T_{max} (hr)	AUC (ng*min/ml)	$T_{1/2}$ (hr)	C_{max} (nM)	T_{max} (hr)	AUC (ng*min/ml)	$T_{1/2}$ (hr)	
8.94	1.0%	2	287	—	1611	2.8	—	—	—	—	—	—	—	—	(Barnett et al., 1982)
9.7	1.3%	6	300	—	4079	—	—	—	—	—	91.6	—	6231	—	(Perez-Reyes et al., 1982)
10	1.3%[a]	48	50.9	—	1420	—	—	—	—	—	—	—	—	—	(Ohlsson et al., 1982)
10	1.3%[a]	48	103	—	2450	—	—	—	—	—	—	—	—	—	(Ohlsson et al., 1982)
10.5	1.3%[a]	22	270	—	—	—	57.3	—	—	—	105.1	—	—	—	(McBurney et al., 1986)
12.7	1.6%	2	312	—	2160	—	—	—	—	—	—	—	—	—	(Lindgren et al., 1981)
12.8	2.0%	6	342	—	4253	—	—	—	—	—	125.1	—	7474	—	(Perez-Reyes et al., 1982)
13	2.0%	3	245	—	1960	—	—	—	—	—	—	—	—	—	(Ohlsson et al., 1980)
13.4	1.6%	2	213	—	1420	—	—	—	—	—	—	—	—	—	(Lindgren et al., 1981)
15	1.9%[a]	360	31.8	—	—	98	—	—	—	—	—	—	—	—	(Johansson et al., 1988)
15.8	1.8%	168	268	—	—	—	20.3	—	—	—	71.1	—	—	—	(Huestis et al., 1992)
16	2.5%	6	493	—	5566	—	—	—	—	—	132	—	8728		(Perez-Reyes et al., 1982)

0.25mg/kg	2.3%[a]	6	152	—	1350	1.5	7.57	—	276	2.2	39.5	—	2394	3.7	(Kauert et al., 2007)
0.4 mg/kg	3.2%[a]	4	357	—	5286	1.6	51.1	—	1866	2.1	386	—	22056	5.5	(Toennes et al., 2011)
29.3	9.8%	8	430	—	4584	—	27.8	—	1452	—	88.3	—	5412		(Hunault et al., 2008)
29.3	2.9%	8	394	—	—	—		—	—	—	—	—	—	—	(Hunault et al., 2014)
33.8	3.6%	168	516	—	—	—	22.7	—	—	—	157	—	—	—	(Huestis et al., 1992)
0.5 mg/kg	4.6%[a]	6	252	—	2418	1.4	10.9	—	480	1.9	67.9	—	4008	3	(Kauert et al., 2007)
49.1	16.4%	8	645	—	6786	—	49.6	—	2202		173	—	8982		(Hunault et al., 2008)
49.1	4.9%	8	534	—	—	—		—	—	—	—	—	—	—	(Hunault et al., 2014)
50.6	6.9%	3.5	954	—	—	—	38.9	—	—	—	—	—	—	—	(Newmeyer et al., 2017b)
50.6	6.9%	3.5	362	—	—	—	10.3	—	—	—	—	—	—	—	(Newmeyer et al., 2017b)
54	6.8%	22	242	0.25	6600	—	30.3	—	1140	—	195	—	12600	—	(Schwope et al., 2011)
54	6.8%	30	53.1	—	1746	—	16.4	—	684	—	54.0	—	12180	—	(Desrosiers et al., 2014)
54	6.8%	30	152	—	10680	—	31.8	—	3900	—	141	—	73860	—	(Desrosiers et al., 2014)
69.4	23.1%	8	735	—	9024	—	47.8	—	2424	—	158	—	9654	—	(Hunault et al., 2008)
69.4	6.9%	8	605	—	—	—	—	—	—	—		—	—	—	(Hunault et al., 2014)
70	7.0%	8	66.5	—	—	—	5.45	—	—	—	22.4	—	—	—	(Brenneisen et al., 2010)

Formulation: all studies used cannabinoid spiked cannabis cigarettes except for (Hunault et al., 2008), (Toennes et al., 2011), and (Hunault et al., 2014), where cannabis cigarettes + tobacco (300 mg cannabis + 700 mg tobacco) were used. [a] 800 mg cannabis cigarette weight was assumed

Supplementary Table 1.3. Mean PK endpoints for THC and its metabolites following oral administration of THC

Dose (mg)	Sampling duration (hr)	For-mu-lation	THC				11-OH-THC				COOH-THC				Reference
			C_{max} (nM)	T_{max} (hr)	AUC (ng*min/ml)	$T_{1/2}$ (hr)	C_{max} (nM)	T_{max} (hr)	AUC (ng*min/ml)	$T_{1/2}$ (hr)	C_{max} (nM)	T_{max} (hr)	AUC (ng*min/ml)	$T_{1/2}$ (hr)	
2.5	12	F	4.20	—	173	—	—	—	—	—	—	—	—	—	(Marinol, 2017)
4.25	48	F	5.76	—	225	5.41	7.66	—	642	11.6	—	—	—	—	(Parikh et al., 2016)
4.25	48	F	4.83	—	546	9.35	3.72	—	757	11.2	—	—	—	—	(Oh et al., 2017)
5	12	F	9.41	—	370	—	—	—	—	—	—	—	—	—	(2017)
5	8	I	9.29	—	189	1.19	14.2	—	648	3.27	—	—	—	—	(Klumpers et al., 2012)
5	10.5	F	14.9	3.2	1836	—	9.08	3.3	888	—	201	4.4	34896	—	(Karschner et al., 2011)
5	48	F	7.00	—	231	2.68	9.93	—	798	11.8	—	—	—	—	(Parikh et al., 2016)
5	48	F	6.96	—	266	4.82	9.44	—	670	12.5	—	—	—	—	(Oh et al., 2017)
5	48	F	8.27	—	628	10.4	6.54	—	890	11.1	—	—	—	—	(Oh et al., 2017)
6.5	8	I	14.1	—	287	1.33	18.0	—	849	5.31	—	—	—	—	(Klumpers et al., 2012)
8	8	I	14.9	—	377	1.32	18.5	—	1087	5.23	—	—	—	—	(Klumpers et al., 2012)
10	12	F	25.1	—	912	—	—	—	—	—	—	—	—	—	(2017)
10	24	C	12.9	1.1	358	—	14.8	1.5	928	—	103	124	14596	—	(Nadulski et al., 2005)
10	130	E	8.2	—	—	—	5.40	—	—	—	56.5	—	—	—	(Vandrey et al., 2017)

10	2	B	41.6	2.0	—	—	—	—	—	—	—	—	—	—	(Fusar-Poli et al., 2009)
10	24	C	12.9	1.0	450	—	14.8	1.37	1003	—	103	115	14983	—	(Nadulski et al., 2005)
10	24	C	16.8	1.0	564	—	17.4	1.38	1118	—	88.4	95	11652	—	(Nadulski et al., 2005)
15	72	B	29.9	—	9600	25	17.9	—	—	12	197	—	—	37	(Wall et al., 1983)
15	72	G	8.59	—	966	7.5	8.47	—	1440	—	74.6	—	40020	—	(Sachse-Seeboth et al., 2009)
15	10.5	F	45.5	3.4	3012	—	33.6	3.4	2544	—	388	4.9	60954	—	(Karschner et al., 2011)
15	12	F	15.9	—	—	—	9.08	—	—	—	—	—	—	—	(Lile et al., 2013)
16.5	24	H	31.0	—	—	—	25.4	—	—	—	218	—	—	—	(Ménétrey et al., 2005)
20	24	B	29.6	—	—	—	26.6	—	—	—	189	—	—	—	(Wall and Perez-Reyes, 1981)
20	72	B	44.5	—	16000	25	20.0	—	—	—	258	—	—	25	(Wall et al., 1983)
20	6	D	14 - 35	—	1020	—		—	—	—		—	—	—	(Ohlsson et al., 1980)
20	10	D	15.9	1.5	—	—		—	—	—		—	—	—	(Agurell et al., 1981)
20	24	F	22.8		—	—	21.1	—	—	—	218	—	—	—	(Ménétrey et al., 2005)
20	10	D	19.1	2	—	—		—	—	—		—	—	—	(Agurell et al., 1981)

20	10	D	25.4	2	—	—		—	—	—		—	—	—	(Agurell et al., 1981)
25	130	E	28.5	—	—	—	17.8	—	—	—	167	—	—	—	(Vandrey et al., 2017)
30	12	F	31.8	—	—	—	15.1	—	—	—	—	—	—	—	(Lile et al., 2013)
45	12	F	57.2	—	—	—	30.3	—	—	—	—	—	—	—	(Lile et al., 2013)
45.7	24	H	68.5	—	—	—	69.2	—	—	—	519	—	—	—	(Ménétrey et al., 2005)
50	130	E	26.9	—	—	—	17.3	—	—	—	230	—	—	—	(Vandrey et al., 2017)
50.6	3.5	E	127	—	—	—	40.5	—	—	—	—	—	—	—	(Newmeyer et al., 2017b)
50.6	3.5	E	82.4	—	—	—	27.6	—	—	—	—	—	—	—	(Newmeyer et al., 2017b)
50.6	50	E	132	—	—	—	44.3	—	—	—	313	—	—	—	(Newmeyer et al., 2017a)
50.6	50	E	66.9	—	—	—	30.3	—	—	—	306	—	—	—	(Newmeyer et al., 2017a)
60	12	F	143	—	—	—	33.3	—	—	—	—	—	—	—	(Lile et al., 2013)
75	12	F	127	—	—	—	45.4	—	—	—	—	—	—	—	(Lile et al., 2013)
90	12	F	165	—	—	—	60.5	—	—	—	—	—	—	—	(Lile et al., 2013)

[a] Formulation: A – corn oil encapsulated in gelatin capsule; B – sesame oil encapsulated in gelatin capsule; C – cannabis extract; D – chocolate cookie; E – brownie; F – Dronabinol; G – coconut oil; H – milk decoction; I – Namisol

Chapter 2. Hepatic enzymes relevant to the disposition of THC and its psychoactive metabolite, 11-OH-THC

The work in this chapter was previously published

in

Drug Metabolism and Disposition. 2019, 47(3): 249-256

2.1. ABSTRACT

Cannabis use by pregnant women is increasing. To predict developmental risk to the offspring from such use, in-utero fetal exposure to (-)-Δ^9-tetrahydrocannabinol (THC), the main psychoactive cannabinoid in cannabis and its active psychoactive metabolite, 11-OH-THC, needs to be determined. Since such measurement is not possible, PBPK modeling and simulation can provide an alternative method to estimate fetal exposure to cannabinoids. To do so, PK parameters for the disposition of THC and 11-OH-THC need to be elucidated. Here, we report a first step to estimate these parameters, namely those related to maternal metabolism of THC/11-OH-THC in HLMs at plasma concentrations observed after smoking cannabis. Using recombinant P450 and UGT enzymes, CYP1A1, 1A2, 2C9, 2C19, 2D6, 3A4, 3A5, 3A7, and UGT1A9 and UGT2B7 were found to be involved in the disposition of THC/11-OH-THC. Using pooled HLMs, the fraction metabolized (fm) by relevant enzymes was measured using selective enzyme inhibitors then adjusted for enzyme cross-inhibition. As previously reported, CYP2C9 was the major enzyme responsible for depletion of THC and formation of 11-OH-THC with fm of 0.82 and 0.99, respectively (mean ± SD), whereas CYP2D6 and CYP2C19 were minor contributors. 11-OH-THC was depleted by UGT and P450 enzymes with fm of 0.60 ± 0.05 and 0.40 ± 0.05, respectively (mean ± SD), with UGT2B7, UGT1A9, CYP2C9, and CYP3A4 as contributors. These mechanistic data represent the first set of drug-dependent parameters necessary to predict maternal-fetal cannabinoid exposure during pregnancy using PBPK modeling.

2.2. INTRODUCTION

As mentioned in the **Chapter 1**, up to 7.1% of pregnant women in the United Stated used cannabis at some point during pregnancy (SAMHSA, 2017). Furthermore, the prevalence of cannabis use by pregnant women has been increasing (Brown et al., 2017). The average concentrations of the psychoactive cannabinoid in cannabis, (-)-Δ^9-tetrahydrocannabinol (THC) have been steadily increasing, with the most recent content (weight/weight) estimated at 12% (ElSohly et al., 2016). To estimate fetal exposure (and therefore risk) to THC and its psychoactive metabolite, 11-OH-THC (**Figure 1.2**), maternal-fetal exposure to these compounds needs to be measured or predicted. Conducting PK studies in pregnant women is not possible due to ethical and logistical reasons. Maternal exposure to drugs drives

drug fetal exposure. Therefore, an alternative is to predict the maternal-fetal exposure to these cannabinoids during pregnancy using physiologically-based pharmacokinetic (PBPK) models where gestational-age dependent changes in expression of hepatic drug metabolizing enzymes (DMEs) and transporters can be incorporated (Ke et al., 2012; Ke et al., 2014a; Zhang et al., 2017b; Zhang and Unadkat, 2017). The latter is important as activity of many cytochrome P450 enzymes is either induced or repressed during pregnancy (Anderson, 2005; Ke et al., 2014b).

In order to predict the disposition of THC/11-OH-THC during pregnancy, amongst other parameters, one must first identify the DMEs involved in the biotransformation of THC and 11-OH-THC and the fraction metabolized (fm) via these pathways. In vitro studies have identified CYP2C9, 3A4, 2C19 and 2D6 as DMEs responsible for the formation of THC metabolites (Stout and Cimino, 2014). Of these, CYP2C9 and CYP2C19 are the hepatic DMEs responsible for the formation of 11-OH-THC (Bland et al., 2005; Watanabe et al., 2007). Through in vivo studies, CYP2C9 and CYP3A4 have been identified as important DMEs involved in 11-OH-THC clearance (Sachse-Seeboth et al., 2009; Stott et al., 2013). Additionally, UDP-glucuronosyltransferase (UGT) enzymes, UGT1A9 and UGT1A10 are the hepatic DMEs responsible for the glucuronidation of 11-OH-THC in vitro (Mazur et al., 2009b).

Despite the above data, there are key drug parameters missing that are necessary for PBPK modeling and simulation (M & S). In vitro metabolic studies have focused on THC metabolite formation rather than on THC depletion. As such, there may be additional enzymes responsible for the clearance of THC. In addition, the enzymes involved in depletion of 11-OH-THC have not all been identified. Furthermore, the fm via each enzyme, a necessary parameter for PBPK M & S, is missing. Lastly, most in vitro studies have examined the metabolism of supraphysiological cannabinoid concentrations which may not be representative of enzyme contributions at cannabinoid concentrations observed in vivo. Therefore, the aims of **Chapter 2** were to profile the hepatic metabolic pathways of THC and 11-OH-THC by: 1) identifying the relevant recombinant enzymes (both P450s and UGTs) capable of metabolizing these compounds, and 2) using the results from the above studies as a guide to quantify the fm via the identified enzymes in pooled HLMs at plasma concentrations of THC and 11-OH-THC observed after smoking cannabis. The results from these studies are the first step in generating the maternal

mechanistic PK parameters necessary to build a linked THC/11-OH-THC PBPK model (see **Chapter 4**) that can be used to predict maternal-fetal exposure to THC/11-OH-THC (see **Chapter 5**).

2.3. MATERIALS AND METHODS

2.3.1. Chemicals and reagents.

(-)-Δ^9-THC (1 mg/ml), (±) 11-OH-THC (0.1 mg/ml), and (±) 11-nor-9-carboxy-Δ9-THC (COOH-THC) (0.1 mg/ml) DEA-exempt methanol stocks and deuterated internal standards [(-)-Δ^9-THC-D3, (±) 11-OH-THC-D3, (±) COOH-THC-D3] were purchased from Cerilliant (Round Rock, TX). Low-binding (LB) microcentrifuge tubes (made of chemical-resistant polypropylene), bovine serum albumin (BSA) (fraction V - heat-shock treated), acetonitrile, and formic acid (liquid chromatography-mass spectrometry (LC/MS) grade) were purchased from Fisher Scientific (Hampton, NH). Amber silanized glass vials were purchased from Waters Corporation (Milford, MA). β-Nicotinamide adenine dinucleotide phosphate (NADP+), D-glucose 6-phosphate (G6P), glucose-6-phosphate dehydrogenase (G6PDH), uridine 5'-diphosphoglucuronic acid (UDPGA), and all chemical inhibitors and probes were purchased from Sigma-Aldrich (St. Louis, MO). Milli-Q water was used in all preparations. All other chemicals and reagents were obtained at the highest quality available commercially.

2.3.2. Recombinant enzymes and HLMs.

Recombinant cytochrome P450 (CYP19, 1A1, 1A2, 2A6, 2B6, 2C8, 2C9*1 (Arg144), 2C19, 2D6*1, 2E1, 3A4, 3A5, 3A7) and UDP-glucuronosyltransferase (UGT1A4, 1A9, 1A10, and 2B7) expressed in baculovirus infected insect cells (SupersomesTM) and pooled adult HLMs (n=50, equal mixed gender) were purchased from Corning (Corning, NY).

2.3.3. Cannabinoid in vitro assay experiment optimization.

THC has low solubility, high protein and non-specific binding to plastic and glassware (Garrett and Hunt, 1974). Due to these reasons, experimental reactions were optimized for cannabinoid adsorption, solubility, and extraction. To limit adsorption, initial studies were performed in amber silanized glass. Due to practical and economic reasons, later studies were performed in LB microcentrifuge tubes.

Depletion kinetics of THC was similar in silanized glass versus LB tubes (data now shown). BSA was added to reactions to combat low solubility and limit adsorption. This analytical strategy has been previously suggested for improving radioimmunoassay of THC (Cook et al., 1976). To improve recovery of cannabinoids from reactions, a freeze-liquid technique previously described by Prasad and Singh, 2009 was used (Prasad and Singh, 2009).

2.3.4. Reaction phenotyping using recombinant enzymes.

In silanized amber glass vials, to 0.1 M potassium phosphate buffer (pH 7.4), the following was added (shown as final concentrations): either 500 nM THC or 100 nM 11-OH-THC, recombinant cytochrome P450 (rCYP) enzyme (2 – 40 pmole), and BSA so the final total protein concentration (BSA + rCYP) was 0.2 mg/ml. Mixtures were pre-incubated in a shaking-block heater for 10 minutes at 37°C and 300 RPM. Reactions were initiated with NADPH regenerating system (final concentrations: 1.3 mM NADP+, 3.3 mM G6P, 3.3 mM MgCl2, 0.4 unit/ml G6PDH). Reactions using recombinant UGT enzymes were set up as above with the following changes: recombinant UGT enzymes (0.05-0.75 mg/ml), 0.2% BSA, 5 mM MgCl2, 25 µg/ml alamethicin. Reactions were incubated for 15 minutes on ice to allow for pore-formation by alamethicin, then pre-incubated at 37°C as described above. Reactions were initiated by adding UDPGA (2.5 mM – final concentration). Negative control reactions were set up the same as above and initiated with buffer instead of co-factors. At designated time points, 50 µL of reaction mixture was terminated by adding to 100 µL ice-cold acetonitrile containing internal standards (IS; THC-D3, 11-OH-THC-D3, COOH-THC-D3) in LB tubes. Samples were centrifuged at 10,000 x g for 5 minutes to pellet the protein content. Supernatant was removed and incubated at -20°C for >1 hour to separate the aqueous and organic layers. The top organic layer was removed, placed in LC glass insert vials, and stored at -20ºC until analysis by LC-MS/MS. Two independent experiments in duplicate were performed.

2.3.5. Reaction phenotyping using HLMs.

In LB tubes, to 0.1M potassium phosphate buffer (pH 7.4) containing 0.2% BSA either 1) 500 nM THC and 0.02 mg/ml HLM or 2) 50 nM 11-OH-THC and 0.1 mg/ml HLM was added (showing final concentrations). The cannabinoid concentrations were chosen to represent clinically observed

concentrations after smoking cannabis (Hunault et al., 2008). Assay conditions were optimized to keep HLM concentration low (<0.5 mg/ml) and sampling time short (<30 min), as previously suggested (Jones and Houston, 2004), as well as keep the maximum substrate depletion at ~75% in order to limit errors when fitting models to data (Nath and Atkins, 2006). Negative control reactions were initiated with buffer instead of co-factors. THC or 11-OH-THC was incubated in the presence and absence of selective P450 inhibitors: 10 μM sulfaphenazole (CYP2C9), 2 μM itraconazole (CYP3A), 30 μM omeprazole (CYP2C19), 1 μM quinidine (CYP2D6), 10 μM furafylline (CYP1A). 11-OH-THC was additionally incubated in the presence and absence of selective UGT inhibitors: 2.5 μM niflumic acid (UGT1A9) and 2 mM fluconazole (UGT2B7). All inhibitors, except for furafylline, were added prior to initiating reaction with co-factor. Since furafylline is a mechanism-based inhibitor, the reaction mixture was pre-incubated in the presence of NADPH regenerating system for 15 minutes at 37ºC with shaking and reaction was initiated by the addition of THC. Organic solvent content was <0.75% v/v except for incubations with fluconazole where organic content was 3%. Control reactions had matching organic content. Reactions were terminated and processed as described for reactions using recombinant enzymes. Calibration curves for THC, 11-OH-THC, and COOH-THC were prepared in buffer with 0.2% BSA and incubated and processed in an identical fashion as the reactions. Three independent experiments, each in duplicate, were performed.

2.3.6. Cross-inhibition of selective enzyme inhibitors.

Each selective P450 inhibitor was incubated in 0.1M potassium phosphate buffer (pH 7.4) containing either 1) 0.5 mg/ml HLM, 0.2% BSA, and 40 μM (S)-mephenytoin (CYP2C19 probe) or 2) 0.1 mg/ml HLM, 0.2% BSA, and a cocktail containing the following P450 probes: 5 μM diclofenac (CYP2C9), 10 μM testosterone (CYP3A), 5 μM dextromethorphan (CYP2D6). Incubations (50 μL final volume) were initiated with NADPH regenerating system. Reactions were terminated with addition of 100 μL ice-cold acetonitrile contain tolbutamide as the IS. The formation of 4-OH-mephenytoin (4-OH-MEP) at 30 minutes, or formation of 4-OH-diclofenac (4-OH-DCL), 6β-OH-testosterone (6β-OH-TES), and dextrorphan (DXO), at 20 minutes was monitored. The P450 probe cocktail was adapted from Chen et al., 2016 and was checked for protein and time linearity. While the time and HLM concentrations for the P450 probe cocktail incubation were chosen to best represent the cannabinoid reaction phenotyping using

HLMs set up, the quantification limitation of S-mephenytoin necessitated higher HLM concentration and longer incubation time. The selective UGT inhibitors were incubated as described in HLM reaction phenotyping section with a cocktail which (among other UGT probes) included 20 µM propofol (UGT1A9) and 10 µM naloxone hydrochloride (UGT2B7). The UGT cocktail has been previously described by Bhatt et al., 2018. Reactions (50 µL) were terminated by adding 100 µL ice-cold acetonitrile containing androsterone glucuronide as the IS. The formation of metabolites propofol-glucuronide (PPF-gluc) and naloxone-3-glucuronide (NLX-3-gluc) at 30 minutes was monitored. Three independent experiments, each in triplicate, were performed.

2.3.7. LC-MS/MS analysis.

Samples were analyzed with Acquity ultra-performance liquid chromatography (UPLC) system (Waters Corporation, Milford, MA) coupled to an AB Sciex Triple Quad 6500 (SCIEX, Framingham, MA) using Acquity UPLC BEH C18 column (1.7 µM 2.1 x 50 mm) with attached C18 x 2mm guard column. LC-MS/MS method for quantification of cannabinoids, P450, and UGT probes was adapted from Hudson et al., 2003, Chen et al., 2016, and Bhatt et al., 2018, respectively. The LC flow gradient and multiple reaction monitoring parameters and are listed in **Supplementary Table 2.1** and, **Supplementary Table 2.2,** respectively.

2.3.8. Analysis of kinetic parameters.

The depletion rate-constant (k_{dep}) was obtained by fitting the THC or 11-OH-THC concentration-time profile with a first-order monoexponential decay equation (**Eq. 1**), where C_t is the concentration of substrate remaining at a given time point (t) and C_0 is the substrate concentration at t=0.

$$C_t = C_0 e^{-k_{dep} * t} \quad (1)$$

The 11-OH-THC formation rate-constant (k_{form}) was obtained by fitting the 11-OH-THC concentration-time profile using **Eq. 2** where M_t and M_{max} are metabolite concentrations at a given time point (t) and maximum metabolite formed, respectively. M_{max} was bound to not exceed the input THC concentrations of 500 nM. To note, there was no significant depletion of 11-OH-THC at 0.02 mg/ml HLM

(data not shown), and as such, **Eq. 2** includes only the formation and not the depletion rate-constants of 11-OH-THC. Furthermore, while COOH-THC was monitored in all reactions, there was no observed formation of COOH-THC (see **Section 2.4**) so no formation kinetics was established for COOH-THC.

$$M_t = M_{max}\ 1 - e^{-k_{form}*t} \tag{2}$$

Depletion clearance (CL_{dep}) of THC or 11-OH-THC and formation clearance (CL_{form}) of 11-OH-THC were calculated as shown in **Eq. 3-4**, where [HLM] and [rCYP] are the protein or recombinant enzyme concentrations (mg/ml or pmol/ml).

$$CL_{dep} = \frac{k_{dep}}{rCYP\,or\,HLM} \tag{3}$$

$$CL_{form} = \frac{k_{form}}{HLM} \tag{4}$$

Fraction metabolized (fm) was calculated from k_{dep} or k_{form} in the presence and absence of inhibitor (i) as shown in **Eq.** 5.

$$fm = 1 - \left(\frac{k_{dep\ or\ form,i}}{k_{dep\ or\ form}}\right) \tag{5}$$

2.3.9. Adjusting fm for inhibitor cross-inhibition.

The cannabinoid fm values were adjusted for P450 and UGT inhibitor cross-inhibition (**Eq. 6**) as previously described (Njuguna et al., 2016).

$$\begin{bmatrix} a_{11} & a_{12} & a_{13} & a_{14} \\ a_{21} & a_{22} & a_{23} & a_{24} \\ a_{31} & a_{32} & a_{33} & a_{34} \\ a_{41} & a_{42} & a_{43} & a_{44} \end{bmatrix} * \begin{bmatrix} x_1 \\ x_2 \\ x_3 \\ x_4 \end{bmatrix} = \begin{bmatrix} b_1 \\ b_2 \\ b_3 \\ b_4 \end{bmatrix} \tag{6}$$

For example, **Eq. 6** solves x=A-1*b where x is the adjusted P450 fm matrix (see **Table 2.4**), A is the P450 cross-inhibition matrix (see **Table 2.2**), and b is the experimentally observed P450 fm (non-adjusted) matrix (see **Table 2.1**). To adjust for the cross-inhibition of UGT inhibitors a 2x2 cross-inhibition (a_{11}-a_{22})

(see **Table 2.3**) and 2x1 experimental fm (b_1-b_2) matrix was used. A stochastic simulation approach for error propagation of the adjusted fm values was used. Briefly, a truncated normal distribution (with bounds $0<\mu<1$) using the mean and standard deviation (SD) of each measured cross-inhibition (e.g. a_{11}-a_{44}) or experimental fm (e.g. b_1-b_4) parameter was simulated and **Eq. 6** was solved by choosing randomly from the normal distributions. The mean and SD from 1000 iterations are reported in **Table 2.4**. If the solution for the adjusted fm values was negative, the fm was labeled as negligible.

2.3.10. Data analysis.

Integration of the chromatographic peaks was performed using Analyst v1.6 (Framingham, MA). Model fitting of concentration-time curves and all plotting was performed using GraphPad Prism 7 (La Jolla, CA). Adjustment of fraction metabolized was performed using MATLAB R2016b (Natick, MA).

2.4. RESULTS

2.4.1. Reaction phenotyping using recombinant enzymes

THC (500 nM) was depleted by recombinant CYP1A1, 1A2, 2C9, 2C19, 2D6, 3A4, 3A5, and 3A7 (**Figure2.1A**). CYP1A1 and CYP2C9 had the highest THC depletion clearance. Recombinant CYP19, 2A6, 2B6, 2C8, and 2E1 did not significantly deplete THC.

11-OH-THC was formed from THC (500 nM) by recombinant CYP1A2, 2C9, 2C19, and 2D6 (**Figure 2.1B**). CYP2C19 and CYP2C9 had the highest 11-OH-THC formation clearance. 11-OH-THC was not formed by recombinant CYP1A1, 3A4, 3A5, and 3A7 even though these enzymes turned over THC. In the chromatographs of THC incubations with recombinant CYP1A1, 2D6, 3A4/5/7, there was a peak that co-eluted with 11-OH-THC in the 331→ 313 *m/z* transition at a consistent retention time (data not shown), indicating formation of an additional monohydroxylated THC metabolite. No formation of COOH-THC was detected in the aforementioned experiments.

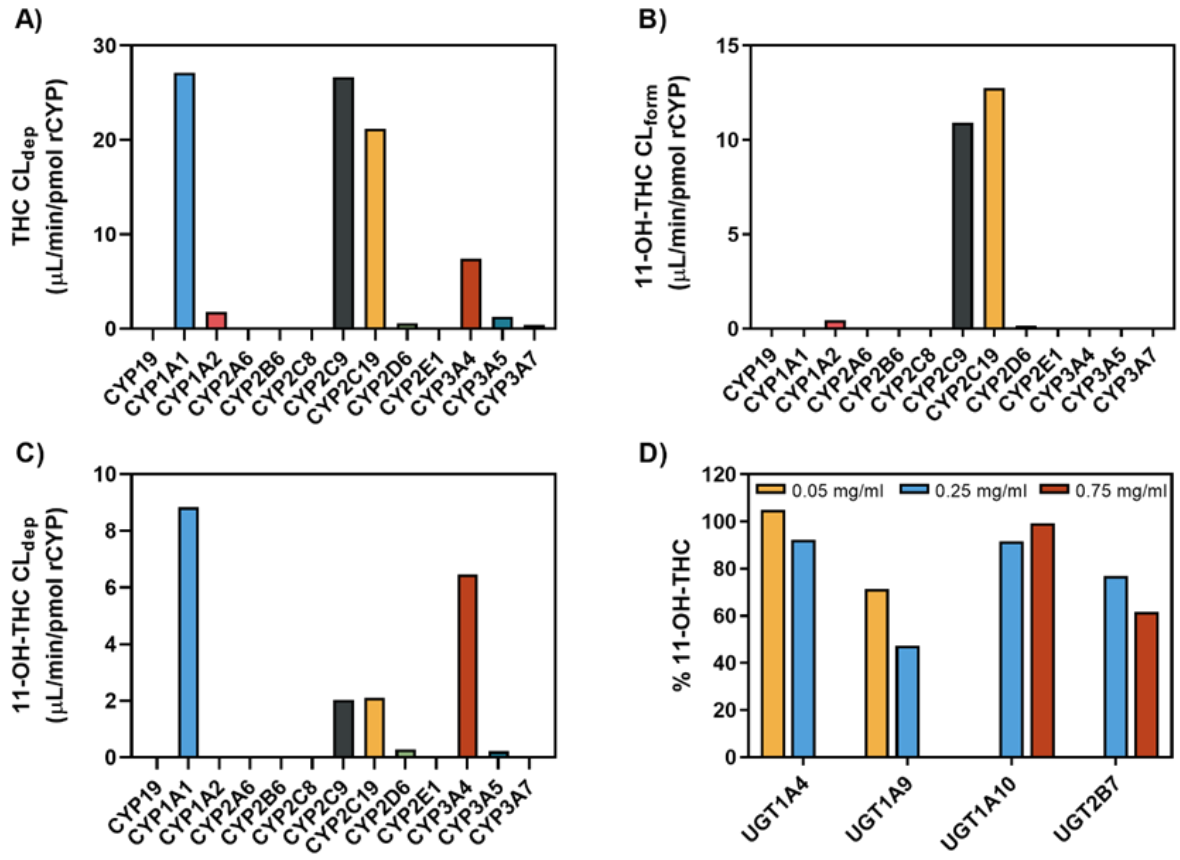

Figure 2.1 Reaction phenotyping using recombinant enzymes.

A) Depletion clearance of THC (500 nM) and B) formation clearance of 11-OH-THC from THC (500 nM) by recombinant P450 enzymes. C) Depletion clearance of 11-OH-THC (50 nM) by recombinant P450 enzymes. D) Enzyme – concentration dependent depletion of 11-OH-THC (50 nM) by recombinant UGT enzymes at 30 minutes. There was no depletion of THC by recombinant UGT enzymes at the highest enzyme concentrations tested (data not shown). Data shown are mean of duplicate determinations (no standard deviation was able to be calculated).

11-OH-THC (50 nM) was depleted by recombinant CYP1A1, 2C9, 2C19, 2D6, 3A4, and 3A5 (**Figure 2.1C**). Recombinant CYP1A1 and CYP3A4 had the highest 11-OH-THC depletion clearance. Recombinant CYP19, 1A2, 2A6, 2B6, 2C8, 2E1, and 3A7 did not significantly deplete 11-OH-THC. Recombinant CYP2C9 and CYP2C19 were the only enzymes that formed COOH-THC (data not shown).

THC was not significantly depleted by any of the recombinant UGT enzymes tested (data not shown). In contrast, 11-OH-THC (50 nM) was depleted in an enzyme-concentration dependent manner by recombinant UGT1A9 and UGT2B7 but not by UGT1A10 and UGT1A4 (**Figure 2.1D**).

2.4.2. Reaction phenotyping using pooled HLMs

Reaction phenotyping at a concentration of THC (500 nM) observed after smoking cannabis (Hunault et al., 2008), was performed in pooled adult HLMs using selective P450 inhibitors for the relevant hepatic enzymes identified from recombinant reaction phenotyping assays (**Figure 2.2**). In control reactions (no inhibitor), CL_{dep} of THC was 3.65 ± 0.36 ml/min/mg and CL_{form} of 11-OH-THC was 1.74 ± 0.42 ml/min/mg. Based off the formation clearance of 11-OH-THC in control reactions, approximately 48% of THC was metabolized to 11-OH-THC. THC depletion was inhibited 78 ± 3% by sulfaphenazole (10 µM) and <25% by itraconazole (2 µM), omeprazole (30 µM), and quinidine (1 µM) (**Figure 2.2A**). The depletion clearance of THC in the presence of furafylline (10 µM) was larger than in control reactions and as such, furafylline was found not be an inhibitor of THC depletion. The reason for this faster depletion is likely due to initiation of reactions with THC, rather than NADPH, and thus not allowing time for protein and non-specific binding of THC.

11-OH-THC formation was inhibited 90 ± 0.94% and 54 ± 7.0% by sulfaphenazole (10 µM) and omeprazole (30 µM), respectively and <25% by itraconazole (2 µM) and quinidine (1 µM) (**Figure 2.2B**). There was no COOH-THC detected in any of the aforementioned experiments, likely due to assay detection limitations. There was no THC depletion via UGT enzymes in pooled HLMs (tested using 0.25 mg/ml HLM), confirming previous results observed in recombinant UGT enzymes (data not shown).

Reaction phenotyping at a concentration of 11-OH-THC (50 nM) observed after smoking cannabis (Hunault et al., 2008), was performed in pooled adult HLMs using selective P450 and UGT inhibitors (**Figure 2.3**). In control reactions, 11-OH-THC was depleted by UGT and P450 enzymes with CL_{dep} of 0.458 ± 0.025 ml/min/mg and 0.299 ± 0.096 ml/min/mg, respectively. As such, UGT and P450 enzymes accounted for 60 ± 4.5% and 40 ± 4.5% of 11-OH-THC depletion in HLMs, respectively (**Figure 2.3A**). In P450-mediated reactions, 11-OH-THC depletion was inhibited 37 ± 8.3% and 61 ± 12%, by sulfaphenazole (10 µM) and itraconazole (2 µM), respectively (**Figure 2.3B**). Omeprazole (30 µM) and quinidine (1 µM) did not significantly inhibit depletion of 11-OH-THC (data not shown). COOH-THC was not detected in any of the aforementioned experiments. In UGT-mediated reactions, 11-OH-THC

depletion was inhibited 60 ± 5.5% and 67 ± 3.6% by fluconazole (2 mM) and niflumic acid (2.5 µM), respectively **(Figure 2.3C**).

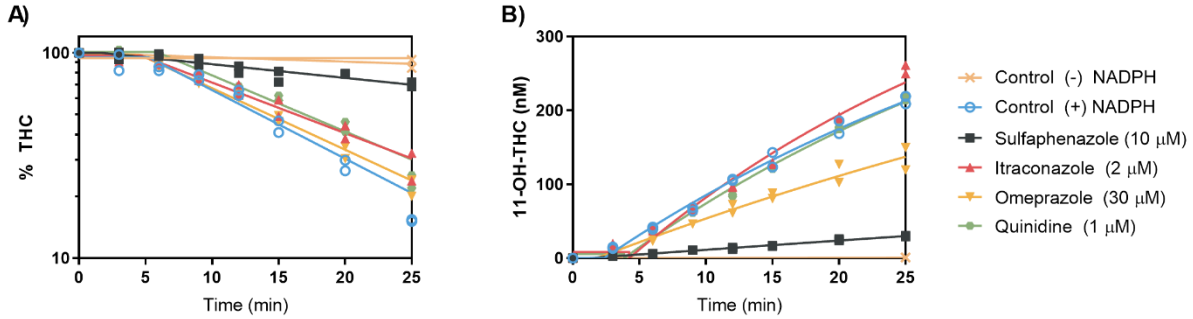

Figure 2.2. THC reaction phenotyping using pooled adults HLMs.

Representative depletion of A) 500 nM THC, a concentration observed after smoking cannabis, and formation of B) 11-OH-THC from THC (500 nM) was monitored in the presence and absence of selective P450 inhibitors. Sulfaphenazole (10 µM) inhibited THC depletion and 11-OH-THC formation by the greatest extent, indicating CYP2C9 is the major enzyme responsible for THC turnover to 11-OH-THC. Panels show data from one representative experiment with duplicate determinations and fit with a model (**Eq. 1** and **2** for k_{dep} and k_{form}, respectively) that includes the observed time lag. The fm mean ± SD calculated using CL_{dep} and CL_{form} (**Eq. 3** and **4**) from three independent experiments are shown in **Table 2.1.**

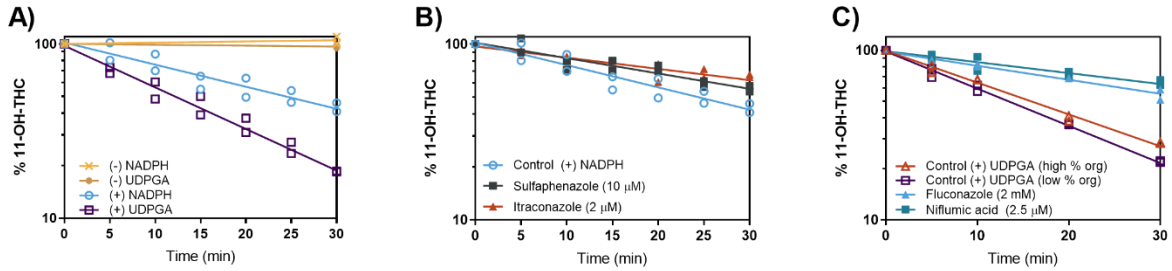

Figure 2.3. 11-OH-THC reaction phenotyping using pooled adult HLMs.

A) Representative depletion of 50 nM 11-OH-THC, a concentration observed after smoking cannabis, is greater by UGT then P450 enzymes. B) Itraconazole (2 µM) and sulfaphenazole (10 µM) inhibited the depletion of 11-OH-THC, indicating CYP3A4 and CYP2C9 are both important in the turnover of 11-OH-THC. To note, no COOH-THC formation was observed in any of the HLM assays. C) Fluconazole (2 mM) and niflumic acid (2.5 µM) inhibited UGT depletion of 11-OH-THC to a similar degree, indicating that UGT2B7 and UGT1A9 are equally important in the depletion of 11-OH-THC. High and low % organic solvent controls were conducted because of the differential organic solvent content in the presence of the UGT inhibitors. Panels show data from one representative experiment with duplicate determinations and fit with a monoexponential decay curve (**Eq. 1** for k_{dep}). The fm mean ± SD calculated using CL_{dep} (**Eq. 3**) from three independent experiments are shown **Table 2.1**.

Table 2.1. Cannabinoid fm values[a] in HLMs determined using selective P450 or UGT inhibitors and quantified by monitoring either THC/11-OH-THC depletion or formation of 11-OH-THC from THC

Selective Inhibitor	Enzyme	THC depletion	11-OH-THC formation	11-OH-THC depletion
Sulfaphenazole (10 μM)	CYP2C9	0.78 ± 0.03	0.90 ± 0.01	0.15 ± 0.04
Itraconazole (2 μM)	CYP3A	0.22 ± 0.05	-0.11 ± 0.09	0.24 ± 0.06
Omeprazole (30 μM)	CYP2C19	0.13 ± 0.11	0.54 ± 0.07	negligible
Quinidine (1 μM)	CYP2D6	0.15 ± 0.10	0.18 ± 0.20	negligible
Fluconazole (2 mM)	UGT2B7	negligible	N/A	0.36 ± 0.05
Niflumic acid (2.5 μM)	UGT1A9	negligible	N/A	0.41 ± 0.04

HLM incubations were conducted with observed concentrations of THC (500 nM) and 11-OH-THC (50 nM) after smoking cannabis. Inhibition of 11-OH-THC depletion by omeprazole and quinidine was negligible (data not shown). Data shown are mean ± SD of three independent experiments with each experiment conducted in duplicate. [a] data not corrected for cross-inhibition of enzyme by the inhibitors.

2.4.3. Cross-inhibition of selective enzyme inhibitors

To accurately determine the fractional contribution of enzymes involved in cannabinoid disposition, the cross-inhibition of the selective P450 and UGT inhibitors was determined. While the inhibitors used efficiently inhibited their respective probe (82-99% inhibition – see bolded valued in **Table 2.2**), there was also significant cross-inhibition, ranging from 2 – 75% (see **Table 2.2**). For example, sulfaphenazole (10 μM) inhibited CYP3A4-mediated 6β-OH-TES formation by 28 ± 12% while itraconazole (2 μM) inhibited CYP2C9-mediated 4-OH-DCL formation by 44 ± 12%. Omeprazole (30 μM) showed the highest degree of cross-inhibition (range 27 – 75%) while quinidine (1 μM) showed the least degree of cross-inhibition (range -33 – 13%).

There was severe cross-inhibition by the UGT selective inhibitors (**Table 2.3**). Fluconazole (2 mM) inhibited UGT1A9-mediated formation of PPF-gluc by 27 ± 14% while niflumic acid (2.5 μM) inhibited UGT2B7-mediated formation of NLX-3-gluc by 49 ± 33%.

Table 2.2. Fractional cross-inhibition of P450 enzymes by P450-selective inhibitors in HLMs

Inhibitor	Selective Probe			
	4-OH-DCL CYP2C9	6β-OH-TES CYP3A	4-OH-MEP CYP2C19	DXO CYP2D6
Sulfaphenazole (10 μM)	**0.99 ± 0.00**	0.28 ± 0.12	0.02 ± 0.07	0.18 ± 0.17
Itraconazole (2 μM)	0.44 ± 0.12	**0.98 ± 0.00**	0.13 ± 0.07	0.27 ± 0.18
Omeprazole (30 μM)	0.75 ± 0.01	0.68 ± 0.07	**0.82 ± 0.07**	0.27 ± 0.16
Quinidine (1 μM)	0.13 ± 0.05	0.12 ± 0.19	-0.33 ± 0.26	**0.90 ± 0.03**

Bolded values represent the fractional inhibition of enzymes by their corresponding selective inhibitor. Data shown are mean ± SD of three independent experiments with each experiment conducted in triplicate.

Table 2.3. Fractional cross-inhibition of UGT enzymes by UGT-selective inhibitors in HLMs

Inhibitor	Selective Probe	
	NLX-3-gluc UGT2B7	PPF-gluc UGT1A9
Fluconazole (2 mM)	**0.65 ± 0.19**	0.27 ± 0.14
Niflumic acid (2.5 μM)	0.49 ± 0.33	**0.89 ± 0.02**

Bolded values represent the fractional inhibition of enzymes by their corresponding selective inhibitor. Data shown are mean ± SD of three independent experiments with each experiment conducted in triplicate.

2.4.4. Adjusted cannabinoid fm values

Using a previously established methodology described by Njuguna et al., 2016, the fm values determined using selective inhibitors (unadjusted) in **Table 2.1** were adjusted for their P450 and UGT inhibitor cross-inhibition shown in **Table 2.2** and **Table 2.3**, respectively, using **Eq. 6**. **Table 2.4** shows the adjusted fm values and SD using error propagation via stochastic simulation. CYP2C9 and CYP2D6 were the major and minor (fm = 0.82 ± 0.08, 0.17 ± 0.15, respectively) DMEs responsible for THC depletion. CYP2C9 was the major DME that formed 11-OH-THC (fm = 0.99 ± 0.10); however, there was a minor contribution from CYP2C19 and CYP2D6 (fm = 0.07 ± 0.18 and 0.24 ± 0.22, respectively). Of the total UGT depletion of 11-OH-THC, UGT2B7 and UGT1A9 fm values were 0.67 ± 4.14 and 0.33 ± 3.98, respectively. Of the total P450 depletion of 11-OH-THC, CYP3A and CYP2C9 fm values were 0.69 ± 0.28

and 0.31 ± 0.18, respectively. When combining UGT and P450 mediated 11-OH-THC depletion, UGT2B7 was the major DME (fm = 0.45 ± 2.78) followed by CYP3A (fm = 0.20 ± 0.08). The sum of the adjusted fm values approximates 1 for THC and 11-OH-THC depletion, but is larger than 1 for the 11-OH-THC formation (**Figure 2.4**).

Table 2.4. Cannabinoid fm values in HLMs adjusted for inhibitor cross-inhibition

Enzyme	THC depletion	11-OH-THC formation	11-OH-THC depletion
CYP2C9	0.82 ± 0.08	0.99 ± 0.10	0.09 ± 0.05
CYP3A	negligible[a]	negligible[a]	0.20 ± 0.08
CYP2C19	negligible[a]	0.07 ± 0.18	negligible[c]
CYP2D6	0.17 ± 0.15	0.24 ± 0.22	negligible[c]
UGT2B7	negligible[b]	N/A	0.45 ± 2.78
UGT1A9	negligible[b]	N/A	0.22 ± 2.65

Data shown are mean ± SD of fm values from **Table 2.1** adjusted for inhibitor cross-inhibition (P450 enzymes –**Table 2.2.** and UGT enzymes –**Table 2.3**) using **Eq. 6**. [a] fm values are set to negligible because the adjusted fm result was negative (THC depletion fm: CYP3A = -0.12 ± 0.16, CYP2C19 = -0.53 ± 0.19; 11-OH-THC formation fm: CYP3A = -0.48 ± 0.19). [b] no observed depletion of THC by UGT enzymes. [c] no significant inhibition of 11-OH-THC depletion observed in the presence of omeprazole and quinidine. N/A – not applicable since UGT enzymes did not form 11-OH-THC.

2.5. DISCUSSION

The aims of this work were to 1) investigate the recombinant enzymes that can metabolize THC and 11-OH-THC and 2) use this information as a guide to quantify the fm of the relevant maternal hepatic enzymes at concentrations of THC and 11-OH-THC observed after smoking cannabis. The mechanistic data generated represents the first set of drug-dependent parameters necessary to build a linked THC/11-OH-THC PBPK model to prospectively predict maternal-fetal cannabinoid exposure during pregnancy.

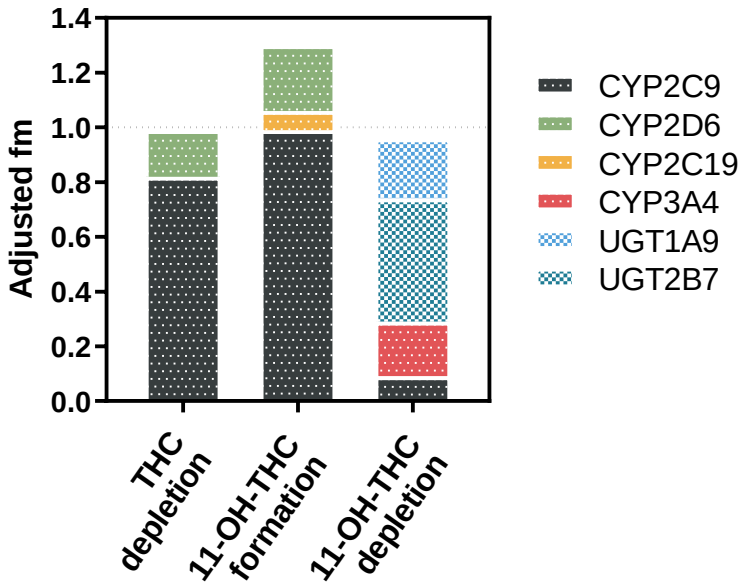

Figure 2.4. Final hepatic enzyme contributions to THC and 11-OH-THC disposition. The sum of fm values for THC and 11-OH-THC depletion after cross-inhibition adjustment is close to 1 but the sum for 11-OH-THC formation is greater than 1 (likely due to error propagation caused by the cross-inhibition adjustment). Data shown are mean fm values after cross-inhibition adjustment (**Eq. 6**,**Table 2.4**). Of note, while the UGT2B7 and UGT1A9 fm values were estimated with poor confidence (see **Table 2.4**) due to severe cross-inhibition of the selective inhibitors, the total UGT contribution (fm = 0.60 ± 0.05) was estimated with confidence. Clinical data supports our fm estimates. For example, CYP2C9 fm for THC depletion must be at least 0.66 since there was a 3-fold increase in THC AUC in CYP2C9 polymorphic subjects after oral administration of THC (Sachse-Seeboth et al., 2009). Further discussion can be found in text.

THC is metabolized to more than 40 metabolites (Agurell et al., 1986). Standards for most of these metabolites are not readily available, therefore, to elucidate the enzymes important in the disposition of THC and the 11-OH-THC, one needs to conduct substrate depletion studies as well as monitor the formation of 11-OH-THC from THC. Furthermore, to capture enzyme contributions that are clinically relevant, the concentration of substrate chosen in depletion experiments needs to be representative of those observed in vivo. After smoking a cannabis cigarette containing 9.8%, 16.4%, and 23.1% weight/weight THC, the maximum THC plasma concentrations (C_{max}) values were 430 nM, 645 nM, and 735 nM while the 11-OH-THC C_{max} values were 28 nM, 50 nM, and 48 nM, respectively (Hunault et al., 2008). The average THC potency was 12% in 2014 (ElSohly et al., 2016). Therefore, the chosen 500 nM THC and 50 nM 11-OH-THC reflect plasma concentrations after smoking cannabis of contemporary potency. Furthermore, the chosen THC concentration was lower than the estimated K_m for

THC depletion of 3.76 ± 1.28 μM (Benito-Gallo et al., 2016) and the estimated K_m for 11-OH-THC formation of 0.80 ± 0.12 μM (Bland et al., 2005).

Our reaction phenotyping studies with recombinant enzymes generated novel data that CYP1A1, 1A2, 3A5, and 3A7 depleted THC but of these enzymes, only CYP1A2 formed 11-OH-THC. Our data corroborates previous reports that found CYP2C9, 2C19, 2D6, and 3A4 are important in the metabolism of THC (Watanabe et al., 2007). Interestingly, the THC depletion clearance of CYP1A1 was higher than CYP2C9, the major DME of THC (**Figure 2.1A**). While the contribution of CYP1A1 is negligible in the liver, CYP1A1, the major DME in the lung (Zhang et al., 2006), may be important for cannabinoid lung disposition. There is no current direct evidence of lung cannabinoid metabolism in human, however, biotransformation of THC to 11-OH-THC is observed in rat lung homogenate and dog and guinea pig perfused lung (Nakazawa and Costa, 1971; Widman et al., 1975; Halldin et al., 1984). Since metabolism of THC by the human lung may be an important drug parameter in the cannabinoid PBPK, further studies need to be conducted to establish the contribution of lung metabolism to THC disposition, especially if CYP1A1 is induced by smoking cannabis.

Maternal THC exposure drives fetal THC exposure. Therefore, we used the recombinant enzyme data to guide reaction phenotyping studies of hepatic enzymes that are responsible for the maternal hepatic clearance of THC. Our data corroborates previous studies that demonstrate CYP2C9 is the major DME responsible for THC metabolism in HLMs (Bornheim et al., 1992; Bland et al., 2005; Watanabe et al., 2007). We adjusted the apparent fm determined via selective inhibitors (**Table 2.1**) with the inhibitor cross-inhibition (**Table 2.2** and **Table 2.3**). This was to account for potential overestimation of fm values when the inhibitor selectivity is not optimum. After adjusting for inhibitor cross-inhibition, CYP2C9 was the main DME responsible for THC depletion (fm = 0.82 ± 0.08) with the remaining contribution from CYP2D6 (**Table 2.4**). While there was turnover of THC by CYP3A4 and CYP2C19 in recombinant enzymes, as well as significant inhibition by itraconazole and omeprazole (22 ± 5% and 13 ± 11%, respectively), this inhibition was primarily due to cross-inhibition of CYP2C9 (44 ± 12% and 75 ± 1%, respectively, **Table 2.2).** It should be noted that due to error propagation, there is less confidence when estimating small fm values, such as those for CYP2D6, 3A4, and 2C19.

The formation fm of enzymes responsible for the formation of 11-OH-THC, the main and active metabolite of THC, were reflective of THC enzyme contributions. After adjusting for inhibitor cross-inhibition, CYP2C9 was the main DME responsible for 11-OH-THC formation (fm = 0.99 ± 0.10) with minor contributions from CYP2D6 and CYP2C19. The sum of the 11-OH-THC formation fm values was greater than 1 (**Figure 2.4**). This may be due to the error propagation during fm adjustment, particularly for the smaller fm values for CYP2D6 and CYP2C19.

Reaction phenotyping studies were extended to include the depletion of 11-OH-THC. All the P450 enzymes that metabolized THC also turned over 11-OH-THC except for CYP1A2 and CYP3A7. Like THC, recombinant CYP1A1 had the largest 11-OH-THC depletion clearance (**Figure 2.1C**). A previous extensive screen using recombinant UGT enzymes found that only UGT1A9 and UGT1A10 are relevant to the formation of 11-OH-THC-glucuronide (Mazur et al., 2009b). As such, we verified the 11-OH-THC depletion by UGT1A9 and UGT1A10, and we additionally included UGT1A4, an enzyme that is inducible during pregnancy (Anderson, 2005; Ke et al., 2014b), and UGT2B7, the major UGT expressed in the liver (Achour et al., 2014). We tested 11-OH-THC depletion at protein concentrations five times higher for UGT1A10 compared to UGT1A9 because in the previous study by Mazur et al., 2009, the clearance of 11-OH-THC (V_{max}/K_m) by UGT1A9 was approximately five-fold higher than UGT1A10. Even so, we did not observe significant depletion of 11-OH-THC by UGT1A10. Unlike the previous report, we observed depletion of 11-OH-THC by UGT2B7. In HLMs, UGT enzymes depleted 11-OH-THC at a greater extent than P450 enzymes (fm = 0.60 ± 0.05 vs. 0.40 ± 0.05). In contrast to THC, CYP3A has a larger contribution to 11-OH-THC depletion than CYP2C9 (fm 0.20 ± 0.08 vs. 0.09 ± 0.05) (**Table 2.4**). Furthermore, the reaction phenotyping studies in HLMs identified UGT2B7 as the major DME (fm = 0.45 ± 2.78). It should be noted that there was significant cross-inhibition of the UGT selective inhibitors (**Table 2.3**). Because of this, there was a large uncertainty associated with the adjusted UGT2B7 and UGT1A9 fm values (**Table 2.4**). Selective inhibitors of UGTs are needed to better define these fm values. As such, the total UGT contribution (fm = 0.60 ± 0.05) rather than the individual UGT fm values should be used for PBPK M & S.

Clinical data further confirms that CYP2C9 and CYP3A4 are major contributors in the disposition of THC and 11-OH-THC. After oral administration of 15 mg THC in *CYP2C9*3/*3* homozygotes, which confers decreased CYP2C9 function, there is a three-fold increase in THC $AUC_{(0\text{-}inf)}$ and no change in 11-OH-THC $AUC_{(0\text{-}inf)}$ when compared to wild-type (Sachse-Seeboth et al., 2009). CYP2C9 inhibition leads to an increase in the combined THC/11-OH-THC exposure because CYP2C9 forms and depletes 11-OH-THC. When a oromucosal spray containing 10.8 mg THC/10 mg CBD is co-administered with ketoconazole (CYP3A inhibitor), the THC and 11-OH-THC $AUC_{(0\text{-}inf)}$ is increased 1.84 and 3.62-fold, respectively (Stott et al., 2013). CYP3A THC fm in the liver is insignificant but may be significant in the gut where expression of CYP3A is much greater than CYP2C9. As such, the THC drug-drug interaction with ketoconazole may be due to pre-systemic interactions. Unlike inhibition of CYP2C9, inhibition of CYP3A4 significantly increases 11-OH-THC AUC because CYP3A4 depletes but does not form 11-OH-THC. In both examples, the inhibition of CYP2C9 and CYP3A4 led to changes in the pharmacodynamic effect (increased sedation and euphoric mood). Because 11-OH-THC is equally or even more potent than THC (Perez-Reyes et al., 1972), the combined exposure of THC/11-OH-THC needs to be considered when establishing cannabinoid dose-risk relationship during pregnancy.

The reported cannabinoid metabolic profiling can be extrapolated to pregnant women. During pregnancy, CYP3A4 and CYP2C9 mediated clearance is increased 2 and 1.6-fold, respectively, UGT2B7 activity does not change, and UGT1A9 changes are unknown (Anderson, 2005; Ke et al., 2014b). The changes to DME expression and activity during pregnancy are likely to increase THC clearance and 11-OH-THC formation/clearance. The fetal-to-maternal (F/M) concentration ratio of THC in chronic cannabis users ranged from 0.16 – 0.38 (Blackard and Tennes, 1984). Because the F/M ratio is less than 1, there may be extraction of cannabinoids by the placenta or the fetal liver or both. As such, placental CYP1A1, UGT2B7, and fetal CYP3A7 may limit fetal exposure of THC and 11-OH-THC. Of particular interest is the contribution of placental CYP1A1 to cannabinoid fetal exposure since cannabis tar induces CYP1A1 mRNA (Roth et al., 2001). Studies need to be conducted with placental microsomes/S9 fractions to elucidate the contribution of placental metabolism of THC/11-OH-THC in fetal exposure to these drugs (see **Chapter 5**).

The relevant hepatic enzymes and the corresponding fm values have been established for THC and 11-OH-THC. CYP2C9 is the most important DME for THC depletion and formation of 11-OH-THC, while UGT enzymes represent the major pathway of 11-OH-THC depletion (**Figure 2.4**). In **Chapter 3**, the kinetics (CL_{int}, V_{max}, and K_m) of the main enzymatic pathways, as determined in this **Chapter** via recombinant enzymes and fm in pooled HLMs, are quantified. The mechanistic information presented in **Chapters 2** and **3** is necessary to build a THC/11-OH-THC PBPK model in nonpregnant women (see **Chapter 4**) that then can be used to predict cannabinoid exposure during pregnancy (see **Chapter 5**). Studies need to be conducted to determine the contribution of other enzymes in lungs or the placenta in the clearance of THC/11-OH-THC. In addition, to build a PBPK model of these cannabinoids after oral administration of THC, studies to determine the contribution of intestinal enzymes in the first pass metabolism of THC/11-OH-THC will need to be conducted. However, the goal of this project is to predict THC/11-OH-THC exposure after intravenous administration and inhalation, and as such, the aforementioned studies remain to be conducted.

2.6. SUPPLEMENTAL INFORMATION

Supplementary Table 2.1. LC flow gradient

Time (min)	Water + 0.1% formic acid (%)	Acetonitrile + 0.1% formic acid (%)	Flow rate (ml/min)
Cannabinoid studies			
Initial	40	60	0.3
0.5	40	60	0.3
3.8	5	95	0.3
4.3	5	95	0.3
4.7	40	60	0.3
6.0	40	60	0.3
CYP probes cocktail			
Initial	95	5	0.6
1.0	95	5	0.6
2.0	5	95	0.6
2.5	5	95	0.6
2.6	95	5	0.6
3.2	95	5	0.6
UGT probes cocktail			
Initial	97	3	0.3
1.0	97	3	0.3
4.5	5	95	0.3
5.5	5	95	0.3
5.7	97	3	0.3
7.0	97	3	0.3

Supplementary Table 2.2. MS/MS parameters

Analyte	Parent Ion (*m/z*)	Product Ion (*m/z*)	DP (eV)	CE (V)
Cannabinoid studies				
THC	315.2	193.3	100	33
		123.2	100	45
11-OH-THC	331.4	313.4	150	21
		193.3	150	35
COOH-THC	345.3	327.3	150	23
		299.3	150	27
THC-D3 (IS)	318.3	196.3	100	33
		123.3	100	45
11-OH-THC-D3 (IS)	334.4	316.3	150	21
		196.3	150	35
COOH-THC-D3 (IS)	348.3	330.3	150	23
		302.3	150	27
CYP probe cocktail				
4-OH-Diclofenac	312.0	231.0	40	27
6β-OH-Testosterone	305.3	269.1	90	30
4-OH-mephenytoin	235.0	150.1	45	24
Dextrorphan	258.1	157.0	95	47
Tolbutamide (IS)	271.3	155.0	70	25
UGT probe cocktail				
Naloxone-3-glucuronide	504.0	310.0	70	30
		212.0	70	55
		253.0	70	44
Propofol-glucuronide	353.0	177.0	-70	-30
		113.0	-70	-30
Androsterone-glucuronide (IS)	449.1	255.2	70	25
		273.2	70	30
	467.3	255.2	70	35

IS – internal standard. The first listed transitions were used for quantification

Chapter 3. Quantifying hepatic kinetics of THC and its psychoactive metabolite, 11-OH-THC, through in vitro modeling

The work presented in this chapter has been submitted

to

Drug Metabolism and Disposition

3.1. ABSTRACT

Fetal exposure to the psychoactive cannabinoids in cannabis, THC and its active hydroxy metabolite, 11-OH-THC, may lead to negative fetal outcomes. Physiologically-based pharmacokinetic (PBPK) modeling can predict maternal-fetal exposure of cannabinoids, thus bypassing logistical and ethical hurdles associated with conducting clinical studies during pregnancy. To build a maternal-fetal cannabinoid PBPK model, mechanistic information, such as the drug-metabolizing enzymes (DMEs), fraction metabolized (fm), and kinetic parameters (CL_{int}, V_{max} and K_m) of cannabinoid hepatic metabolism are necessary. We previously identified and quantified the fm's of DMEs involved in hepatic depletion of THC and 11-OH-THC (**Chapter 2**). Here, we extend this work to characterize the enzyme kinetics of THC and 11-OH-THC by monitoring their depletion and formation of some of their metabolites in pooled human liver microsomes. A P450 and UGT kinetic model was fitted to the concentration-time depletion/formation profiles to establish the contribution and kinetics of the individual DME pathways. CYP2C9 pathway was the major pathway for depletion of THC and formation of 11-OH-THC (fm = 0.91, $K_{m,u}$ = 2.91 nM). The remaining THC depletion pathway was attributed to CYP2D6. 11-OH-THC was depleted by UGTs (fm = 0.67 and $K_{m,u}$ = 39.0 nM), CYP3A4 (fm = 0.18, $K_{m,u}$ =824 nM) and CYP2C9 (fm = 0.15, $K_{m,u}$ = 32.7 nM). Our data predict that the disposition of THC will be nonlinear at the higher doses of THC. These mechanistic data will be used to predict THC/11-OH-THC exposure during pregnancy via PBPK modeling and simulation.

3.2. INTRODUCTION

The prevalence of cannabis use during pregnancy is increasing (Brown et al., 2017; SAMHSA, 2017). Studies on fetal risks from cannabis use during pregnancy can be inconclusive or contradictory because many studies rely on self-report of cannabis use and are confounded by factors such as use of other drugs of abuse (e.g. tobacco) and socioeconomic factors (Gunn et al., 2016). When adjusted for tobacco use, clinical, and socioeconomic factors as well as objective assessment of maternal cannabis use, Metz et al., found that such use is associated with increased neonatal morbidity (Metz et al., 2017). While the causative factors for this morbidity are unknown, through animal studies, the psychoactive components of cannabis, THC and its psychoactive metabolite, 11-OH-THC (**Figure 1.2**), have been

found to cause fetal toxicity (Paria et al., 1998; Wang et al., 2006; Tortoriello et al., 2014; Grant et al., 2017). Therefore, fetal risks from maternal cannabis use will depend on the extent of fetal exposure to these cannabinoids. Determining maternal-fetal THC/11-OH-THC exposure, in humans, at different gestational ages is impossible due to ethical concerns and logistical hurdles. Therefore, an alternative is to predict gestational-age dependent maternal and fetal cannabinoid exposure through modeling such as physiologically-based pharmacokinetic modeling and simulation (PBPK M&S).

PBPK M&S requires mechanistic (e.g. drug metabolizing enzymes (DME) involved) and quantitative information (e.g. CL_{int} and fraction metabolized (fm) via an enzyme) on the disposition of the cannabinoids. Once such information is available, the PK of cannabinoids in nonpregnant women can be extrapolated to that in pregnant women by adjusting for pregnancy-induced physiological changes, such as induction or repression of DMEs, plasma protein binding, and body (e.g. fat) composition (Anderson, 2005; Ke et al., 2014b). Then, the predicted maternal cannabinoid plasma concentrations can be used to predict fetal plasma concentrations, as we have successfully done for a variety of drugs (Zhang et al., 2017a; Zhang and Unadkat, 2017).

The adult hepatic enzymes important in THC and 11-OH-THC disposition and the fraction metabolized (fm) via these enzymes at physiologically relevant concentrations of 500 nM and 50 nM, respectively were identified in **Chapter 2** (Patilea-Vrana et al., 2018). For successful PBPK M&S of maternal concentrations of THC/11-OH-THC at varying doses of THC, the kinetics (i.e. V_{max}, K_m, CL_{int}) of these nonlinear processes need to be well characterized. The formation of 11-OH-THC (Bornheim et al., 1992) and depletion of THC (Benito-Gallo et al., 2016) in HLMs have been previously reported. However, the aforementioned reports did not correct for the extensive nonspecific binding of THC and 11-OH-THC to glassware and plasticware (Garrett and Hunt, 1974). Hence, the reported K~~m~~ and CL_{int} values may not to be reliable (Obach, 1997). Therefore, the aims of **Chapter 3** were to 1) determine the depletion and formation kinetics (V_{max}, K_m, CL_{int}) of THC and 11-OH-THC using pooled HLMs that are corrected for nonspecific binding of these highly lipophilic drugs (logP of 6.97 and 5.33 for THC and 11-OH-THC, respectively (Thomas et al., 1990)) and 2) fit a P450 and UGT kinetic model to the in vitro concentration-time profiles to estimate the kinetic parameters via specific enzymatic pathway. The second aim of

Chapter 3 was guided by results from **Chapter 2**, where the most important DMEs of THC/11-OH-THC were identified, that is CYP2C9, CYP3A4 and UTG enzymes, and their fm was quantified (Patilea-Vrana et al., 2018). The mechanistic kinetic parameters generated in **Chapter 2** and **3** are then extrapolated to in vivo and used to predict, through PBPK M&S, in vivo maternal exposure to THC/11-OH-THC after consumption of cannabis of varying THC content (see **Chapter 4**). Then, the predicted maternal THC/11-OH-THC exposure can be used to predict fetal exposure (**Chapter 5**) which can help establish fetal exposure-risk relationship for the cannabinoids.

3.3. MATERIALS AND METHODS

3.3.1. Chemicals and reagents.

(-)-Δ^9-THC (1 mg/ml), (±) 11-OH-THC (0.1 mg/ml), and (±) 11-nor-9-carboxy-Δ^9-THC (COOH-THC) (0.1 mg/ml) DEA-exempt methanol stocks and deuterated internal standards [IS; (-)-Δ^9-THC-D3, (±) 11-OH-THC-D3, (±) COOH-THC-D3] were purchased from Cerilliant (Round Rock, TX). (-)-Δ^9-THC (50 mg/ml) was purchased from Cayman Chemicals (Ann Arbor, MI). Micro ultracentrifuge (UC) polycarbonate tubes and Dulbecco's phosphate-buffered saline (DPBS) were purchased from Thermo Scientific (Asheville, NC). Low-binding (LB) microcentrifuge tubes (made of chemical-resistant polypropylene), bovine serum albumin (BSA) (Fraction V - heat-shock treated), acetonitrile, and formic acid (liquid chromatography-mass spectrometry (LC/MS) grade) were purchased from Fisher Scientific (Hampton, NH). β-nicotinamide adenine dinucleotide phosphate (NADP+), D-glucose 6-phosphate (G6P), glucose-6-phosphate dehydrogenase (G6PDH), uridine 5'-diphosphoglucuronic acid (UDPGA), itraconazole, and sulfaphenazole, were purchased from Sigma-Aldrich (St. Louis, MO). Milli-Q water was used in all preparations. All other chemicals and reagents were obtained at the highest quality available commercially.

3.3.2. Biological materials.

Pooled adult HLMs (n=50, equal mixed gender) were purchased from Corning (Corning, NY). Frozen human plasma from a single healthy donor was purchased from Bloodworks (Seattle, WA).

3.3.3. Cannabinoid HLM incubations.

For P450-mediated depletion, reaction mixtures (500 µL final volume) in LB tubes contained either 1) 0.010 – 14.3 µM THC and 0.02 mg/ml HLM or 2) 0.013 – 60 µM 11-OH-THC and 0.1 mg/ml HLM in 0.1 M potassium phosphate buffer (pH 7.4) containing 0.2% BSA. In a separate set of experiments, 0.02 – 2 µM THC or 0.5 – 5 µM 11-OH-THC was incubated in the presence and absence of 10 µM sulfaphenazole (CYP2C9 selective inhibitor) and 2 µM itraconazole (CYP3A selective inhibitor) as described above. The THC and 11-OH-THC concentration range differed in the presence vs. absence of inhibitors because the former was limited to the nonlinear concentration range. Reactions mixtures were pre-incubated at 37°C for 10 minutes in a heated shaking block to allow for protein and nonspecific binding. P450-mediated depletion was initiated with a NADPH regenerating system (final concentrations: 1.3 mM NADP+, 3.3 mM G6P, 3.3 mM MgCl2, 0.4 unit/ml G6PDH). For UGT-mediated depletion, the mixtures contained 0.013 – 60 µM 11-OH-THC, 0.1 mg/ml HLM, 5 mM MgCl2, and 25 µg/ml alamethicin. Reactions mixtures were incubated for 15 minutes on ice to allow for pore formation then pre-incubated as described above. UGT-mediated depletion was initiated with 2.5 mM UDPGA. The incubation period for each cannabinoid concentration was optimized to achieve ~75% substrate depletion in order to minimize errors associated with estimation of kinetic parameters (V_{max} and K_m) when using the substrate depletion approach (Nath and Atkins, 2006). As such, the lowest and highest cannabinoid concentrations had up to 4- and 90-minute incubation period, respectively. At designated time points, depletion of the cannabinoids was stopped by taking a 50 µL aliquot of the reaction mixture and adding it to 100 µL ice-cold acetonitrile containing the IS (THC-D3, 11-OH-THC-D3, COOH-THC-D3) in LB tubes. Samples were centrifuged for 5 minutes at 10,000 x g, the supernatant was removed, and placed at -20°C for >1 hour to separate organic and aqueous phases. The top organic layer was added to LC glass inserts and stored at -20°C until analysis by LC-MS/MS. Four independent experiments for THC depletion and three independent experiments for 11-OH-THC depletion, each with duplicate determinations, were performed.

3.3.4. Incubation protein binding.

Microsomal binding of THC and 11-OH-THC at C_{max} concentrations observed after smoking cannabis of contemporary THC content (Hunault et al., 2014) was measured using the tube adsorption method as previously described (Ishigam et al., 2001; Isoherranen et al., 2004). Briefly, in LB tubes, 500

nM or 50 nM 11-OH-THC were incubated in either 0.1 M potassium phosphate buffer (group 1) or buffer containing 0.2% BSA and 0.02 or 0.1 mg/ml HLM for THC and 11-OH-THC, respectively (group 2). Mixtures were incubated for 20 minutes at 37°C with shaking to allow for protein and nonspecific binding, then either 100 µL of ice-cold acetonitrile containing IS was added to 50 µL of mixture (subgroup A) or 50 µL aliquot of mixture was removed and added to 100 µL ice-cold acetonitrile containing IS (subgroup B). Samples were centrifuged and processed for LC-MS/MS as described above. We assumed that addition of acetonitrile to the mixture solution desorbs and solubilizes all cannabinoid adsorbed to LB tubes. As such, in group 1 (buffer only) and group 2 (buffer + BSA + HLM), C1A and C2A are the concentration of total unbound cannabinoid in buffer or total bound and unbound cannabinoid in the presence of proteins after desorption from the LB tube surface, respectively. C1B and C2B are the concentration of total unbound cannabinoid in buffer or total bound and unbound cannabinoid in the presence of proteins after adsorption to LB tube surface, respectively. The partition ratio, R, of unbound cannabinoid in buffer to LB surface wall was calculated using **Eq. 7**.

$$R = \frac{C1_B}{C1_A - C1_B} \tag{7}$$

The unbound concentration of cannabinoid in incubation mixtures containing protein (fu_{inc}) was calculated using **Eq. 8**. Four independent experiments with four to six replicates per group were performed.

$$fu_{inc} = R * \left(\frac{C2_A - C2_B}{C2_B} \right) \tag{8}$$

3.3.5. Plasma protein binding.

Although attempts were made to measure the plasma protein binding of THC and 11-OH-THC using the tube adsorption method, their high plasma protein binding made it difficult to quantify the fraction adsorbed to the LB tubes in the presence of plasma proteins. Therefore, as an alternative, ultracentrifugation was used to measure THC and 11-OH-THC plasma protein binding. Diluted plasma (10-fold dilution with DPBS) was incubated with 500 nM THC or 50 nM 11-OH-THC in ultracentrifugation

tubes (150 µL final volume) for 20 minutes at 37°C with shaking to allow for protein and nonspecific binding. Samples were centrifuged using Sorval Discovery M150 SE centrifuge and S100-AT3 rotor (Thermo Scientific) at 435,000 x g for 90 minutes at 37°C. The middle aqueous layer was sampled to obtain the unbound cannabinoid concentration. The total bound and unbound cannabinoid concentration was sampled from control incubations that were incubated similarly but not centrifuged. The fraction unbound in plasma (fu_p) was extrapolated using **Eq. 9** (Schuhmacher et al., 2000), where fu_d is the fraction unbound in diluted plasma and plasma DF is the dilution factor of 0.1.

$$fu_p = \frac{DF * fu_d}{1 - fu_d * (1 - DF)} \tag{9}$$

3.3.6. LC-MS/MS analysis.

Acquity UPLC BEH C18 column (1.7 µM 2.1 x 50 mm) attached to C18 x 2mm guard column was used for chromatographic separation. Samples were analyzed with Acquity ultra-performance liquid chromatography (UPLC) system (Waters Corporation, Milford, MA) coupled to an AB Sciex Triple Quad 6500 (SCIEX, Framingham, MA). Acetonitrile or water containing 0.1% formic acid was used as organic and aqueous mobile phases, respectively. LC flow gradient and multiple reaction monitoring parameters used were as previously described (Patilea-Vrana et al., 2018). Integration of the chromatographic peaks was performed using Analyst v1.6 (Framingham, MA).

3.3.7. Data analyses using substrate depletion and metabolite formation approach.

The depletion rate constant, k_{dep}, at different concentrations of THC and 11-OH-THC was obtained by fitting a monoexponential decay curve (**Eq. 10**) to the THC or 11-OH-THC concentration-time curves where C_t is the substrate concentration at a given timepoint (t) and C_0 is the substrate concentration at t = 0.

$$\frac{C_t}{C_0} = e^{-k_{dep}t} \tag{10}$$

Using the substrate depletion approach (Nath and Atkins, 2006), $k_{dep([S]\rightarrow 0)}$, the depletion rate constant at infinitesimal substrate concentrations, and K_m, the Michaelis-Menten constant, was obtained by fitting **Eq. 11** to k_{dep} versus THC or 11-OH-THC concentrations [S]. V_{max}, the maximal reaction rate, was obtained using **Eq. 12** where [HLM] is the HLM concentration in mg/ml.

$$k_{dep} = k_{dep\ S\rightarrow 0}\left(1-\frac{S}{K_M+S}\right) \tag{11}$$

$$V_{max} = \frac{k_{dep\ S\rightarrow 0}\ ^*K_m}{HLM} \tag{12}$$

Formation kinetic parameters (V_{max} and K_m) of 11-OH-THC were obtained by fitting the Michaelis-Menten relationship (**Eq. 13**) to the 11-OH-THC formation rate (V) versus THC concentration [S].

$$V = \frac{Vmax * S}{K_M + S} \tag{13}$$

A substrate inhibition model was used to fit COOH-THC formation rate (V) versus 11-OH-THC concentration [S] as shown in **Eq. 14**.

$$V = \frac{Vmax * S}{K_M + S * \left(1+\frac{S}{K_i}\right)} \tag{14}$$

The total depletion or formation intrinsic clearance (CL_{int}) was calculated using **Eq. 15**.

$$CL_{int} = \frac{V_{max}}{fu_{inc} * K_m} \tag{15}$$

Data was analyzed using GraphPad Prism 7 (La Jolla, CA).

3.3.8. Modeling of in vitro data.

A P450 kinetic model was built to estimate the P450-mediated kinetics of THC, 11-OH-THC, and COOH-THC and a UGT kinetic model was built to estimate the UGT-mediated depletion of 11-OH-THC. We previously showed that CYP2C9 and CYP2D6 deplete THC with fm of 0.82 ± 0.08 and 0.17 ± 0.15,

respectively, and CYP2C9 forms 11-OH-THC with fm = 0.99 ± 0.10. CYP2C9, CYP3A4, and UGTs (UGT1A9 and UGT2B7) deplete 11-OH-THC with fm of 0.09 ± 0.05, 0.20 ± 0.08, and 0.60 ± 0.05, respectively (Patilea-Vrana et al., 2018). Using the previous data as a guide, the P450 kinetic model was set up as follows: the biotransformation of THC to 11-OH-THC was assigned to CYP2C9 with the remaining THC depletion pathway assigned to CYP2D6. The biotransformation of 11-OH-THC to COOH-THC was assigned to CYP2C9 with two additional 11-OH-THC depletion pathways mediated by CYP2C9 and CYP3A4. We assumed that COOH-THC formation and the additional 11-OH-THC CYP2C9 depletion pathway had the same K_m value. Additionally, based on our previous observations, we assumed COOH-THC was not depleted in the HLM system. While we tested the activity of ALDH enzymes to turn over 11-OH-THC in cytosolic and S9 fractions, we saw minimal depletion (data not shown), and as such, restricted the 11-OH-THC depletion model to P450 and UGT enzymes only.

We chose selective inhibitors of CYP2C9 (sulfaphenazole) and CYP3A (itraconazole) to elucidate the fm and enzyme kinetic parameters (CL_{int}, K_m, V_{max}) via each pathway. Since these inhibitors are not entirely selective, their previously determined inhibition of CYP2C9, CYP3A4, and CYP2D6 (Patilea-Vrana et al., 2018) was incorporated into the P450 kinetic model. We assumed both sulfaphenazole and itraconazole were competitive inhibitors of the P450 enzymes. The UGT kinetic model was not split into specific pathways because we previously were unable to establish UGT1A9 and UGT2B7 fm with confidence due to poor selectivity of UGT inhibitors.

A P450 or UGT kinetic model was fitted to the in vitro concentration-time profiles of THC and 11-OH-THC in the presence and absence of sulfaphenazole and itraconazole. The P450 kinetic model was fitted to COOH-THC concentration-time profile only in the absence of inhibitors since we did not thoroughly establish the identify and fm of DMEs responsible for COOH-THC formation, as done for 11-OH-THC. Since *CYP2C9*3/*3* subjects had a 3.2-fold lower COOH-THC $AUC_{(0\text{-}inf)}$ compared to wild-type subjects with no significant change in 11-OH-THC AUC (Sachse-Seeboth et al., 2009), we attributed biotransformation of COOH-THC to CYP2C9 pathway. We used a naïve pooled approach implemented in Phoenix® 8.1, Certara (Princeton, NJ) to model the in vitro data since the biological source in all experiments was the same pool of HLMs. The general ordinary differential equations (ODE's) are shown

below (**Eq. 16-20**), where INH_{P450} enzyme represents the fractional inhibition of enzyme activity by sulfaphenazole and itraconazole as previously measured using P450 enzyme probes (Patilea-Vrana et al., 2018). The governing ODE's are further explained in **Section 3.6 SUPPLEMENTARY INFORMATION**.

$$V_{THC}\frac{dC_{THC\_dep}}{dt}=-\left(\frac{Vmax_{11\text{–}OH\text{–}THC_{CYP2C9}}*C_{THC}}{Km_{11\text{–}OH\text{–}THC_{CYP2C9}}*\left(\frac{1}{1-INH_{CYP2C9}}\right)+C_{THC}}+\frac{Vmax_{THC_{CYP2D6}}*C_{THC}}{Km_{THC_{CYP2D6}}*\left(\frac{1}{1-INH_{CYP2D6}}\right)+C_{THC}}\right) \quad (16)$$

$$\begin{aligned}V_{THC}\frac{dC_{11\text{–}OH\text{–}THC\_form}}{dt}=&\frac{Vmax_{11\text{–}OH\text{–}THC_{CYP2C9}}*C_{THC}}{Km_{11\text{–}OH\text{–}THC_{CYP2C9}}*\left(\frac{1}{1-INH_{CYP2C9}}\right)+C_{THC}}\\&-\left(\frac{Vmax_{11\text{–}OH\text{–}THC\_dep_{CYP3A}}*C_{11\text{–}OH\text{–}THC}}{Km_{11\text{–}OH\text{–}THC\_dep_{CYP3A}}*\left(\frac{1}{1-INH_{CYP3A}}\right)+C_{11\text{–}OH\text{–}THC}}\right)\\&-\left(\frac{Vmax_{11\text{–}OH\text{–}THC\_dep_{CYP2C9}}*C_{11\text{–}OH\text{–}THC}}{Km_{11\text{–}OH\text{–}THC\_dep_{CYP2C9}}*\left(\frac{1}{1-INH_{CYP2C9}}\right)+C_{11\text{–}OH\text{–}THC}}\right)\\&-\left(\frac{Vmax_{COOH\text{–}THC_{CYP2C9}}*C_{11\text{–}OH\text{–}THC}}{Km_{11\text{–}OH\text{–}THC\_dep_{CYP2C9}}*\left(\frac{1}{1-INH_{CYP2C9}}\right)+C_{11\text{–}OH\text{–}THC}}\right)\end{aligned} \quad (17)$$

$$\begin{aligned}V_{11\text{–}OH\text{–}THC}\frac{dC_{11\text{–}OH\text{–}THC\_dep}}{dt}=&-\left(\frac{Vmax_{11\text{–}OH\text{–}THC\_dep_{CYP3A}}*C_{11\text{–}OH\text{–}THC}}{Km_{11\text{–}OH\text{–}THC\_dep_{CYP3A}}*\left(\frac{1}{1-INH_{CYP3A}}\right)+C_{11\text{–}OH\text{–}THC}}\right)\\&-\left(\frac{Vmax_{11\text{–}OH\text{–}THC\_dep_{CYP2C9}}*C_{11\text{–}OH\text{–}THC}}{Km_{11\text{–}OH\text{–}THC\_dep_{CYP2C9}}*\left(\frac{1}{1-INH_{CYP2C9}}\right)+C_{11\text{–}OH\text{–}THC}}\right)\\&-\left(\frac{Vmax_{COOH\text{–}THC_{CYP2C9}}*C_{11\text{–}OH\text{–}THC}}{Km_{11\text{–}OH\text{–}THC\_dep_{CYP2C9}}*\left(\frac{1}{1-INH_{CYP2C9}}\right)+C_{11\text{–}OH\text{–}THC}}\right)\end{aligned} \quad (18)$$

$$V_{11\text{–}OH\text{–}THC}\frac{dC_{COOH\text{–}THC}}{dt}=\frac{Vmax_{COOH\text{–}THC_{CYP2C9}}*C_{11\text{–}OH\text{–}THC}}{Km_{11\text{–}OH\text{–}THC\_dep_{CYP2C9}}+C_{11\text{–}OH\text{–}THC}} \quad (19)$$

$$V_{11\text{–}OH\text{–}THC}\frac{dC_{11\text{–}OH\text{–}THC\_dep\_UGTs}}{dt}=-\frac{Vmax_{11\text{–}OH\text{–}THC\_dep_{UGTs}}*C_{11\text{–}OH\text{–}THC}}{Km_{11\text{–}OH\text{–}THC\_dep_{UGTs}}+C_{11\text{–}OH\text{–}THC}} \quad (20)$$

Since THC and 11-OH-THC incubations used different HLM concentrations (0.02 mg/ml and 0.1 mg/ml, respectively), V_{THC} and $V_{11\text{-}OH\text{-}THC}$ were normalized by HLM concentration used, namely 0.05 L/mg and 0.01 L/mg, respectively. The normalized volume (L/mg) was multiplied by the starting cannabinoid concentrations (μM) to derive the respective cannabinoid incubation dose (in μmol/mg). For the P450 kinetic model, the datasets of when THC was dosed (THC depletion and 11-OH-THC formation concentration-time profiles) were simultaneously fitted with the datasets of when 11-OH-THC was dosed (11-OH-THC depletion and COOH-THC formation concentration-time profiles). This simultaneous fitting approach allowed for parameter estimation of 11-OH-THC formation and depletion kinetic parameters. When fitting the models to the data, the kinetic parameters from **Table 3.2** were used as initial estimates (obtained as described under the preceding section). Various structural and error models were tested. Model performance was tested via goodness-of-fit and residual plots. Model validation was performed using Montel-Carlo simulations using the final P450 kinetic model and an independent dataset not used during model development.

3.4. RESULTS

3.4.1. Nonspecific, HLM incubation, and plasma protein binding of THC and 11-OH-THC

In the absence and presence of proteins (HLM and BSA), >85% and >90% of THC (500 nM) and 11-OH-THC (50 nM) was bound to the surface of the LB tubes and proteins, respectively (**Table 3.1**). The fraction of THC and 11-OH-THC unbound in plasma (fu_p) was similar but lower than the cannabinoids' corresponding fu_{inc} (**Table 3.1**).

Table 3.1. Non-specific, HLM incubation, and plasma protein binding of THC and 11-OH-THC

Cannabinoid	$f_{adsorbed}$[a]	fu_{inc}[b]	fu_p[c]

THC	0.927 ± 0.041	0.040 ± 0.015	0.011 ± 0.001
11-OH-THC	0.864 ± 0.049	0.061 ± 0.025	0.012 ± 0.002

[a] – The fraction of THC or 11-OH-THC non-specifically bound to the LB tube surface in buffer was calculated using R, the LB surface partition ratio (**Eq. 7**) as $f_{adsorbed} = 1-R/(R+1)$. [b] – Tube adsorption method was used to measure fraction unbound in incubations (fu_{inc}) of THC (500 nM) and 11-OH-THC (50 nM) in the presence of 0.2% BSA and 0.02 or 0.1 mg/ml HLM for THC and 11-OH-THC, respectively. [c] – Ultracentrifugation with diluted plasma was used to measure plasma protein binding (fup) of THC (500 nM) and 11-OH-THC (50 nM). Data shown are mean ± SD of three independent experiments with four – six replicates per experiment.

3.4.2. Estimates of THC, 11-OH-THC, and COOH-THC depletion and formation kinetics using substrate depletion and metabolite formation approach

The kinetic profiles THC/11-OH-THC depletion and 11-OH-THC/COOH-THC formation in pooled HLMs are shown in **Figure 3.1**. Kinetic parameter estimated using substrate depletion and metabolite formation in the presence and absence of sulfaphenazole and itraconazole are shown in **Table 3.2**. While $K_{m,u}$ of THC depletion and 11-OH-THC formation were nearly identical (7.37 ± 4.91 nM and 7.54 ± 3.19 nM, respectively), the THC depletion V_{max} was ~4-fold larger than V_{max} for the formation of 11-OH-THC (**Table 3.2**). Based on the mean CL_{int} values, 26% of THC was metabolized to 11-OH-THC (**Table 3.2**, **Figure 3.1A-B**). Formation of COOH-THC was not detected in the aforementioned experiments. Per average, THC depletion and 11-OH-THC formation CL_{int} decreased 88% and 92% in the presence of sulfaphenazole, respectively (**Table 3.2**, **Figure 3.2A-B**).

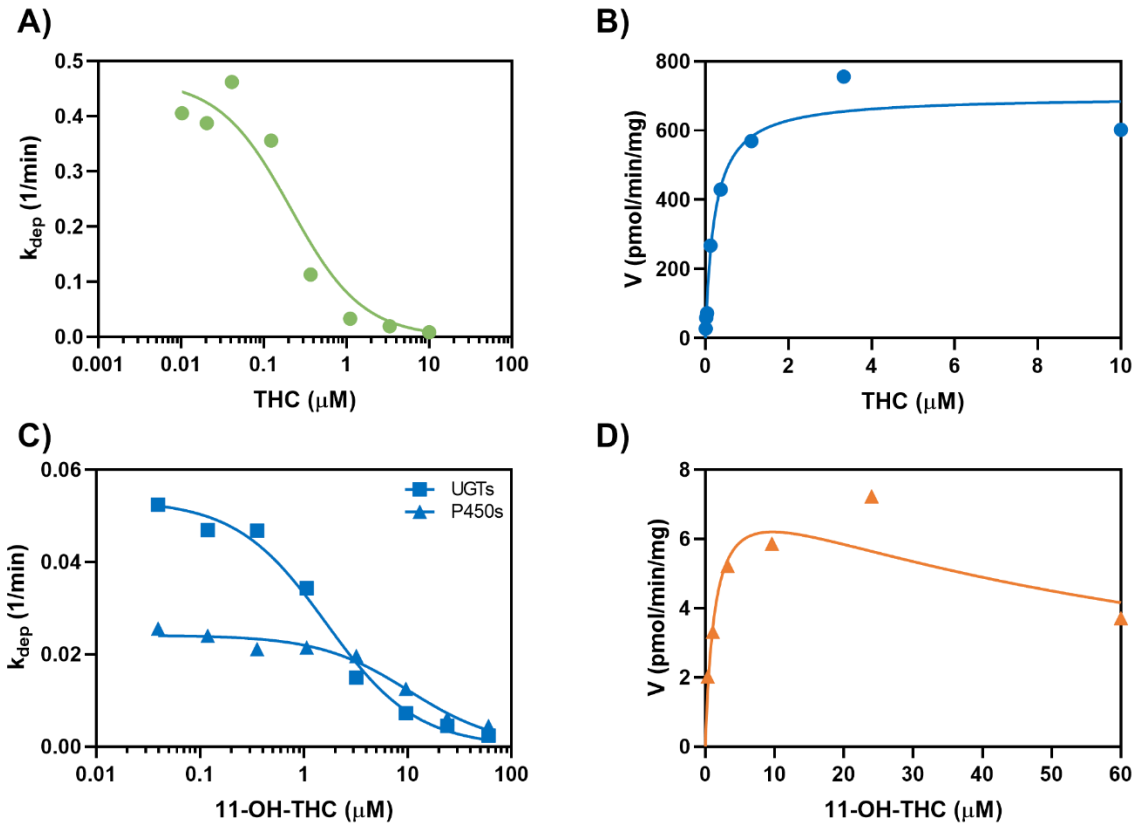

Figure 3.1. In vitro cannabinoid kinetic profiles

Representative kinetic profiles cannabinoid kinetics of A) THC depletion, B) 11-OH-THC formation, C) 11-OH-THC depletion by UGT and P450 enzymes, and D) COOH-THC formation in pooled HLMs from one (of three to four) independent experiments, each with duplicate determinations. Depletion rate-constant (k_{dep}) and formation rate (V) were obtained from cannabinoid concentration-time profiles (see **Supplementary Figure 3.1** for representative profiles). Substrate depletion (**Eq. 11**) and metabolite formation (**Eq. 13**) were used to determine kinetic parameters (V_{max} and K_m). A substrate inhibition model (**Eq. 14**) was used to model COOH-THC formation kinetics. Kinetic parameters estimated from these data were used as initial estimates for the subsequent modeling of cannabinoid depletion and formation kinetics using the P450 and UGT kinetics models shown in **Figure 3.3**.

UGT enzymes had a higher affinity (K_m) but lower capacity (V_{max}) whereas the P450 enzymes had a lower affinity but higher capacity for 11-OH-THC depletion (**Table 3.2**, **Figure 3.1C**). Furthermore, the CL_{int} of UGT enzymes was ~ 2-fold larger than CL_{int} of P450 enzymes (**Table 3.2**). Substrate inhibition (estimated by K_i) of COOH-THC formation was observed at >10 μM 11-OH-THC concentrations (**Figure 3.1D**). Based on the mean CL_{int} values, COOH-THC formation accounted for 2.1% of P450-mediated depletion of 11-OH-THC (**Table 3.2**). Per average, 11-OH-THC P450 depletion CL_{int} decreased 34% and 53% in the presence of sulfaphenazole and itraconazole, respectively (**Figure 3.2C**). Per average, COOH-THC

formation CL_{int} decreased 93% in the presence of sulfaphenazole but was not affected by itraconazole (**Table 3.2**, **Figure 3.2D**).

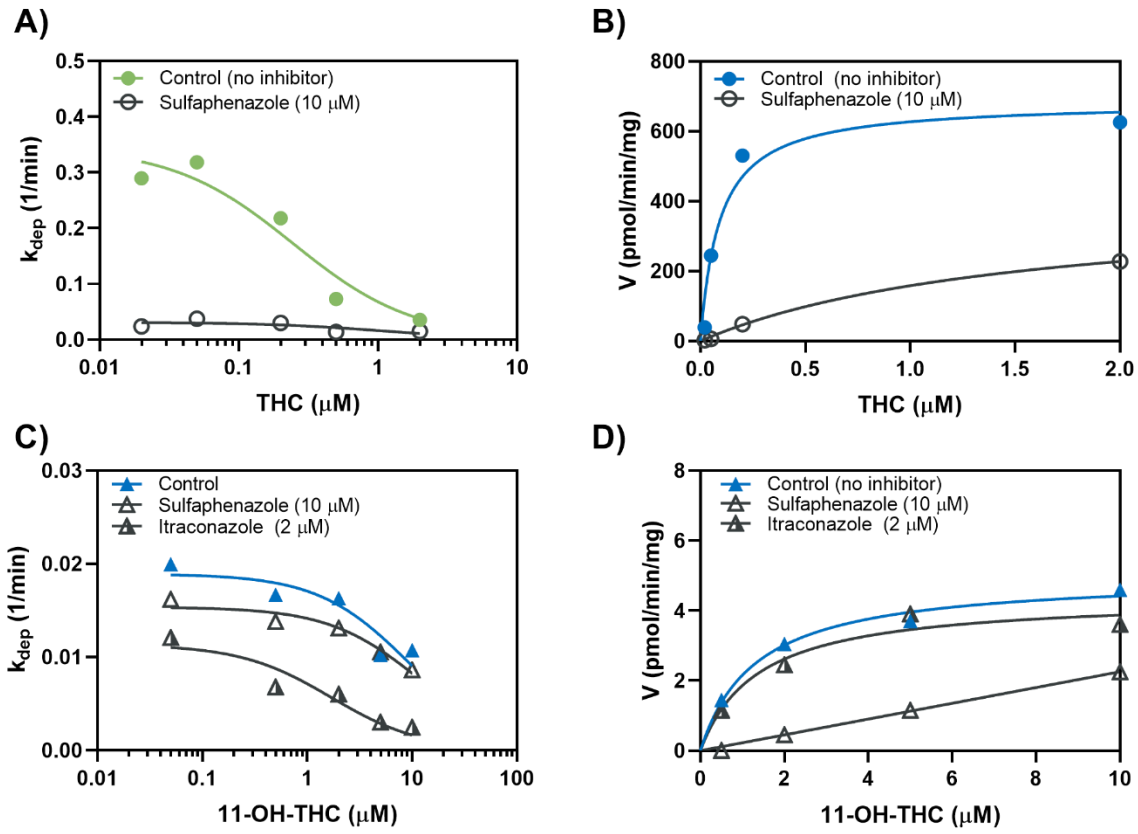

Figure 3.2. Impact of CYP2C9 and CYP3A4 inhibition on cannabinoid kinetic profiles
Representative kinetic profiles of A) THC depletion, B) 11-OH-THC formation, C) 11-OH-THC depletion by P450 enzymes, and D) COOH-THC formation in the presence and absence of sulfaphenazole (CYP2C9 inhibitor) and itraconazole (CYP3A inhibitor) from one (of three) independent experiments, each with duplicate determinations. Inhibition studies were performed over a range of cannabinoid concentrations that spanned the nonlinear kinetic range (see **Figure 3.1**). Substrate depletion (**Eq. 11**) and metabolite formation (**Eq. 13**) were used to determine kinetic parameters (V_{max} and K_m). Representative concentration-time curves are shown in **Supplementary Figure 3.2**.

Table 3.2. Kinetic parameters quantified using the traditional substrate depletion and metabolite formation approach in pooled HLMs

Pathway	Inhibitor	V_{max} pmol/min/mg	K_m[a] µM	$K_{m,u}$[b] nM	CL_{int} ml/min/mg
THC depletion	None	3150 ± 1310	0.18 ± 0.10	7.37 ± 4.91	435 ± 217
	Sulfaphenazole (10 µM)	1064 ± 580	0.57 ± 0.47	24.1 ± 21.3	50.9 ± 22.2
11-OH-THC formation	None	803 ± 162	0.18 ± 0.05	7.54 ± 3.19	111 ± 48.8
	Sulfaphenazole (10 µM)	515 ± 136	1.42 ± 0.13	60.0 ± 21.2	8.66 ± 2.88
11-OH-THC depletion (P450s)	None	2550 ± 107	11.0 ± 0.58	669 ± 296	3.82 ± 1.68
	Sulfaphenazole (10 µM)	1701 ± 96.0	10.5 ± 1.07	679 ± 242	2.52 ± 0.88
	Itraconazole (2 µM)	194 ± 111	1.74 ± 1.09	112 ± 79.8	1.79 ± 0.63
COOH-THC formation	None	7.95 ± 0.60	1.51 ± 0.34c	91.8 ± 45.3	0.088 ± 0.041
	Sulfaphenazole (10 µM)	n.d.	n.d.	n.d.	0.006 ± 0.003d
	Itraconazole (2 µM)	4.57 ± 0.97	0.98 ± 0.55	63.3 ± 41.5	0.094 ± 0.068
11-OH-THC depletion (UGTs)	None	910 ± 99.0	1.87 ± 0.24	114 ± 52.0	8.11 ± 3.85

[a] – not adjusted for incubation binding (fu_{inc}); [b] – adjusted for incubation binding (fu_{inc}); [c] – COOH-THC formation was fitted using a substrate inhibition model (**Eq. 14**) K^i was 52.1 ± 14.3 µM; [d] – CL_{int} was determined from the linear slope of [11-OH-THC] vs. velocity of COOH-THC formation; n.d. – not determined. Inhibition by sulfaphenazole did not lead to saturation of COOH-THC formation and as such, V_{max} and Km could not be determined. Data shown are mean ± SD of three to four independent experiments with duplicate determinations per experiment. Error propagation was applied to the standard deviation of $K_{m,u}$ and CL_{int} using $s_z = \bar{z}\sqrt{\left(\frac{s_x}{\bar{x}}\right)^2 + \left(\frac{s_y}{\bar{y}}\right)^2}$ where $\bar{x} \pm s_x$ and $\bar{y} \pm s_y$ represents the mean ± SD of fu_{inc} and K_m or $CL_{int,u}$, respectively. The values shown here were used as initial estimates for the P450 and UGT kinetic model (**Figure 3.3**).

3.4.3. Quantifying enzyme kinetics of THC/11-OH-THC using the P450 and UGT kinetic models

Based on kinetic parameters in **Table 3.2**. the formation of metabolites (11-OH-THC and COOH-THC) do not completely account for the depletion of their respective parent compounds (THC and 11-OH-THC). Furthermore, phenotyping data detailed in **Chapter 2** demonstrate that multiple DMEs are involved in the disposition of these cannabinoids. That is, the depletion kinetics of THC and 11-OH-THC in **Table 3.2** represent aggregated kinetics of multiple enzymatic pathways and multiple metabolites formed. In order to tease out the metabolic kinetics via specific enzymatic pathways, we formulated the P450 and UGT kinetic models (**Figure 3.3**) using previous data on the identity and fm of the DMEs responsible for the disposition of THC and 11-OH-THC as shown in **Chapter 2** (Patilea-Vrana et al., 2018).

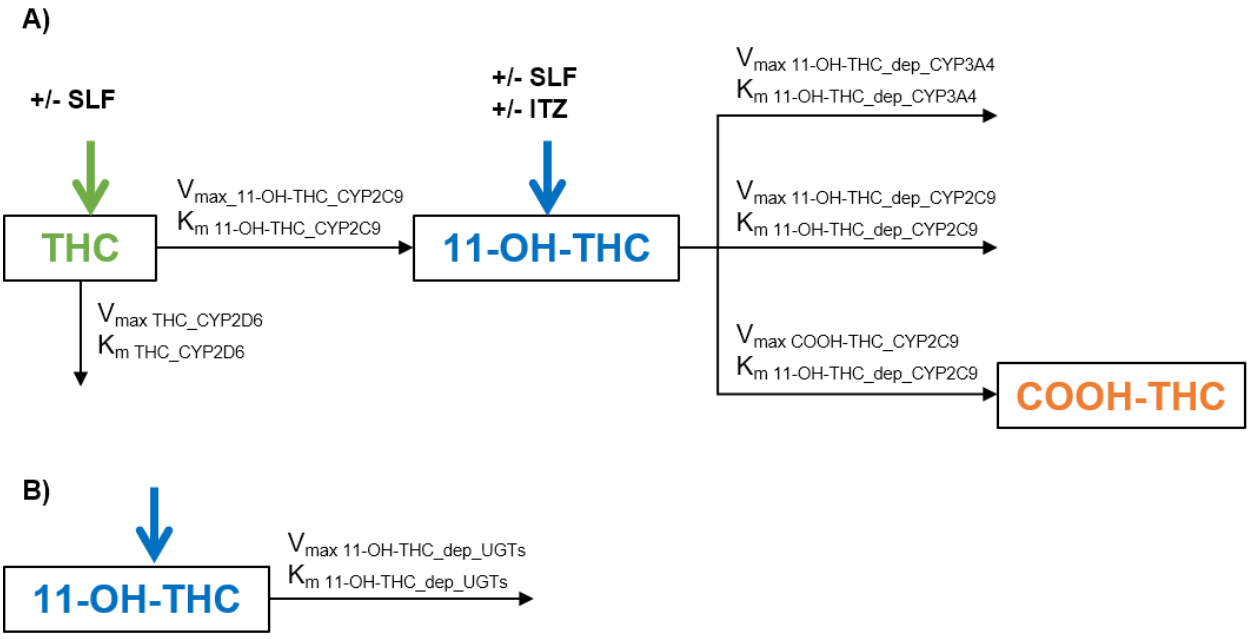

Figure 3.3. In vitro (P450 and UGT) kinetic models.
The A) P450 kinetic model was developed to account for individual depletion (dep) or formation P450 pathways using previous data that identified the enzymes and their respective fm values that are relevant to THC and 11-OH-THC disposition in pooled HLMs as described in **Chapter 2**, **Table 2.4**. The UGT kinetic model was not split up to account for individual UGT pathways due to lack of selective UGT inhibitors (see **Chapter 2**). The P450 and UGT kinetic models were fitted to the concentration-time profiles of THC, 11-OH-THC, and COOH-THC after incubation with either THC (green arrow) or 11-OH-THC (blue arrow) in the absence of presence of sulfaphenazole (SLF, CYP2C9 inhibitor) and itraconazole (ITZ, CYP3A inhibitor). Kinetic models were fit to data from three to four independent experiments. Kinetic parameters from **Table 3.2** were used as initial estimates. Description of the governing ordinary differential equations can be found in **Section 3.6 SUPPLEMENTARY INFORMATION**.

We used the data from **Table 3.2** as initial estimates in the kinetic P450 and UGT kinetic models. While COOH-THC showed substrate inhibition at 11-OH-THC concentrations greater than 10 μM (**Figure 3.1D**, **Table 3.2**), including substrate inhibition in the model did not have a significant decrease in the -2LL or AIC values (data not shown). Therefore, COOH-THC formation was modeled without substrate inhibition. Because the identity and fm of DME's responsible for COOH-THC formation are not relevant to the depletion kinetics of THC and 11-OH-THC, they were not characterized. Thus, only the formation of COOH-THC in the absence of inhibitors was modeled. The absence of COOH-THC concentration-time data did not affect 11-OH-THC parameter estimation in the presence of inhibitors since formation of COOH-THC accounted for only a small percentage of 11-OH-THC depletion (data not shown).

Goodness-of-fit plots of the P450 and UGT kinetic models show good fit to the observed concentration-time profiles of THC depletion, 11-OH-THC formation/depletion, and COOH-THC formation (**Figure 3.4**). Furthermore, the observed vs. predicted concentrations closely follow the line of unity (**Supplementary Figure 3.3**).

The final parameter estimates and CV% of the estimates from the P450 and UGT kinetic models are summarized in **Table 3.3** and **Figure 3.5**. Final fm estimates using the CL_{int} estimates from the P450 and UGT kinetic models are summarized in **Table 3.4**. The overall THC depletion CL_{int} was 236 ml/min/mg with 11-OH-THC formation (CL_{int} = 214 ml/min/mg) by CYP2C9 accounting for 91% of THC depletion. CYP2D6 mediated the remaining 9% of THC depletion. To note, since CYP2D6 is highly polymorphic enzyme, the CYP2D6 fm would decrease in CYP2D6 poor metabolizers while CYP2C9 fm would approach 1. THC affinity ($K_{m,u}$) for CYP2C9 was 79-fold larger than that for CYP2D6. The final CL_{int} parameter estimates for THC depletion and 11-OH-THC formation are ~2-fold smaller and larger, respectively, when compared to the kinetic parameters estimated using substrate depletion and metabolite formation approach in **Table 3.2**.

The overall 11-OH-THC depletion CL_{int} was 12.9 ml/min/mg. P450 and UGT enzymes accounted for 23% and 67% of total 11-OH-THC depletion CL_{int}, respectively. 11-OH-THC $K_{m,u}$ for CYP2C9 was lower than that for CYP3A4 (32.7 nM vs. 824 nM). Nevertheless, due to the difference in V_{max} value of the enzymes, CYP2C9 and CYP3A4 contribution to the total P450-mediated 11-OH-THC depletion was 45%

and 55%, respectively. COOH-THC formation accounted for 3.7% of overall 11-OH-THC P450-mediated depletion. The final CL_{int} parameter estimates for 11-OH-THC depletion are comparable to the kinetic parameters estimated using substrate depletion approach in **Table 3.2**. Furthermore, the fm values estimated using in vitro modeling are comparable to adjusted fm measured using selective inhibitors as shown in **Chapter 2**, **Table 2.4**.

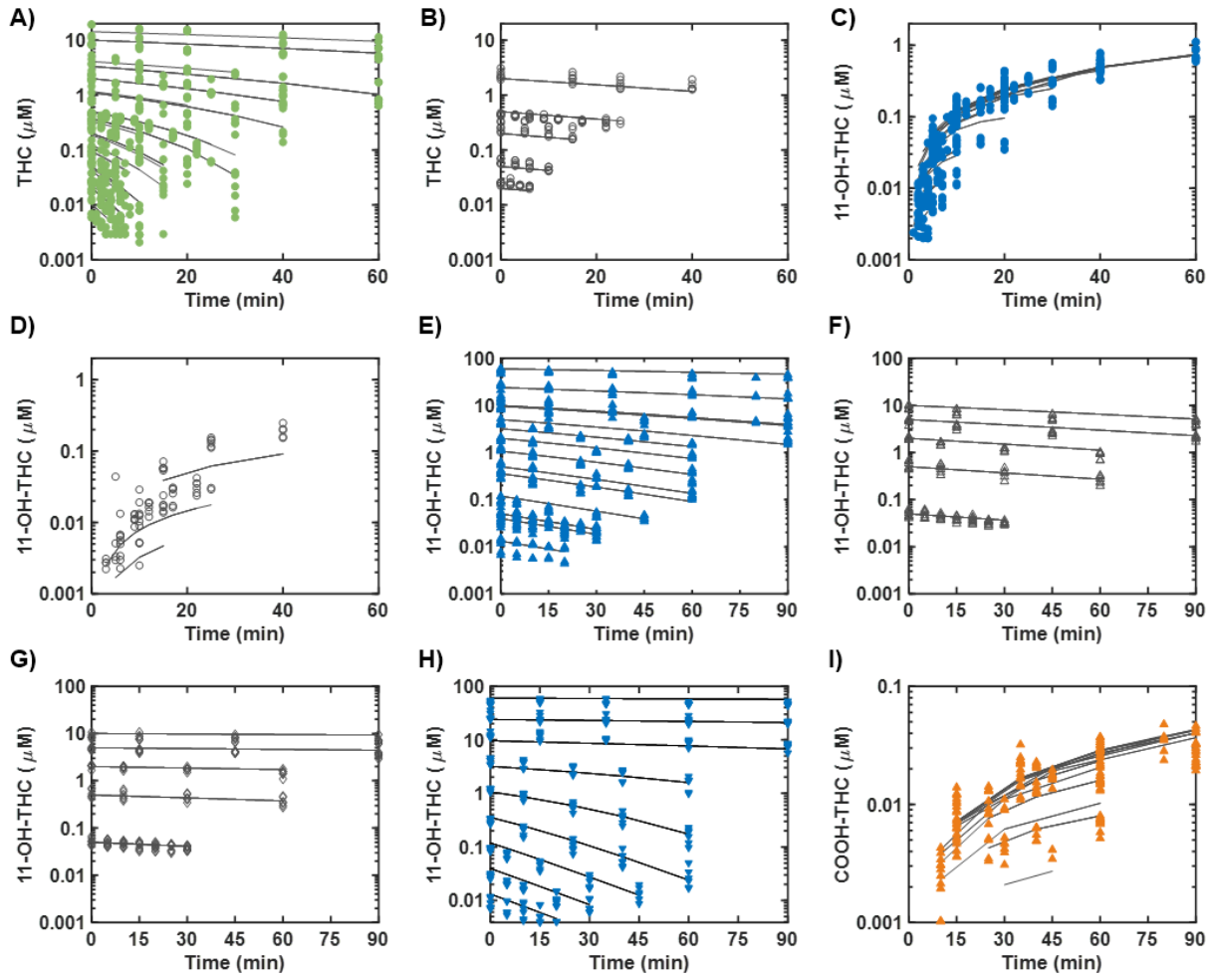

Figure 3.4. Goodness-of-fit plot of in vitro kinetic models.
Observed (dots) and model fit (lines) of in vitro concentration-time profiles of THC in the A) absence and B) presence of sulfaphenazole, 11-OH-THC formation in the C) absence and D) presence of sulfaphenazole, 11-OH-THC depletion by P450 enzymes in the E) absence and presence of F) sulfaphenazole and G) itraconazole, H) 11-OH-THC depletion by UGT enzymes and I) and COOH-THC formation in the absence of inhibitors. Each line represents a different incubation concentration of THC or 11-OH-THC. Additional goodness-of-fit graphs are shown in **Supplementary Figure 3.3**.

The P450 kinetic model was validated using an independent data set and Monte-Carlo simulations (**Supplementary Figure 3.4**). Using the final P450 kinetic model parameter estimates, ten individual Monte-Carlo simulations of THC concentration-time profiles were generated and compared with observed data from an independent incubation of 500 nM THC with HLMs. The simulations were in good agreement with the observed data (**Supplementary Figure 3.4**).

Table 3.3. **Kinetic parameters estimate and CV% using in vitro kinetic modeling**

Pathway	**Enzyme(s)**	**V_{max} pmol/min/mg**	**K_m µM**	**$K_{m,u}$ nM**	**CL_{int} ml/min/mg**
THC depletion[a]	P450s	—	—	—	236 (48%)
11-OH-THC formation	CYP2C9	624 (1.5%)	0.07 (3.6%)	2.91 (36%)	214 (34%)
Unknown[b]	CYP2D6	4905 (17%)	5.48 (20%)	231 (44%)	21.3 (34%)
11-OH-THC depletion[a]	P450s/UGTs	—	—	—	12.9 (26%)
COOH-THC formation	CYP2C9	4.83 (1.7%)	0.50 (3.7%)	32.7 (44%)	0.15 (34%)
Unknown[b]	CYP2C9	54.4 (5.6%)	0.50 (3.7%)	32.7 (44%)	1.70 (34%)
Unknown[b]	CYP3A	1826 (6.3%)	12.8 (8.1%)	824 (59%)	2.21 (34%)
Unknown[b]	UGT2B7/1A9	343 (3.7%)	0.64 (4.4%)	39.0 (44%)	8.80 (44%)

[a] Depletion of THC or 11-OH-THC signifies total (aggregated) depletion and is reported as the sum of the CL_{int} values of the various enzymatic pathways. [b] Metabolite formed not-measured. The P450 and UGT kinetic models were fitted to data from three to four independent experiments (see **Section 3.3 METHODS** and for description of the kinetic models). Kinetic parameters shown in **Table 3.2** were used as initial estimates. Data shown are parameter estimate and the confidence in these estimates (CV%). $K_{m,u}$ and CL_{int} parameter estimates and CV% were corrected for incubation binding using fu_{inc} (**Table 3.1**).

Table 3.4. **Fractional metabolism (fm) estimated using the in vitro kinetic models**

Enzyme	**THC depletion**	**11-OH-THC formation**	**11-OH-THC depletion**
CYP2C9	0.91 (0.4%)	1 (fixed)	0.15 (3.6%)
CYP3A	0 (fixed)	0 (fixed)	0.18 (3.0%)
CYP2D6	0.09 (4.4%)	0 (fixed)	0 (fixed)
UGTs	0 (fixed)	0 (fixed)	0.67 (12%)

fm values were calculated using CL_{int} values (see **Table 3.3**). Data shown are parameter estimates and CV% of the estimates.

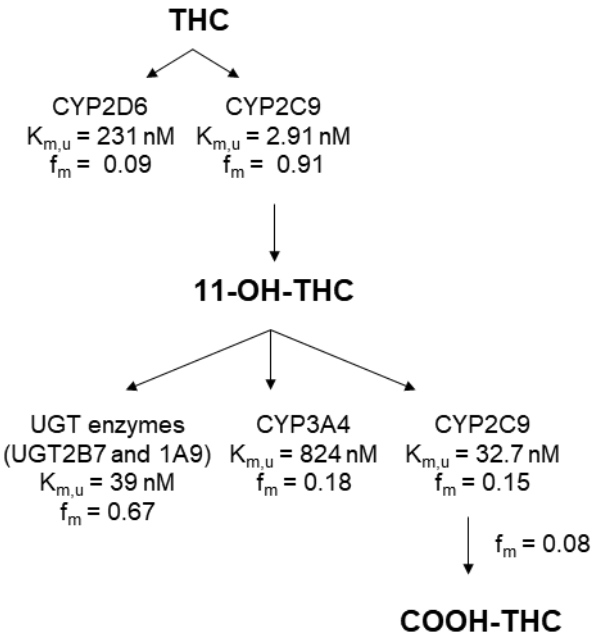

Figure 3.5. Enzymatic pathways and kinetics of THC, 11-OH-THC, and COOH-THC in HLMs.

3.5. DISCUSSION

We previously identified that CYP2C9 is the most relevant P450 enzyme to the depletion and formation of THC and 11-OH-THC, respectively, while UGT enzymes, CYP3A4, and CYP2C9 are the most relevant DMEs to the depletion of 11-OH-THC (Patilea-Vrana et al., 2018). However, we previously determined cannabinoid fm values using maximum plasma concentrations (C_{max}) observed after smoking cannabis, i.e. 500 nM THC and 50 nM 11-OH-THC (Hunault et al., 2014). Since THC concentrations quickly decline after inhalation C_{max} has been reached, it is necessary to elucidate the enzyme kinetics that drive cannabinoid disposition at various concentrations. Here, we extend our previous work detailed in **Chapter 2** and provide kinetic parameter estimates (V_{max}, K_m, CL_{int}) of the relevant enzymatic pathways responsible for THC and 11-OH-THC disposition. These parameters, in addition to estimates of plasma protein binding (fu_p), provide the hepatic metabolism parameters necessary to eventually predict cannabinoid exposure during pregnancy via PBPK M & S (see **Chapter 4**).

We quantified the metabolic kinetics of THC and 11-OH-THC using the substrate depletion and metabolite formation approach in pooled HLMs (**Figure 3.1**). However, the depletion approach cannot

account for nonlinearity in the concentration-time profile when fitting the data using a monoexponential decay curve (usual practice) nor can the metabolite formation approach account for subsequent metabolite depletion. Furthermore, since THC and 11-OH-THC are metabolized by multiple enzymes, the metabolic kinetics are representative of total, or aggregated, enzyme kinetics. To accurately estimate the relevant kinetic parameters, we fitted a sequential P450 and UGT kinetic model simultaneously to THC depletion, 11-OH-THC formation, and 11-OH-THC depletion concentration-time profiles using a naïve-pooled approach (**Figure 3.3**)**.** The modeling approach improved parameter estimate by accounting for the aforementioned limitations. For example, based off CL_{int} values in **Table 3.2**, 11-OH-THC formation accounted for 26% of THC depletion, however, CL_{int} estimates using the P450 model in **Table 3.3** estimate that 91% of THC is metabolized to 11-OH-THC. Indeed, previous studies has shown 11-OH-THC is the major metabolite of THC (Agurell et al., 1986) and furthermore, at THC concentrations less than K_m, 11-OH-THC formation accounted for majority of THC depletion (**Supplementary Table 3.1**). Lastly, previously established cross-inhibition of sulfaphenazole and itraconazole was incorporated into the P450 kinetic model, thus improving the accuracy of the estimated enzyme kinetic parameters.

The microsomal protein binding of drugs in HLM incubations is an important parameter for correctly estimating the vitro K_m and CL_{int} and therefore accurate prediction of in vivo hepatic clearance of THC/11-OH-THC (Obach, 1997). THC and 11-OH-THC are lipophilic compounds with logP of 6.97 and 5.33, respectively (Thomas et al., 1990) and as such, have high microsomal protein and non-specific binding. In the absence of microsomal proteins, THC and 11-OH-THC were extensively (>85%) bound to the LB tubes (**Table 3.1**). Indeed, others have also reported that polycarbonate and polypropylene containers show extensive nonspecific THC binding (up to 80%) (Garrett and Hunt, 1974). Silanized glass can reduce nonspecific binding of drugs, however, we found that the THC depletion kinetics were comparable between silanized glass and LB tubes (data not shown). Therefore, due to ease of use, we adopted to use the LB tubes for all subsequent studies. In our studies, THC and 11-OH-THC fuinc was 0.040 ± 0.015 and 0.061 ± 0.025, respectively (**Table 3.1**). This binding was dependent on BSA concentrations when tested between 0.02 – 2% BSA but independent of the microsomal concentration (0.02 and 0.1 mg/ml) when 0.2% BSA was included (data not shown). Lastly, we measured plasma protein binding at a single concentration of THC (500 nM) and 11-OH-THC (50 nM) because a previous

study reported that this binding is linear across THC concentrations spanning 0.00318 – 3.18 µM (Garrett and Hunt, 1974).

Formation of 11-OH-THC by CYP2C9 (fm = 0.91) accounted for most THC depletion while the remaining depletion pathway (fm = 0.09) was attributed to CYP2D6 (**Table 3.4**). This is consistent with our in vitro results in **Chapter 2** as well as PK studies in CYP2C9 polymorphic subjects (Sachse-Seeboth et al., 2009; Patilea-Vrana et al., 2018). It should be noted that in our previous study, we also saw metabolism of THC by recombinant CYP1A1/2, 2C19, 3A4/5, but the contributions via these enzymes were not significant in HLMs at 500 nM THC (Patilea-Vrana et al., 2018). Metabolites from the minor THC depletion pathway can be due to hydroxylation of THC at the C8 position on the alicyclic ring that forms 8α/β-OH-THC or positions of the pentyl chain (Bornheim et al., 1992; Watanabe et al., 2007; Dinis-Oliveira, 2016). The total (aggregated) THC depletion CL_{int} was 236 ml/min/mg (**Table 3.3**). The depletion K_m and CL_{int} of THC in HLMs has been reported by others to be 3.76 µM and 2.24 ml/min/mg, respectively by Benito-Gallo et al. (Benito-Gallo et al., 2016). The presence of BSA in our study which led to THC fu_{inc} of 0.04 is much smaller than the predicted fu_{inc} by Benito-Gallo et al. of 0.51 and as such, differences in protein binding may contribute to the difference in CL_{int}. The reason for the difference in the CL_{int} estimate is unknown. Formation kinetics of 11-OH-THC were $K_{m,u}$ = 2.91 nM and CL_{int} = 214 ml/min/mg (**Table 3.3**). Bland et al., found that 11-OH-THC formation from THC had an apparent K_m of 0.8 µM (tested at 0.25 – 20 µM THC), however, we cannot compare this value with the $K_{m,u}$ reported here (2.91 nM) since fu_{inc} was not reported in the aforementioned study.

Here, we provide the first report of 11-OH-THC depletion kinetic estimates. Like our previous results in **Chapter 2**, UGT enzymes (fm = 0.67) have a higher contribution to 11-OH-THC depletion compared to P450 enzymes (fm = 0.23). The affinity of CYP2C9 for 11-OH-THC is higher than that for CYP3A4 ($K_{m,u}$ of 32.7 nM vs. 824 nM) but the reverse is true for CL_{int} (CL_{int} of 2.21 vs. 1.70 ml/min/mg) indicating both enzymes will likely play a significant role in the clearance of 11-OH-THC. This conclusion is consistent with two studies. In the first, after oral administration of THC, 11-OH-THC plasma $AUC_{(0\text{-}inf)}$ did not change in *CYP2C9*3/*3* subjects even though THC plasma $AUC_{(0\text{-}inf)}$ increased three-fold, thus indicating that CYP2C9 impacts both the formation and depletion of 11-OH-THC. In the second, 11-OH-

THC plasma $AUC_{(0\text{-}inf)}$ increased 1.84 – fold when Sativex®, an oromucosal spray containing equal part THC and CBD, was co-administered with ketoconazole, a CYP3A inhibitor. COOH-THC accounted for 3.7% of total 11-OH-THC depletion. Other metabolites, such as 8β-11-di-OH-THC may have been formed (Dinis-Oliveira, 2016). Indeed, when 11-OH-THC is administered IV, 80% of the total radiolabeled dose is excreted in feces, mainly as unchanged 11-OH-THC and 8β-11-di-OH-THC (Lemberger et al., 1972a).

The measured THC and 11-OH-THC fu_p (**Table 3.1**) using ultracentrifugation is consistent with previous reports of THC and 11-OH-THC plasma protein binding of <0.01 – 0.03 (Garrett and Hunt, 1974; Widman et al., 1974; Fanali et al., 2011; Benito-Gallo et al., 2016). Adjusting the C_{max} of THC and 11-OH-THC after inhalation or oral administration of cannabis by the fu_p (**Table 3.1**), the THC and 11-OH-THC unbound C_{max} can reach 8.08 nM and 0.60 nM, and 1.82 nM and 0.24 nM for inhalation and oral administration, respectively (Hunault et al., 2008; Lile et al., 2013). This suggests that 11-OH-THC formation may be saturated during smoking but not oral administration because the THC unbound plasma concentration is larger than 11-OH-THC $K_{m,u}$ of 2.91 nM for the former but not latter. However, the observed data on the PK of THC are contradictory. THC and 11-OH-THC C_{max} and $AUC_{0\text{-}8hr}$ did not increase with dose when cannabis cigarettes containing 9.8%, 16.4%, and 23.1% (weight/weight) THC were smoked (Hunault et al., 2008). But, in a similar study design completed by the same group, the THC C_{max} values increased in proportion with dose (Hunault et al., 2014). After intravenous or inhalational administration of THC, the plasma concentration of THC decline extremely rapidly with a half-life of 2.8 min (Hunt and Jones, 1980). Thus, for an unbound THC C_{max} of 8.08 nM, it would take less than 6 min for the unbound THC plasma concentration to drop to < 2.91 nM, the $K_{m,u}$ for the formation of 11-OH-THC. Thus, it is not surprising that it would be difficult to observe nonlinear PK of THC in vivo.

The metabolic parameters generated thus far (fm, CL_{int}, V_{max}, and K_m) will be included in the maternal-fetal PBPK model to predict cannabinoid exposure during pregnancy (see **Chapter 5**). CYP2C9, CYP3A4, and CYP2D6 are induced during pregnancy 1.6 – 2-fold (Anderson, 2005; Ke et al., 2014b), and thus can increase the depletion/formation of THC and 11-OH-THC. Alterations during pregnancy in the concentration of plasma binding proteins may also impact the maternal and thus fetal cannabinoid

clearances. Albumin concentrations decrease however lipoprotein concentration increase with gestational age (Wiznitzer et al., 2009; Ke et al., 2014b). Using zonal ultracentrifugation, 63% of THC was associated to the lipoprotein fraction, primarily to low density lipoprotein (LDL) (Klausner et al., 1975). Thus, the total impact of all the above changes on maternal-fetal exposure to THC/11-OH-THC remains to be determined via PBPK M&S.

In summary, we report the in vitro enzyme kinetics of THC and 11-OH-THC (**Table 3.3**, **Figure 3.5**). THC is mainly metabolized to 11-OH-THC by CYP2C9 with affinity ($K_{m,u}$) that can be lower than unbound plasma concentrations after inhalation but not oral administration of cannabis. While this may lead to saturation of CYP2C9 metabolism in vivo, the fast decline in plasma concentrations due to rapid distribution and clearance likely results in minimal or no observable THC PK nonlinearity in vivo. CYP2C9 and CYP3A both will likely contribute to the clearance of 11-OH-THC in vivo. The mechanistic information provided here was extrapolated to in vivo and used to build and verify a PBPK model of THC and 11-OH-THC disposition in nonpregnant population (see **Chapter 4**). The nonpregnant THC/11-OH-THC model was extrapolated to a pregnant population using the m-f-PBPK model and used to simulate maternal and fetal THC and 11-OH-THC concentrations during pregnancy (**Chapter 5**).

3.6. SUPPLEMENTARY INFORMATION

The cannabinoid HLM concentration-time curves were fitted using the ordinary differential equations (ODE's) shown below (**Supplementary Eq. 21-29**) (see **Figure 3.3).** CTR, SLF, and ITZ subscripts represent the control (no inhibitor), sulfaphenazole, and itraconazole incubations, respectively (see **Supplementary Figure 3.1** and **Supplementary Figure 3.2**).

$$V_{THC}\frac{dC_{THC_{CTR}}}{dt} = -\frac{Vmax_{11-OH-THC_{CYP2C9}} \times C_{THC_{CTR}}}{Km_{11-OH-THC_{CYP2C9}} + C_{THC_{CTR}}} - \frac{Vmax_{THC_{CYP2D6}} \times C_{THC_{CTR}}}{Km_{THC_{CYP2D6}} + C_{THC_{CTR}}} \tag{21}$$

$$V_{THC}\frac{dC_{THC_{SLF}}}{dt} = -\frac{Vmax_{11-OH-THC_{CYP2C9}} \times C_{THC_{SLF}}}{Km_{11-OH-THC_{CYP2C9}} \times \left(\frac{1}{1-SLF_{CYP2C9}}\right) + C_{THC_{SLF}}} - \frac{Vmax_{THC_{CYP2D6}} \times C_{THC_{SLF}}}{Km_{THC_{CYP2D6}} \times \left(\frac{1}{1-SLF_{CYP2D6}}\right) + C_{THC_{SLF}}} \tag{22}$$

$$\begin{aligned} V_{THC}\frac{dC_{11-OH-THC_{CTR}}}{dt} = {} & \frac{Vmax_{11-OH-THC_{CYP2C9}} \times C_{THC_{CTR}}}{Km_{11-OH-THC_{CYP2C9}} + C_{THC_{CTR}}} \\ & - \frac{Vmax_{11-OH-THC_{CYP3A4}} \times C_{11-OH-THC_{CTR}}}{Km_{THC_{CYP3A4}} + C_{11-OH-THC_{CTR}}} \\ & - \frac{Vmax_{11-OH-THC_{CYP2C9}} \times C_{11-OH-THC_{CTR}}}{Km_{11-OH-THC_{CYP2C9}} + C_{11-OH-THC_{CTR}}} \\ & - \frac{Vmax_{COOH-THC_{CYP2C9}} \times C_{11-OH-THC_{CTR}}}{Km_{11-OH-THC_{CYP2C9}} + C_{11-OH-THC_{CTR}}} \end{aligned} \tag{23}$$

$$\begin{aligned} V_{THC}\frac{dC_{11-OH-THC_{SLF}}}{dt} = {} & \frac{Vmax_{11-OH-THC_{CYP2C9}} \times C_{THC_{SLF}}}{Km_{11-OH-THC_{CYP2C9}} \times \left(\frac{1}{1-SLF_{CYP2C9}}\right) + C_{THC_{SLF}}} \\ & - \frac{Vmax_{11-OH-THC_{CYP3A4}} \times C_{11-OH-THC_{SLF}}}{Km_{11-OH-THC_{CYP3A4}} \times \left(\frac{1}{1-SLF_{CYP3A4}}\right) + C_{11-OH-THC_{SLF}}} \\ & - \frac{Vmax_{11-OH-THC_{CYP2C9}} \times C_{11-OH-THC_{SLF}}}{Km_{11-OH-THC_{CYP2C9}} \times \left(\frac{1}{1-SLF_{CYP2C9}}\right) + C_{11-OH-THC_{SLF}}} \\ & - \frac{Vmax_{COOH-THC_{CYP2C9}} \times C_{11-OH-THC_{SLF}}}{Km_{11-OH-THC_{CYP2C9}} \times \left(\frac{1}{1-SLF_{CYP2C9}}\right) + C_{11-OH-THC_{SLF}}} \end{aligned} \tag{24}$$

$$V_{11\text{-}OH\text{-}THC}\frac{dC_{11\text{-}OH\text{-}THC_{dep_{CTR}}}}{dt}=-\frac{Vmax_{11\text{-}OH\text{-}THC_{CYP3A4}}\times C_{11\text{-}OH\text{-}THC_{dep_{CTR}}}}{Km_{11\text{-}OH\text{-}THC_{CYP3A4}}+C_{11\text{-}OH\text{-}THC_{dep_{CTR}}}}-\frac{Vmax_{11\text{-}OH\text{-}THC_{CYP2C9}}\times C_{11\text{-}OH\text{-}THC_{dep_{CTR}}}}{Km_{11\text{-}OH\text{-}THC_{CYP2C9}}+C_{11\text{-}OH\text{-}THC_{dep_{CTR}}}}-\frac{Vmax_{COOH\text{-}THC_{CYP2C9}}\times C_{11\text{-}OH\text{-}THC_{dep_{CTR}}}}{Km_{11\text{-}OH\text{-}THC_{CYP2C9}}+C_{11\text{-}OH\text{-}THC_{dep_{CTR}}}} \quad (25)$$

$$V_{11\text{-}OH\text{-}THC}\frac{dC_{11\text{-}OH\text{-}THC_{dep_{SLF}}}}{dt}=-\frac{Vmax_{11\text{-}OH\text{-}THC_{CYP3A4}}\times C_{11\text{-}OH\text{-}THC_{dep_{SLF}}}}{Km_{11\text{-}OH\text{-}THC_{CYP3A4}}\times\left(\frac{1}{1-SLF_{CYP3A4}}\right)+C_{11\text{-}OH\text{-}THC_{dep_{SLF}}}}-\frac{Vmax_{11\text{-}OH\text{-}THC_{CYP2C9}}\times C_{11\text{-}OH\text{-}THC_{dep_{SLF}}}}{Km_{11\text{-}OH\text{-}THC_{CYP2C9}}\times\left(\frac{1}{1-SLF_{CYP2C9}}\right)+C_{11\text{-}OH\text{-}THC_{dep_{SLF}}}}-\frac{Vmax_{COOH\text{-}THC_{CYP2C9}}\times C_{11\text{-}OH\text{-}THC_{dep_{SLF}}}}{Km_{11\text{-}OH\text{-}THC_{CYP2C9}}\times\left(\frac{1}{1-SLF_{CYP2C9}}\right)+C_{11\text{-}OH\text{-}THC_{dep_{SLF}}}} \quad (26)$$

$$V_{11\text{-}OH\text{-}THC}\frac{dC_{11\text{-}OH\text{-}THC_{dep_{ITZ}}}}{dt}=-\frac{Vmax_{11\text{-}OH\text{-}THC_{CYP3A4}}\times C_{11\text{-}OH\text{-}THC_{dep_{ITZ}}}}{Km_{11\text{-}OH\text{-}THC_{CYP3A4}}\times\left(\frac{1}{1-ITZ_{CYP3A4}}\right)+C_{11\text{-}OH\text{-}THC_{dep_{ITZ}}}}-\frac{Vmax_{11\text{-}OH\text{-}THC_{CYP2C9}}\times C_{11\text{-}OH\text{-}THC_{dep_{ITZ}}}}{Km_{11\text{-}OH\text{-}THC_{CYP2C9}}\times\left(\frac{1}{1-ITZ_{CYP2C9}}\right)+C_{11\text{-}OH\text{-}THC_{dep_{ITZ}}}}-\frac{Vmax_{COOH\text{-}THC_{CYP2C9}}\times C_{11\text{-}OH\text{-}THC_{dep_{ITZ}}}}{Km_{11\text{-}OH\text{-}THC_{CYP2C9}}\times\left(\frac{1}{1-ITZ_{CYP2C9}}\right)+C_{11\text{-}OH\text{-}THC_{dep_{ITZ}}}} \quad (27)$$

$$V_{11\text{-}OH\text{-}THC}\frac{dC_{COOH\text{-}THC_{CTR}}}{dt}=\frac{Vmax_{COOH\text{-}THC_{CYP2C9}}\times C_{COOH\text{-}THC_{CTR}}}{Km_{11\text{-}OH\text{-}THC_{CYP2C9}}+C_{COOH\text{-}THC_{CTR}}} \quad (28)$$

$$V_{11\text{-}OH\text{-}THC}\frac{dC_{11\text{-}OH\text{-}THC_{dep_{UGT}}}}{dt}=-\frac{Vmax_{11\text{-}OH\text{-}THC_{UGT}}\times C_{11\text{-}OH\text{-}THC_{dep_{UGT}}}}{Km_{11\text{-}OH\text{-}THC_{UGT}}+C_{11\text{-}OH\text{-}THC_{dep_{UGT}}}} \quad (29)$$

We assumed that CYP2C9 Km for COOH-THC formation and the secondary CYP2C9 mediated 11-OH-THC depletion pathway was the same. In addition, we assumed sulfaphenazole and itraconazole inhibit P450 enzymes competitively.

V_{THC} and $V_{11\text{-}OH\text{-}THC}$ are the incubation volumes normalized for HLM protein concentration (0.02 mg/ml and 0.1 mg/ml THC and 11-OH-THC incubations, respectively)**.** These were set at 0.05 L/mg and 0.01 L/mg, respectively. Doses were also normalized by the HLM concentration and are expressed as µmol/mg.

$C_{THC_{CTR}}$ and $C_{11\text{-}OH\_THC_{CTR}}$ are the observed THC and 11-OH-THC concentrations when 0.010 – 14.3 µM THC was incubated in the absence of inhibitors. $C_{11\text{-}OH\text{-}THC\_dep\ CTR}$ and $C_{COOH\text{-}THC_{CTR}}$ are the observed 11-OH-THC and COOH-THC concentrations when 0.013 – 60 µM 11-OH-THC was incubated with NADPH (P450 metabolism) in the absence of inhibitors. $C_{11\text{-}OH\text{-}THC\_dep_{UGT}}$ are the observed 11-OH-THC concentrations when 0.013 – 60 µM 11-OH-THC was incubated with UDPGA (UGT metabolism).

In a limited dataset, 0.02 – 2 µM THC and 0.5 – 5 µM 11-OH-THC was incubated in the presence of sulfaphenazole (SLF – CYP2C9 inhibitor) and itraconazole (ITZ – CYP3A inhibitor). $C_{THC_{SLF}}$ and $C_{11\text{-}OH\text{-}THC_{SLF}}$ are the observed THC and 11-OH-THC concentrations in the presence of SLF when THC was incubated with HLMs. $C_{11\text{-}OH\text{-}THC\_dep\ SLF}$ and $C_{11\text{-}OH\text{-}THC\_dep\ ITZ}$ are the observed 11-OH-THC concentrations in the presence of SLF and ITZ when 11-OH-THC was incubated with HLMs. Since COOH-THC accounts for <5% of 11-OH-THC P450 depletion and COOH-THC kinetics are not the focus on this study, only the control observations were modeled.

The inhibition of SLF and ITZ has been previously established in **Chapter 2** (**Table 2.2**). SLF_{2C9}, $SLF_{2D6,}$ and SLF_{3A4} is the sulfaphenazole fractional inhibition of CYP2C9 (SLF_{CYP2C9} = 0.99), CYP2D6 (SLF_{CYP2D6} = 0.18), and CYP3A4 (SLF_{CYP3A4} = 0.28). ITZ_{CYP3A4} and ITZ_{CYP2C9} and is the itraconazole fractional inhibition of CYP3A4 (ITZ_{CYP3A4} = 0.98), CYP2C9 (ITZ_{CYP2C9} = 0.44). Competitive inhibition of the P450 enzymes by SLF and ITZ was assumed.

The P450 kinetic model (**Supplementary Eq. 1-8**) was applied by simultaneously fitting all observed data (i.e. THC, 11-OH-THC, COOH-THC in the presence and absence of inhibitors) from incubations mediated by P450 enzymes. The UGT kinetic model (**Supplementary Eq. 9**) was applied by fitting all observed data from incubation mediated by UGT enzymes.

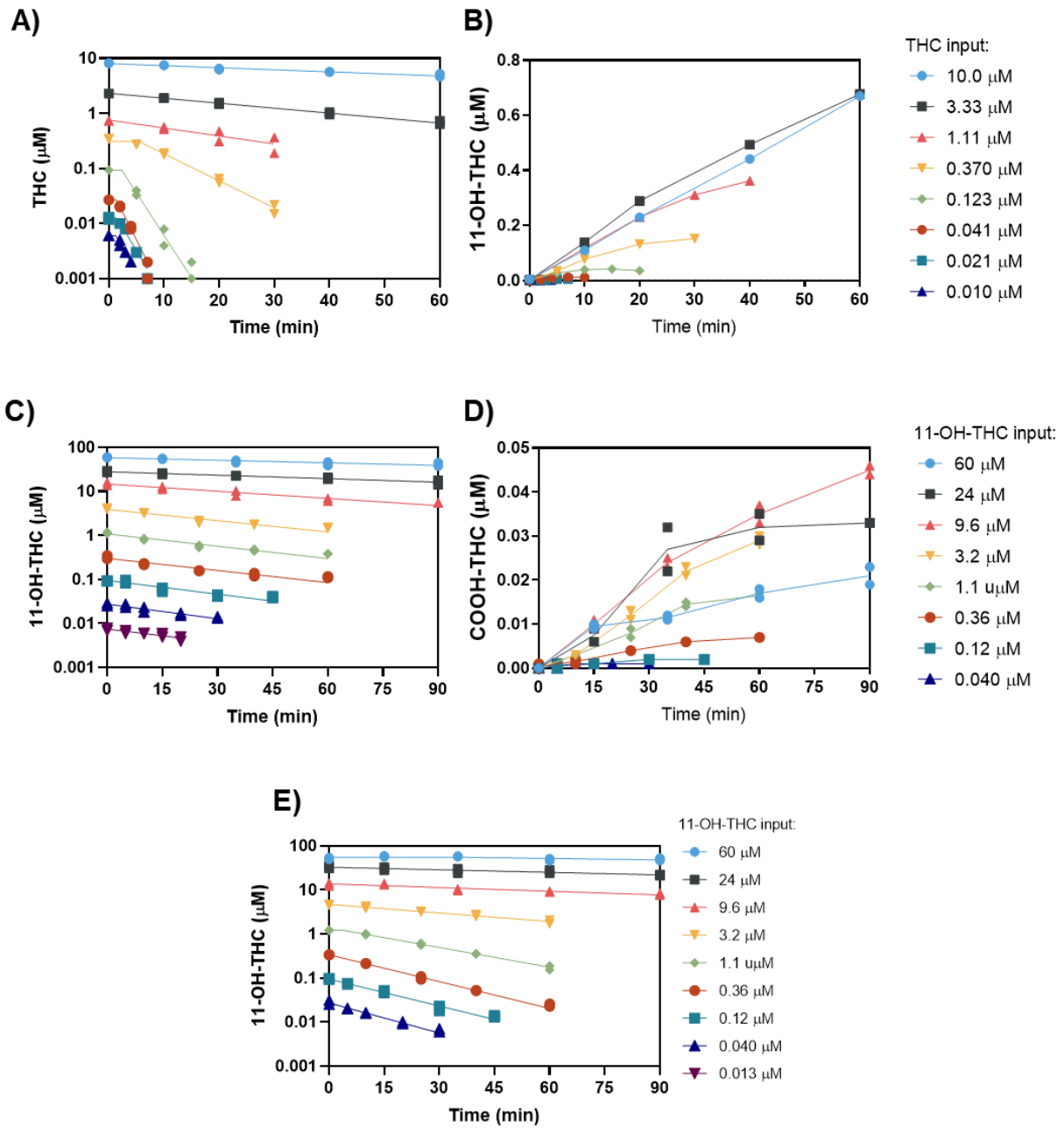

Supplementary Figure 3.1. In vitro concentration-time profiles of THC and its metabolites

Representative concentration-time profiles of A) THC depletion and B) 11-OH-THC formation at different THC concentrations in pooled HLMs. Representative concentration-time profiles of C) 11-OH-THC depletion by P450 enzymes D) COOH-THC formation and E) 11-OH-THC depletion by UGT enzymes at different 11-OH-THC concentrations in pooled HLMs. Depletion rate constant (k_{dep}) was obtained by fitting **Eq. 11** to the concentration-time curves (panels A, C, E). Formation rate (V) was obtained through linear fit of the metabolite concentration-time profile of timepoints that corresponded to <20% parent (Panels B and D). Data shown is representative of one (of three to four) independent experiments, each with duplicate determinations.

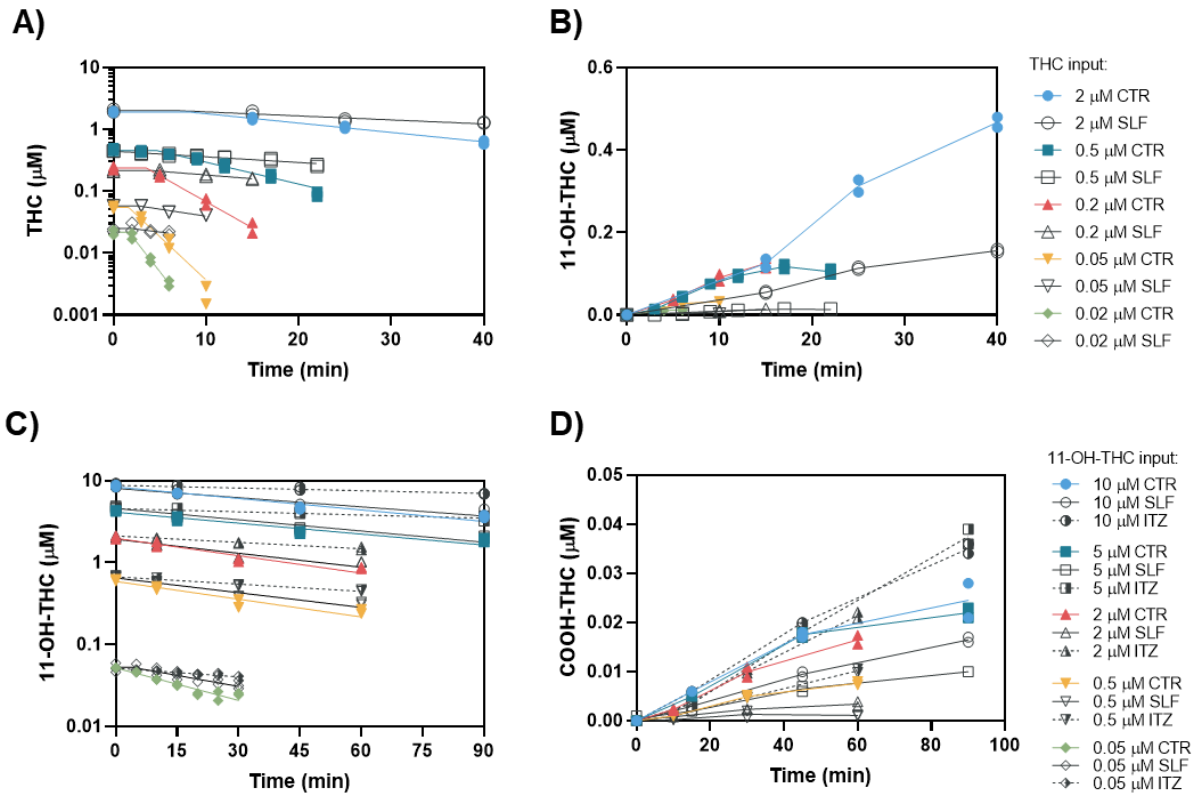

Supplementary Figure 3.2. Impact of P450 inhibition on cannabinoid disposition in vitro

Representative concentration-time profiles of A) THC depletion and B) 11-OH-THC formation at different THC concentrations in the absence (DMSO control with no inhibitor, CTR) and presence of sulfaphenazole (SLF; CYP2C9 inhibitor) in pooled HLMs. Representative concentration-time profiles of C) 11-OH-THC depletion by P450 enzymes D) COOH-THC formation at different 11-OH-THC concentrations in the absence and presence of SLF and itraconazole (ITZ; CYP3A inhibitor) pooled HLMs. These experiments were conducted with limited THC/11-OH-THC concentrations that are within the nonlinear range (see **Figure 3.1**). k_{dep} and V were obtained as described in **Supplementary Figure 3.1**. Data shown is representative from one (of three) independent experiments, each with duplicate determinations.

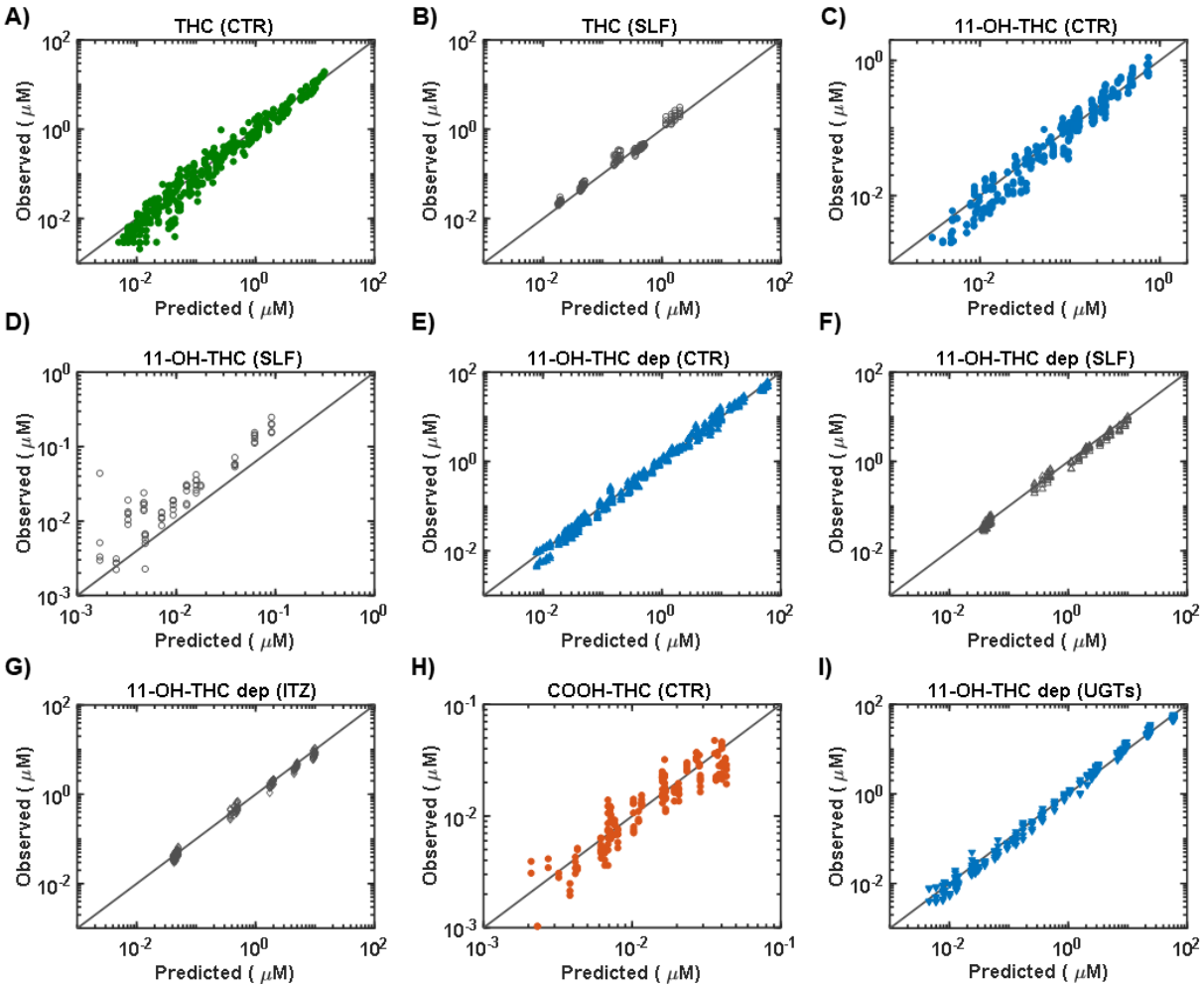

Supplementary Figure 3.3. Goodness-of-fit plot of P450 and UGT kinetic models

Predicted versus observed concentrations (dots) and the line of unity for P450 (panels A-H) and UGT (panel I) kinetic models.

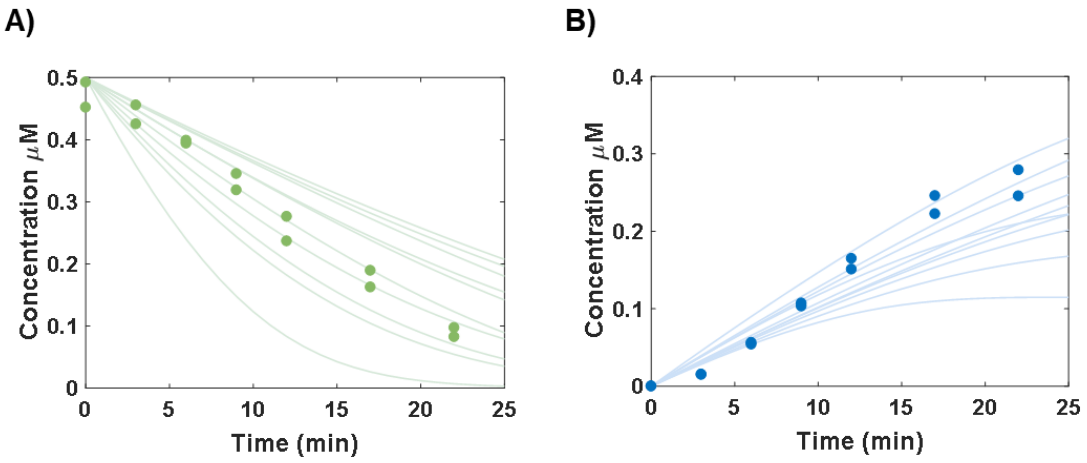

Supplementary Figure 3.4. Model validation of in vitro P450 kinetic model

Monte-Carlo simulations (lines, 10 individual simulations) using P450 kinetic model estimates (**Table 3.3**) shows good agreement with observed concentrations (dots) from an independent dataset with duplicate determinations of A) 500 nM THC depletion and subsequent B) 11-OH-THC formation in pooled HLMs.

Chapter 4. Development and verification of a linked THC/11-OH-THC PBPK model in a healthy nonpregnant population

4.1. ABSTRACT

The prevalence of cannabis use among pregnant women is rising. The impact of increased in utero exposure to cannabis to fetal outcomes is unknown. The psychoactive cannabinoid, THC and its active hydroxy metabolite, 11-OH-THC, have been shown to perpetrate fetal risk in preclinical studies. Therefore, to elucidate the impact of maternal cannabis use on fetal outcomes, the maternal THC and 11-OH-THC exposure must be known. Since measuring cannabinoid maternal concentrations in the clinic is logistically and ethically difficult, we used PBPK modeling and simulation as an alternative, non-invasive approach to predict THC and 11-OH-THC concentrations throughout pregnancy. Here, we extrapolated the in vitro mechanistic PK information outlined in **Chapters 2** and **3** to build a linked THC/11-OH-THC PBPK model in a healthy nonpregnant population and verified with observed data after IV administration and inhalation of THC. Inhalation was chosen as the administration route since it is the most popular. The in vitro to in vivo extrapolation (IVIVE) of both THC and 11-OH-THC disposition was successful. The bioavailability (F_{inh}) of THC after inhalation was higher in chronic versus casual cannabis users (F_{inh} = 0.35 and 0.19, respectively). THC clearance was not sensitive to small alterations in intrinsic clearance (CL_{int}) whereas 11-OH-THC was. Based off this data, it is expected that THC exposure will not change during pregnancy but 11-OH-THC exposure will decrease. By building and verifying the linked THC/11-OH-THC PBPK model in a healthy nonpregnant population, a mechanistic physiological and pharmacokinetic platform now exists that can be extrapolated for predictions beyond pregnancy, such as impact of drug-drug interactions and genetic polymorphism on disposition of THC and 11-OH-THC.

4.2. INTRODUCTION

Epidemiological studies have shown that maternal marijuana (cannabis) use is associated with neonatal morbidity and subtle but persistent neurodevelopmental consequences (Huizink, 2014; Gunn et al., 2016; Metz et al., 2017; Stickrath, 2019). However, these results are confounded by factors such as reliance on self-reporting of cannabis use, concurrent tobacco and alcohol use, socioeconomic background, and types (e.g. joints, edibles) and modes (e.g. smoking, vaping, eating) of cannabis products consumed. Prospective clinical studies are required to establish the independent risk associated with maternal cannabis, however, such studies are not ethical. Animal and in vitro studies have identified

(-)-Δ^9-tetrahydrocannabinol (THC), the psychotropic component of cannabis, and its active metabolite, 11-OH-THC, as potential perpetrators of fetal developmental risk (Paria et al., 1995; Wang et al., 2006; Tortoriello et al., 2014; Costa et al., 2015). But these studies cannot be translated to humans without taking into consideration of differences in maternal-fetal exposure to these cannabinoids. As such, in order to anticipate the risk associated with maternal cannabis use, the THC and 11-OH-THC exposure during pregnancy must be predicted as quantifying this exposure is logistically difficult (maternal) or not possible (fetal).

A non-invasive approach to predicting cannabinoid exposure in such special populations is via physiologically based pharmacokinetic modeling and simulation (PBPK M & S). PBPK models incorporate physiological and drug dependent information to mechanistically predict drug disposition in vivo. Drug dependent information includes the identity of the drug metabolizing enzymes (DMEs) and their kinetics. We have previously identified the hepatic enzymes responsible for the disposition of THC and 11-OH-THC (**Chapter 2**) (Patilea-Vrana et al., 2018) and their kinetics (**Chapter 3**). Once a PBPK model is developed and verified in a healthy population, the model can be extrapolated to pregnant populations by accounting for gestational-age physiological changes, such as increase in DME expression. For example, the activity of the two major DME's relevant to THC and 11-OH-THC disposition, cytochrome P450 enzymes CYP2C9 and CYP3A4, increase 1.5 – and 2 -fold, respectively, during pregnancy (Anderson, 2005; Ke et al., 2014b). We have previously demonstrated successful prediction of maternal and fetal drug concentrations at term for drugs that are substrate of CYP2C9 and CYP3A4 using PBPK M & S (Ke et al., 2012; Ke et al., 2014a; Zhang and Unadkat, 2017). Using a similar approach, extrapolations of THC and 11-OH-THC can be made from healthy nonpregnant to pregnant populations.

Therefore, the aims of this study were to i) extrapolate the previously quantified in vitro enzyme kinetics of THC and 11-OH-THC shown in **Chapter 3** to build and ii) verify a linked THC/11-OH-THC PBPK model after IV and inhalation of THC in a healthy nonpregnant population. The final THC and 11-OH-THC models were verified after IV and inhalation but not oral administration of THC since mechanistic data on extrahepatic metabolism is missing. Importantly, smoking cannabis is the most popular route of administration, and thus relevant (Schauer et al., 2016). The predictions of THC and 11-OH-THC

concentrations during pregnancy via PBPK M & S are a crucial component in establishing the pharmacologically relevant concentrations necessary to use in preclinical studies, and therefore translate preclinical fetal safety and toxicity of in utero cannabis exposure to humans. While the focus of our study was to extrapolate cannabinoid disposition to pregnancy, the linked THC/11-OH-THC model can be mechanistically extrapolated to predict cannabinoid disposition in other special populations, such as disease populations, subjects with genetic polymorphism, and drug-drug interactions.

4.3. MATERIALS AND METHODS

4.3.1. General workflow of the linked THC/11-OH-THC PBPK model development

The workflow of the linked THC/11-OH-THC PBPK model using is depicted in **Figure 4.1.** The THC and 11-OH-THC models were developed using Simcyp (Simcyp® Population-based Simulator Version 16, Simcyp Limited, Sheffield, UK). The parent model for THC was developed first and verified using observed data after IV administration of THC. Simulations of THC after inhalation were conducted using the final THC IV model with in vivo estimated adsorption parameters (absorption rate constant - ka and inhalation bioavailability - F_{inh}) and compared to observed values. Due to lack of viable datasets where 11-OH-THC was administered independently, the metabolite 11-OH-THC model was developed using an IV THC training dataset where 11-OH-THC was monitored. The 11-OH-THC model was verified using observed data after inhalation of THC. Since the purpose of the inhalation datasets was to verify the 11-OH-THC model, THC F_{inh} was optimized in order for the simulated THC AUC_{0-t} and C_{max} to approximate observed values. Finally, the linked THC/11-OH-THC PBPK model was adjusted for gestational-dependent physiological changes and used to simulate THC and 11-OH-THC disposition during pregnancy.

The inclusion criteria for clinical studies used for model development included single dose studies in healthy individuals of IV and inhalation of THC and 11-OH-THC with no exclusion made for sample size, gender, frequency of cannabis use, or bioanalytical methodology. Where available, the following pharmacokinetic (PK) parameters were collected: area under the curve (AUC), maximum plasma concentrations (C_{max}), clearance (CL), volume of distribution at steady-state (V_{ss}) and terminal half-life

($t_{1/2}$). If available, concentration-time profiles were digitized using the online semi-automatic tool WebPlotDigitizer (https://automeris.io/WebPlotDigitizer/). If the AUC was not reported but the concentration-time profile was provide, AUC was estimated via noncompartmental analysis in Phoenix® 8.1, Certara (Princeton, NJ). The details and observed PK parameters for IV and inhalation datasets can be found in **Supplementary Tables 4.1** and **4.2**, respectively.

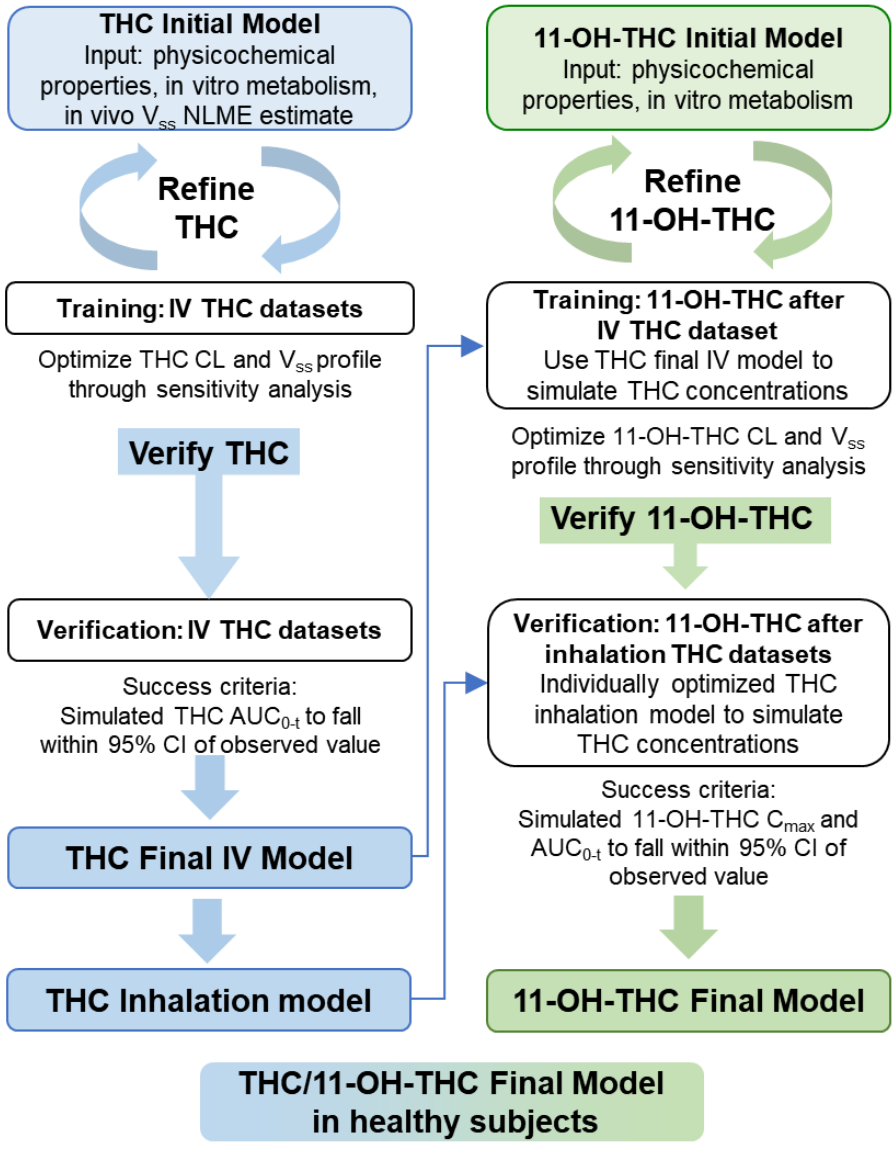

Figure 4.1. General workflow of THC and 11-OH-THC PBPK model development and verification in a healthy nonpregnant population.

In order to assess the quality of the observed data and identify any potential outliers, the THC and 11-OH-THC concentration-time profiles were normalized with respect to THC dose (**Supplementary Figure 4.1**). As shown in **Supplementary Figure 4.1A**, studies that used thin layer chromatograph (TLC) had similar trends in the initial decrease of THC concentrations but remarkably different profiles in the elimination phase when compared to all other studies. For example, THC clearance estimated by via TLC (Wall et al., 1983) was 12-15 L/hr whereas studies that used high performance liquid chromatography - standard ultraviolet (HLPC- UV) (Hunt and Jones, 1980) or gas chromatograph-mass spectrometry (GC-MS) (Ohlsson et al., 1982; Kelly and Jones, 1992; Naef et al., 2004) estimated THC clearance between 36-59 L/hr (see **Supplementary Table 4.1**). A similarly much longer half-life can be observed in the TLC studies by (Lemberger et al., 1970; Lemberger et al., 1971; Lemberger et al., 1972b; Wall et al., 1983) when compared to the remaining studies (**Supplementary Figure 4.1A**). It should be noted the TLC studies were from two different groups so it is likely that the analytical methodology of TLC versus HLPC-UV or GC-MS may contribute to the difference. As such, any TLC studies were removed and not used during THC or 11-OH-THC model training and verification. Lastly, the study from Brenneisen et al., 2010 was removed from the inhalation datasets since both THC and 11-OH-THC concentrations were at least an order of magnitude smaller than all other studies. The reason for this discrepancy is unknown. All of the studies had small samples size (n = 3-22), mostly male subjects, and were of younger age. Due to these characteristics, there is larger interindividual and interstudy variability (see **Supplementary Tables 4.1-4.2**). A designation of chronic and casual cannabis users was given using an arbitrary cutoff of cannabis use more or less than twice a week, respectively (**Table 4.2-4.3**).

4.3.2. Model training and verification for THC

Input values for the final THC PBPK model are listed in **Table 4.1**. Physicochemical properties for THC were collected from literature. To note, the THC blood-to-plasma (B:P) ratio reported by Giroud et al., 2001 was chosen over the reported THC B:P of 0.39 by Schwilke et al., 2009 even though the latter had a larger sample size (n = 8 versus 75) because the latter value required an adjustment of the hematocrit to 0.61, which is outside of the range of hematocrit levels for healthy individuals (Giroud et al., 2001; Schwilke et al., 2009). Furthermore, we originally built the initial THC model using our previously

measured unbound fraction in plasma (fu_p) of 0.011 (**Chapter 3, Table 3.1**), but later optimized THC fu_p using the Simcyp Prediction Toolbox.

Table 4.1. Drug-dependent parameters of THC and 11-OH-THC used for PBPK M & S

Parameter	THC	Reference	11-OH-THC	Reference
Physicochemical properties				
Molecular weight (g/mol)	314.5	ChEMBL	330.5	ChEMBL
Log of octanol:water partition coefficient ($logP_{o:w}$)	6.97	(Thomas et al., 1990)	5.33	(Thomas et al., 1990)
Compound type	Neutral	ChEMBL	Neutral	ChEMBL
Blood-to-plasma (B:P)	0.667	(Giroud et al., 2001)	0.625	(Giroud et al., 2001)
fu_{plasma}	0.002	Predicted in Simcyp	0.005	Optimized
Plasma binding proteins	HSA Lipoprotein (63% bound)	(Klausner et al., 1975)	HSA Lipoprotein (63% bound)	Assumed same as THC
Distribution – full PBPK model				
V_{ss} (L/kg)	6.5	Estimated using NLME	3.8	Predicted[a]
Kp scaler	0.004	Adjusted to match Vss. Kp values predicted [a]	—	
Lipid binding scaler	—		0.059	Predicted in Simcyp
Lung ka (hr^{-1})	12	Estimated using NLME	—	
Lung F_{inh}	0.22	Estimated using NLME	—	
Elimination – enzyme kinetics				
CYP2C9				
V_{max} (pmol/min/mg) (metabolite formed: 11-OH-THC)	624	Measured	—	
K_m (μM) (fu_{inc})	0.07 (0.04)	Measured	—	
V_{max1} (pmol/min/mg) (metabolite formed: COOH-THC)	—		4.83	Measured
K_m (μM) (fu_{inc})	—		0.50 (0.06)	Measured
V_{max2} (pmol/min/mg)	—		54.4	Measured
K_m (μM) (fu_{inc})	—		0.50 (0.06)	Measured
CYP3A4				
V_{max} (pmol/min/mg)	4905	Measured	1826	Measured
K_m (μM) (fu_{inc})	5.48 (0.04)	Measured	12.8 (0.06)	Measured
Additional HLM CL (UGTs)[b]				
CL_{int} (μl/min/mg) (fu_{inc})	—		537 (0.06)	Measured
CL_R (L/hr)	0	(Wall and Perez-Reyes, 1981)	0	(Lemberger et al., 1972a)
CL_{bile} (L/hr)	0	(Wall and Perez-Reyes, 1981)	0	(Lemberger et al., 1972a)

[a] Distribution predicted via Rodgers and Rowland (Simcyp Method 2). [b] We have previously identified UGT1A9 and UGT2B7 deplete 11-OH-THC using recombinant enzymes, but we were unable to differentiate their fractional contributions due to the lack of selective inhibitors (Patilea-Vrana et al., 2018).

We have previously measured the in vitro kinetics (V_{max} and K_m) of THC via CYP2C9 (major pathway, fm = 0.91) and CYP2D6 (fm = 0.09) (**Chapter 3, Table 3.4**). These values, which are listed in **Table 4.1,** were extrapolated to in vivo using enzyme expression levels as listed in the Simcyp Virtual Healthy Population. Renal and biliary clearance were set to 0 L/hr since less than 5% of administered THC dose is excreted unchanged in urine and feces (Wall and Perez-Reyes, 1981).

As shown in **Supplementary Table 4.1**, the reported THC V_{ss} ranges from 0.6 – 8.9 L/kg (Hunt and Jones, 1980; Kelly and Jones, 1992; Naef et al., 2004). However, the smaller V_{ss} values also have smaller sampling times (8 versus 24 hours). Indeed, a theoretical simulation (**Supplementary Figure 4.3C)** demonstrates that lower sampling times can severely underestimate the true V_{ss} and an optimum sampling time would have to be at least 56 hours. Because of these limitations, the observed THC V_{ss} was estimated by fitting a three-compartment model to the digitized concentration-time profiles after IV administration of THC using a nonlinear mixed effects (NLME) model in Phoenix® 8.1, Certara (Princeton, NJ) (**Supplementary Figure 4.2A**). The goodness-of-fit plot in **Supplementary Figure 4.2B** shows good model fit of the observed THC concentrations after IV administration. The NLME V_{ss} estimate was 6.4 L/kg (39%). Within Simcyp, the Rodgers and Rowland (Simcyp Method 2) was selected for predicting tissue distribution and a Kp scaler of 0.004 was used for the predicted value to match the NLME V_{ss} estimate.

Data from Ohlsson et al., 1982 was used as training dataset for the THC IV model. This dataset was chosen because it had the longest sampling time of 48 hours (Ohlsson et al., 1982). As described above, and shown in **Supplementary Figure 4.2C**, sampling times greater than 12 and 56 hours are necessary to accurately estimate the THC CL and V_{ss}. No change was made in the model for chronic versus casual users. The THC IV model was verified using the remaining THC IV datasets.

Since there is no mechanistic information on lung disposition of THC in humans, the absorption of THC after inhalation (ka and F_{inh}) was estimated by fitting a three-compartment model simultaneously to the digitized THC concentration-time profiles after IV and inhalation using NLME modeling (**Supplementary Figure 4.2A**). Goodness-of-fit plots show good model fit of the observed THC concentration after inhalation (**Supplementary Figure 4.2B**). The NLME estimates for ka and F_{inh} are 12

min^{-1} (12%) and 0.22 (33%). These parameters were incorporated into the inhalation PBPK model to simulate THC concentrations after inhalation and compared with observed values.

4.3.3. Model training and verification for 11-OH-THC

Input values for the final 11-OH-THC PBPK model are listed in **Table 4.1**. As for THC, physicochemical properties were collected from literature. Due to similar high lipophilicity, we assumed the same percentage of 11-OH-THC bound to lipoprotein (63%) as THC. Originally, we built the initial 11-OH-THC model using our previously measured fu_p of 0.012 (**Chapter 3, Table 3.1**), but later optimized this value via manual sensitivity analysis. The Rodgers and Rowland method (Simcyp Method 2) using a lipid binding scaler (ψ) was used to predict 11-OH-THC distribution. The lipid binding scaler back-calculates the maximum extent of cellular lipid binding (P_{max}) by correlating neutral lipid and neutral phospholipid binding in red blood cells to that in tissue (**Eq. 24-26**).

$$P_{max} = \frac{K_{pu,rbc} - f_{IW,rbc} - 0.7f_{NP,rbc}}{f_{NL,rbc} + 0.3f_{NP,rbc}} \tag{24}$$

$$\psi = \frac{P_{max}}{P_{o:w}} \tag{25}$$

$$K_{pu} = f_{EW} + \frac{X_{IW}}{X_{EW}} f_{IW} + \left(\frac{\psi \times P_{o:w} \times f_{NL} + (0.3 \times \psi \times P_{o:w} + 0.7) f_{NP}}{X_{EW}} \right) + Ka_{PR}[PR]_t \tag{26}$$

where K_{pu}, and $K_{pu,rbc}$ are the unbound tissue and erythrocyte partition coefficient, f_{EW}, $f_{IW,rbc}$, $f_{NP,rbc}$, $f_{NL,rbc}$, f_{NL}, f_{NP} are the fraction of extracellular and intracellular water, neutral phospholipids, and neutral phospholipids in red blood cells (rbc) or tissue, X_{IW}, X_{EW} are the ionized drug in intracellular and extracellular water, Ka_{PR} and $[PR]_t$ are the affinity constant for and tissue concentrations of extracellular tissue protein (albumin or protein), respectively. This is a necessary adjustment since the Rodgers and Rowland prediction method greatly overestimates V_{ss} for compounds with $logP_{o:w} > 4$ (Haddad et al., 2000; Rodgers and Rowland, 2007).

We have previously quantified the enzyme kinetics for 11-OH-THC clearance in vitro (**Table 4.1**). UGT enzymes (fm = 0.60), CYP3A4 (fm = 0.18), and CYP2C9 (fm = 0.15) are the DME's responsible for metabolism of 11-OH-THC (**Chapter 3, Table 3.4**). We have previously identified UGT2B7 and UGT1A9 are the UGT isoforms that deplete 11-OH-THC in vitro, however, we were unable to distinguish their fractional contributions accurately due to lack of selective inhibitors (Patilea-Vrana et al., 2018). As such, UGT CL_{int} was listed as HLM-other in the Simcyp model. No renal or biliary clearance was selected for 11-OH-THC. There is negligible excretion of unchanged 11-OH-THC in the urine but up to 20% of radiolabeled 11-OH-THC dose is excreted unchanged in feces (Lemberger et al., 1972a; Lemberger et al., 1973). However, the unchanged 11-OH-THC in feces may be 11-OH-THC deconjugated by bacterial β-glucuronidase. Furthermore, there is no current information on the transport of 11-OH-THC by biliary efflux transporters, such as P-gp or BCRP.

Metabolite exposure (area under the curve - AUC) and the concentration-time profile will depend on the parent AUC, the metabolite formation and elimination clearance, and V_{ss}. As such, ideally, 11-OH-THC elimination clearance and V_{ss} should be first optimized and verified using data after IV administration of 11-OH-THC. Otherwise, it is difficult to distinguish between the formation and elimination clearance of the metabolite if using datasets where the parent drug was administered. However, the only IV administration datasets of 11-OH-THC used TLC to quantify 11-OH-THC concentrations (Lemberger et al., 1972a; Lemberger et al., 1973) and have been removed for reasons outlined above. As such, optimization of 11-OH-THC AUC and concentration-time profile was performed using the final IV THC model and data after IV THC administration from Naef et al. 2004. No other datasets of 11-OH-THC formation after IV administration of THC were available for verification (the studies by Wall et al., 1981 and Wall et al., 1983 were removed because they used TLC as the bioanalytical method). As such, 11-OH-THC model was verified using THC inhalation datasets after optimization of THC F_{inh} in order to approximate the observed THC AUC_{0-t}. This was to ensure that THC AUC and concentration-time profile was well simulated in order to allow for verification of 11-OH-THC disposition.

4.3.4. Model verification and performance assessment

For each verification dataset, ten trials were run and the trial design was set to match the number of subjects, age range, and proportion of females as shown in **Table 4.2** and **4.3**. In order for the THC and 11-OH-THC models to be considered successful, the simulated PK parameters needed to be within the 95% confidence interval of the observed value. Since all the observed studies had small sample size less than 30 subjects, a t-distribution was used to calculate the 95% confidence interval. THC model verification was performed using the simulated THC $AUC_{0\text{-}t}$ after IV administration of THC. 11-OH-THC model verification was performed using the 11-OH-THC C_{max}, 11-OH-THC $AUC_{0\text{-}t,}$ and combined (THC + 11-OH-THC) $AUC_{0\text{-}t}$ after THC inhalation. To note, no success criteria was assigned to THC $AUC_{0\text{-}t}$ and C_{max} after THC inhalation because F_{inh} was individually optimized in order to verify 11-OH-THC. Additional model assessment was performed by comparing the predicted versus observed concentrations and PK parameters. Bias and precision were calculated via the mean relative error (MRE) and relative root mean square error (rRMSE) as shown in **Eq. 27** and **28**, respectively (Sheiner and Beal, 1981).

$$\mathrm{MRE} = \frac{1}{n}\sum_{i=1}^{n}\frac{(\mathrm{Pred}_i - \mathrm{Obs}_i)}{\mathrm{Obs}_i}\times 100 \tag{27}$$

$$\mathrm{rRMSE} = \sqrt{\frac{1}{n}\sum_{i=1}^{n}\left(\frac{\mathrm{Pred}_i - \mathrm{Obs}_i}{\mathrm{Obs}_i}\right)^2}\times 100 \tag{28}$$

Table 4.2. THC IV datasets used for THC and 11-OH-THC training and verification details

Study name	Dose	Sampling time (hr)	N (subjects)	Females (%)	Age	Average frequency of cannabis use[a]	Reference
Hunt_1980	2 mg	24	6	0.0	22-30	>2x weekly (chronic)	(Hunt and Jones, 1980)
Ohlsson_1980	5 mg	4	11	0.0	18-35	frequent and occasional	(Ohlsson et al., 1980)
Lindgren_1981a	5 mg	4	18	11.1	19-36	Daily (chronic)	(Lindgren et al., 1981)
Lindgren_1981b	5 mg	4	18	11.1	19-36	<1x month (casual)	(Lindgren et al., 1981)
Ohlsson_1982a	5 mg	48	5	0.0	18-35	Daily (chronic)	(Ohlsson et al., 1982)
Ohlsson_1982b	5 mg	48	4	0.0	18-35	<1x month (casual)	(Ohlsson et al., 1982)
Kelly_1992a	5 mg	8	4	0.0	24-45	Daily (chronic)	(Kelly and Jones, 1992)
Kelly_1992b	5 mg	8	4	0.0	24-45	<2-3x month (casual)	(Kelly and Jones, 1992)
Naef_2004	0.053 mg/kg	8	4	50.0	26-35	naïve	(Naef et al., 2004)
Morrison_2009	2.5 mg	2	22	0.0	28±6	2-1000 episodes over last 10 years (casual)	(Morrison et al., 2009)
Barkus_2011	2.5 mg	2	10	0.0	26±4	324 exposures over last 24 years (casual)	(Barkus et al., 2011)

[a] Unless designated in the reference, designation of chronic versus casual users was given arbitrarily to cannabis use of greater and less than twice a week, respectively.

Table 4.3. THC inhalation datasets used for THC simulations and 11-OH-THC verification

Study name	Dose	Sampling time (hr)	N (subjects)	Females (%)	Age	Average frequency of cannabis use[a]	Reference
Ohlsson_1980	13 mg	3	11	0.0	18-35	frequent and occasional	(Ohlsson et al., 1980)
Barnett_1981	8.94 mg	2	6	50.0	25-31	Frequent (chronic)	(Barnett et al., 1982)
Lindgren_1981a	13.4 mg	2	18	11.1	19-36	<1x month (casual)	(Lindgren et al., 1981)
Lindgren_1982b	12.7 mg	2	18	11.1	19-36	Daily (chronic)	(Lindgren et al., 1981)
Ohlsson_1982a	10 mg	48	4	0.0	18-35	<1x month (casual)	(Ohlsson et al., 1982)
Ohlsson_1982b	10 mg	48	5	0.0	18-35	Daily (chronic)	(Ohlsson et al., 1982)
Perez-Reyes_1982a	9.7 mg	6	6	50.0	26-32	4-12x month (chronic)	(Perez-Reyes et al., 1982)
Perez-Reyes_1982b	12.8 mg	6	6	50.0	26-32	4-12x month (chronic)	(Perez-Reyes et al., 1982)
Perez-Reyes_1982b	16 mg	6	6	50.0	26-32	4-12x month (chronic)	(Perez-Reyes et al., 1982)
Johansson_1988	15 mg	360	3	0.0	No info	Daily (chronic)	(Johansson et al., 1988)
McBurney_1986	0.15 mg/kg	22	10	0.0	18-30	Occasional (casual)	(McBurney et al., 1986)
Huestis_1992a	15.8 mg	168	6	0.0	29-36	2-3x week (chronic)	(Huestis et al., 1992)
Huestis_1992b	33.8 mg	168	6	0.0	29-36	2-3x week (chronic)	(Huestis et al., 1992)
Kauert_2007a	0.25 mg/kg	6	10	10.0	19-21	Occasional (casual)	(Kauert et al., 2007)
Kauert_2007b	0.50 mg/kg	6	10	10.0	19-21	Occasional (casual)	(Kauert et al., 2007)
Hunault_2008a	29.3 mg	8	18	0.0	18-33	2-9x month (chronic)	(Hunault et al., 2008)
Hunault_2008b	49.1 mg	8	20	0.0	18-33	2-9x month (chronic)	(Hunault et al., 2008)
Hunault_2008c	69.4 mg	8	20	0.0	18-33	2-9x month (chronic)	(Hunault et al., 2008)
Toennes_2008a	0.5 mg/kg	8	12	33.3	20-27	<4x week (casual)	(Toennes et al., 2008)
Toennes_2008b	0.5 mg/kg	8	12	25.0	20-31	>4x week (chronic)	(Toennes et al., 2008)
Schwope_2011a	54 mg	22	10	10.0	19-46	2x month (casual)	(Schwope et al., 2011)
Toennes_2011	0.4 mg/kg	4	19	26.3	19-38	<4x week (casual)	(Toennes et al., 2011)
Desrosiers_2014a	54 mg	30	14	28.6	19-38	2x month (casual)	(Desrosiers et al., 2014)
Desrosiers_2014b	54 mg	30	11	27.3	22-41	4.5x day (chronic)	(Desrosiers et al., 2014)
Hunault_2014a	29.3 mg	8	18	0.0	18-45	2-9x month (chronic)	(Hunault et al., 2014)
Hunault_2014b	49.1 mg	8	20	0.0	18-45	2-9x month (chronic)	(Hunault et al., 2014)
Hunault_2014c	69.4 mg	8	20	0.0	18-45	2-9x month (chronic)	(Hunault et al., 2014)

Study name	Dose	Sampling time (hr)	N (subjects)	Females (%)	Age	Average frequency of cannabis use[a]	Reference
Newmeyer_2017a	50.6 mg	3.5	9	33.3	21-46	2-8x month (casual)	(Newmeyer et al., 2017b)
Newmeyer_2017b	50.6 mg	3.5	11	18.2	19-38	daily (chronic)	(Newmeyer et al., 2017b)

[a] Unless designated in the reference, designation of chronic versus casual users is given arbitrarily to cannabis use of greater and less than twice a week, respectively.

4.4. RESULTS

4.4.1. THC model development and verification

The initial THC and 11-OH-THC models were built using physicochemical properties collected from literature, enzyme kinetics as we have previously quantified in **Chapter 3**, and NLME estimated in vivo values for THC V_{ss}, ka, and F_{inh} (**Supplementary Figure 4.2**). The final model input values are shown in **Table 4.1**. During model training, THC and 11-OH-THC fu_p were adjusted from 0.011 and 0.012 to 0.0022 and 0.005, respectively. All other input parameters remained unchanged.

The observed and simulated concentration-time profiles of THC after IV administration are shown in **Figure 4.2**. The IV THC training set used from Ohlsson et al., 1982 included both chronic and casual users, however, there were no difference in the THC concentration-time profiles or AUC_{0-t} (Ohlsson et al., 1982). As such, no modification was made in the THC PBPK IV model for casual and chronic users. Verification of the THC IV PBPK model is shown in **Table 4.4**. Overall, the predicted THC concentration-time profiles were similar to the observed profiles with 70% of the simulated values within two-fold of the observed values. Seven out of eight simulated THC AUC_{0-t} were within the 95% confidence interval of the observed value. For the Lindgren_1981a dataset, the simulated AUC_{0-t} was underestimated, however it was close to the confidence interval limit. Nevertheless, all simulated THC AUC_{0-t} were within two-fold of the observed value (data not shown). The bias (MRE) and precision (rRMSE) for predicted THC AUC_{0-t} after IV administration were -6% and 20%, respectively. Give the success criteria and bias and precision, the THC IV model performed well.

4.4.2. Simulation of THC after inhalation of cannabis

Using the final THC IV model and the NLME estimates for inhalation absorption (ka = 12 h^{-1} and F_{inh} = 0.22 – **Supplementary Figure 4.2**), inhalation of THC was simulated and compared to the studies shown in **Figure 4.3**. Of the 27 THC inhalation datasets, 13 did not meet the success criteria for AUC_{0-t} (data not shown). Furthermore, as shown in **Figure 4.3A**, seven of the 27 predicted AUC_{0-t} were not within two-fold of the observed value. Interestingly, there was very little bias (MRE = 1%) but poor precision (rRMSE = 88%). This was in part because THC AUC_{0-t} and C_{max} was generally underpredicted

overpredicted for chronic and casual users, respectively. For any simulated value that did not originally fall within the 95% confidence interval of the observed value, F_{inh} was optimized via manual sensitivity in order to approximate the observed value (**Supplementary Table 4.3**). As shown in **Figure 4.3C**, chronic users had a higher F_{inh} compared to casual users (mean F_{inh}= 0.19±0.14 and 0.35±0.19, respectively).

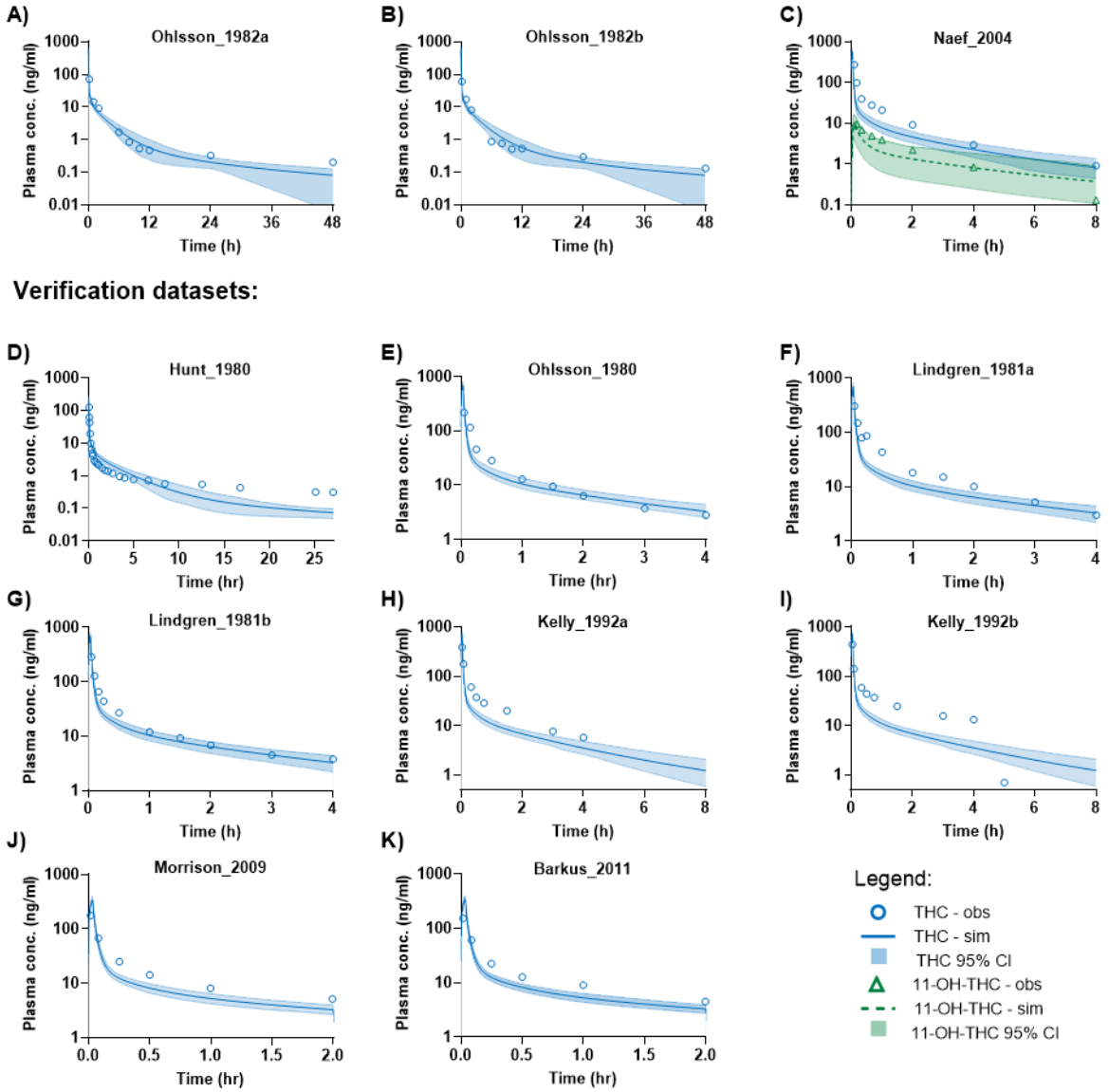

Figure 4.2. Observed and simulated THC and 11-OH-THC profiles after IV administration of THC. Datasets from Ohlsson et al. 1982 (panel A-B) and Naef et al. 2004 (panel C) were used as training sets for THC and 11-OH-THC model development, respectively, while all other datasets (panels D-K) were used for verification of THC (11-OH-THC was verified using inhalation datasets since only one IV THC study had measured 11-OH-THC concentrations). Markers, lines, and shaded area represent mean observed concentrations, simulated concentrations, and the 95% confidence interval of the simulated concentrations, respectively.

Table 4.4. Verification of THC model using IV THC datasets

Study	AUC_{0-t} (ng*hr/ml)			
	Simulated	Observed	95% CI limits	
Hunt_1980	32	26	17	34
Ohlsson_1980	64	60	57	64
Lindgren_1981a	**64**	81	65	96
Lindgren_1981b	64	58	47	68
Kelly_1992a	76	101	49	153
Kelly_1992b	76	122	48	196
Morrison_2009	28	31	28	34
Barkus_2011	28	29	24	35

Bolded numbers did not meet the success criteria (the simulated AUC_{0-t} did not fall within the confidence interval of observed value).

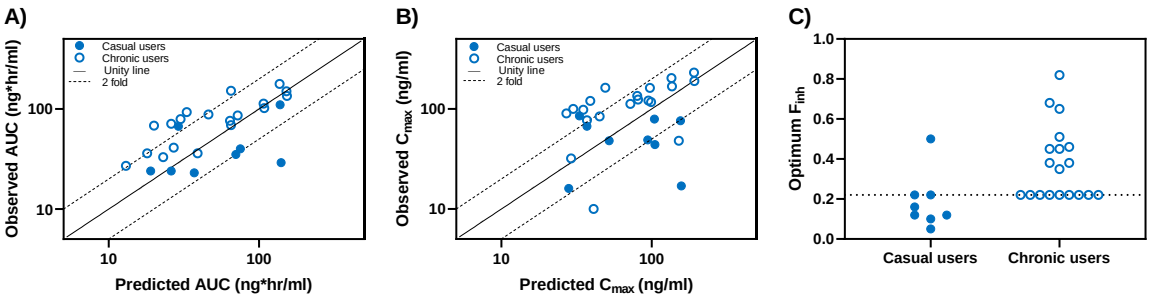

Figure 4.3. Simulation of THC after inhalation using in vivo estimated parameters

Observed and simulated THC A) AUC_{0-t} and B) C_{max} after inhalation of THC. The final THC IV model and NLME estimated absorption parameters (ka = 12 h^{-1} and F_{inh} = 0.22) were used in all simulations. To note, dashed line in panel C is at F_{inh} = 0.22. The THC AUC_{0-t} and C_{max} for casual users is typically overestimated while the reverse is true for chronic users. This suggests that casual and chronic users require a lower and higher F_{inh}, respectively. While F_{inh} of 0.22 results in little bias (MRE = 1%) and thus is acceptable to use for general THC inhalation simulations, the large variability (rRMSE = 88%) due to difference in casual and chronic users requires individual refinement of F_{inh}.

4.4.3. 11-OH-THC model development and verification

The training for the initial 11-OH-THC model was performed using the dataset from Naef et al., 2004 since it was the only dataset that had 11-OH-THC concentrations after IV administration of THC. The THC and 11-OH-THC concentration training curves for the training dataset can be seen in **Figure 4.2C**. Model verification of 11-OH-THC was performed using THC inhalation datasets with F_{inh} optimized such as simulated THC AUC_{0-t} approximated the observed value. This was done to ensure that the AUC

and concentration-time profile of the parent compound (THC) was well characterized in order to verify the disposition of the metabolite (11-OH-THC). The optimize F_{inh} and simulated THC C_{max} and AUC_{0-t} for the inhalation verification datasets are shown in **Supplementary Figure 4.4**.

The simulated and observed THC and 11-OH-THC concentration-time profiles after inhalation of THC are shown in **Figure 4.4**. To note, only nine of the 16 the verification datasets reported the THC and 11-OH-THC concentration-time profiles. Furthermore, while it was difficult to digitize the Desrosiers_2014a and b datasets and many of the values were below the lower limit of quantification, the authors did report C_{max} and AUC_{0-t} parameters (Desrosiers et al., 2014). Overall, the simulated 11-OH-THC concentrations are comparable to the observed values, however there is variability among the studies. Twelve out of the 16 simulated 11-OH-THC C_{max} met the success criteria, whereas 12 out of 14 simulated 11-OH-THC AUC_{0-t} met the success criteria. When considering the combined THC and 11-OH-THC AUC_{0-t}, all of the verification datasets met the success criteria. To note, the two datasets from Newmeyer et al., 2017 only reported 11-OH-THC C_{max} and not AUC_{0-t} (Newmeyer et al., 2017b). The 11-OH-THC bias and precision was as follows: MRE = 87% and 151% for C_{max} and MRE = 15% and rRMSE = 60% for AUC_{0-t}. As shown further in **Figure 4.5A**, while 11-OH-THC C_{max} tended to be overestimated, majority of the values are within two-fold of the observed, except for the Newmeyer_2017a dataset. Furthermore, as shown in **Figure 4.5B**, all of the simulated AUC_{0-t} were within two-fold of the observed values, except for the Huestis_1992b dataset. Due to these outliers, the precision for 11-OH-THC C_{max} and AUC_{0-t} was worsened. Further inspection shows good agreement between the simulated versus observed THC and 11-OH-THC concentrations (**Figure 4.5C**). Indeed, 80% and 79% of the simulated THC and 11-OH-THC concentrations, respectively, were within two-fold of the observed value (**Figure 4.5D-E**). Pooling together the success criteria, the bias and precision, as well as the additional model performance, the 11-OH-THC model performs well.

Using the final linked THC/11-OH-THC model, sensitivity analysis was performed to identify sensitive parameters to THC CL, THC V_{ss}, and 11-OH-THC to THC AUC ratio (M/P AUC) (**Figure 4.6**). THC predicted CL was 57 L/hr, making THC a high clearance compound. As such, THC clearance is blood-flow limited and it was not sensitive to change in intrinsic clearance (CL_{int}), fu_p, or fu_{mic}. For

example, a 10-fold decrease in THC overall CL_{int} leads to a 1.6-fold decrease in THC plasma CL. THC predicted V_{ss} was 6.4 L/hr. As such, THC V_{ss} was the most sensitive to distribution into the adipose and fu_p. Since 11-OH-THC AUC depends both on the formation from THC and elimination from the liver, sensitivity analysis was run for the M/P AUC. As anticipated, M/P AUC was sensitive to changes in 11-OH-THC formation from THC (fm, THC_{plasma}) and changes to 11-OH-THC elimination (CL_{int}). A sensitivity analysis was performed for fu_{mic} since the CL_{int} values used in the PBPK model are in vitro observed values adjusted for microsomal binding, and therefore errors in fu_{mic} will reflect in error in CL_{int} values. For this simulation, fu_{mic} was changed proportionally for both THC and 11-OH-THC. As shown in **Figure 4.6A**, THC CL, and therefore AUC, is not sensitive to fu_{mic} changes. Errors in fu_{mic} impact THC and 11-OH-THC disproportionally, and therefore fu_{mic} was a sensitive parameter to M/P AUC. To demonstrate this, a simulation was run where the total CL_{int} of THC and 11-OH-THC was decreased by 10 or 100-fold while fm and the ratio of 11-OH-THC CL_{int} formation to elimination similar was maintained the same (**Table 4.6**). 11-OH-THC AUC decreased proportional to its CL_{int} whereas THC AUC did not change proportionally to its CL_{int}. Therefore M/P AUC was sensitive to the magnitude of 11-OH-THC CL_{int}.

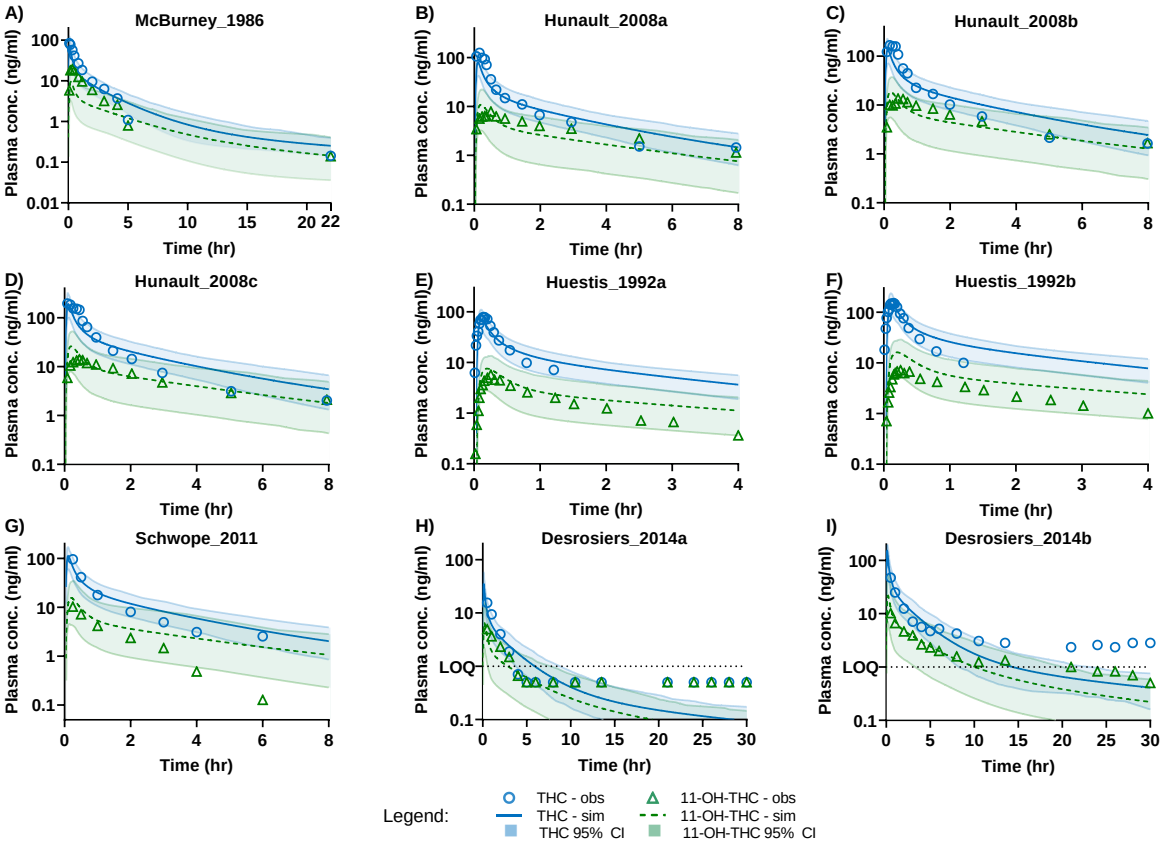

Figure 4.4. Verification of 11-OH-THC PBPK model using THC inhalation datasets.
Due to lack of available 11-OH-THC data in the THC IV studies for verification purposes, THC inhalation datasets were used instead. Since 11-OH-THC exposure is driven by THC exposure, F_{inh} was optimized for each dataset in panels A-I so the simulated THC AUC_{0-t} and C_{max} approximate the observed values (see **Table 5** for further details). Final simulations were run using individually optimized inhalation THC inhalation models linked (see **Supplementary Table 4.3** for details) with 11-OH-THC model optimized using Naef et al. 2004 training set. Markers, lines, and shaded area represent mean observed concentrations, simulated concentrations, and the 95% confidence interval of the simulated concentrations, respectively.

Table 4.5. Verification of 11-OH-THC model using THC inhalation datasets

Study	11-OH-THC C_{max}				11-OH-THC AUC_{0-t}				THC + 11-OH-THC AUC_{0-t}			
	Sim.	Obs.	95% CI or range[b]		Sim.	Obs.	95% CI or range[b]		Sim.	Obs.	95% CI or range[b]	
McBurney_1986	20	19	10	28	**20**	40	23	57	86	107	79	136
Huestis_1992a	7.6	6.7	3.3	10	9	5.7	NC	NC	55	84	NC	NC
Huestis_1992b	16	7.5	3.8	16	20	7.2	NC	NC	117	159	NC	NC
Kauert_2007a	**4.2**	2.5	1.4	3.6	5.8	4.6	2.7	6.5	26	27	17	37
Kauert_2007b	**8.3**	3.6	2.0	5.2	**12**	8.0	5.0	11	53	48	33	63

Study	11-OH-THC C_{max}				11-OH-THC AUC_{0-t}				THC + 11-OH-THC AUC_{0-t}			
	Sim.	Obs.	95% CI or range[b]		Sim.	Obs.	95% CI or range[b]		Sim.	Obs.	95% CI or range[b]	
Hunault_2008a	11	9.2	5.4	13	18	24	16	32	82	101	80	121
Hunault_2008b	18	16	9.3	23	31	37	25	48	138	150	122	177
Hunault_2008c	**26**	16	12	20	43	40	31	49	195	191	156	226
Toennes_2008a	7.7	6.7	3.5	9.9	11	14	9.6	18	48	49	39	59
Toennes_2008b	15	12	5.4	19	23	31	16	46	107	117	80	154
Schwope_2011	16	10	4.0	16	32	19	7.5	42	132	129	33	177
Toennes_2011	20	17	12	22	24	31	20	42	119	119	98	140
Desrosiers_2014a	6.6	5.3	0.0	16	12	11	0.9	36	43	41	5	143
Desrosiers_2014b	22	11	3.6	26	45	65	20	106	182	243	129	480
Newmeyer_2017a[a]	**14**	1.9	0.5	8.7	16	NR	NR	NR	83	NR	NR	NR
Newmeyer_2017b[a]	13	7.2	1.9	31	16	NR	NR	NR	81	NR	NR	NR

[a] Observed and simulated blood C_{max} and AUC [b] The range (min – max) of the observed parameter is listed for the following datasets since no standard deviation was reported: Huestis et al., 1992, Schwope et al., 2011, Desrosiers et al., 2014, Newmeyer et al., 2017. NC – 95% confidence interval not calculated since AUC was estimated via trapezoidal rule of the digitized average concentrations. NR – parameter not reported by Newmeyer et al,. 2017. Bolded numbers did not meet the success criteria (the simulated C_{max} or AUC_{0-t} did not fall within the confidence interval of observed value). To note, THC profiles after inhalation were optimized via F_{inh} in order to ensure THC exposure approximated observed values (see **Supplementary Table 4.2** for optimized F_{inh} values and simulated THC PK parameters for the various verification datasets).

Table 4.6. Simulations to show impact of fu_{mic} or CL_{int} changes to M/P AUC

CL_{int}	CYP2C9 fm	THC CL_{int} (L/hr)	11-OH-THC CL_{int} (L/hr)	Formation/ elimination CL_{int}	Plasma THC AUC (ng*hr/ml)	Plasma 11-OH-THC AUC (ng*hr/ml)	M/P AUC
1X	0.91	840418	57770	13	17	3.7	0.2
0.1X	0.91	84042	5777	13	24	37	1.5
0.01X	0.91	8404	578	13	91	364	4.4

11-OH-THC but not THC plasma AUC increases proportionally to CL_{int} because THC clearance (and thus AUC) has blood-flow limitations whereas 11-OH-THC AUC does not.

4.5. DISCUSSION

The in vitro mechanistic PK information quantified in **Chapters 2** and **3** was extrapolated to in vivo via IVIVE and used to build a linked THC/11-OH-THC PBPK in healthy nonpregnant population. The only parameters that required optimization were THC and 11-OH-THC fu_p. We had previously measured fu_p using ultracentrifugation (**Chapter 3**). During ultracentrifugation, three distinctive layers are formed: a top layer consisting of low-density lipoproteins (LDL) and chylomicrons, a middle layer consisting the unbound drug, and a bottom layer containing albumin and high-density lipoprotein (HDL). For drugs that are highly bound, it is possible to have contamination from the upper layer and thus overestimate fu_p (Brockman et al., 2015). Up to 63% of THC is bound to lipoproteins in plasma, mainly to LDL (Klausner et al., 1975). Therefore it is likely that ultracentrifugation is not a sensitive enough method to accurately measure THC and 11-OH-THC fu_p. Hence, it is not surprising that fu_p needed optimization.

The M/P AUC is defined as $\frac{M}{P} = \frac{fm * CL_p}{fuCL\,int_{met}}$ (Pang et al., 2008). Since the mean simulated and observed M/P AUC after inhalation of THC were the same (0.29 ± 0.05 and 0.29 ± 0.15, respectively, from **Table 4.5**), it means that the combination of fm, 11-OH-THC CL_{int} and fu_b estimates must be correct. Since THC CL_{int} exceed hepatic blood flow, THC plasma CL is blood-flow limited and not as sensitive to changes in CL_{int} (**Figure 4.6**). Therefore, the in vitro estimated THC CL_{int} could be several folds off and the THC PBPK model would still perform well. Furthermore, as seen in the M/P equation, the 11-OH-THC formation clearance has blood-flow limitations (because THC CL_p is blood flow limited) whereas the elimination clearance does not. As such, even though the formation of 11-OH-THC is much greater than its elimination (see CL_{int} values in **Table 4.6**), 11-OH-THC has apparent formation-rate limited kinetics. This helps explain why the observed M/P AUC is less than one and THC and 11-OH-THC have similar half-lives in vivo. When considering the impact of CL_{int} on both THC and 11-OH-THC disposition as outlined above, we conclude that the IVIVE of the mechanistic PK information from **Chapters 2-3** was successful.

The THC and 11-OH-THC models performed well. In all verification instances, majority, if not all, datasets met out success criteria. Given the wide interindividual and interstudy variability, this

performance is acceptable. Overall there was little bias (MRE < 30%) for all estimates except for 11-OH-THC C_{max} after inhalation of THC. The observed maximum time to reach C_{max} (t_{max}) is 0.08-0.50 hours and 0.1 – 0.6 hours for THC and 11-OH-THC (**Supplementary Table 4.2**), respectively, while the simulated t_{max} was 0.11-0.12 hours to 0.19-0.20 hours, respectively. Because of the short time to reach C_{max}, it is possible that many studies were not able to capture the true $C_{max,}$ thus leading to a model overestimation. Furthermore, the simulated value for the dataset from Newmeyer_2017a was a clear outlier (**Figure 4.5A**), thus leading to increased bias. Precision was good for the THC final model (rRMSE < 20%). While the precision for the 11-OH-THC model was less than the THC model, this was in part driven by a few outliers. Nevertheless, majority of the 11-OH-THC PK parameter as well as the simulated concentrations are within two-fold of the observed values (**Figure 4.5**). Given the interstudy variability within the observed data, we can conclude that the 11-OH-THC model performed well.

The inhalation THC model with the in vivo estimated inhalation adsorption parameters (ka = $12h^{-1}$ and F_{inh} = 0.22) did not perform well (**Figure 4.3**). The THC AUC and C_{max} was over- and underestimated for casual and chronic users, respectively. Some have hypothesized that chronic users have an increased rate of THC metabolism (Lemberger et al., 1971). There was no difference in the THC clearance in chronic versus casual users in studies where THC was administered IV (Ohlsson et al., 1982; Kelly and Jones, 1992). As shown in the THC sensitivity an increase in THC CL_{int} would not lead to a change to THC clearance due clearance being blood flow limited (**Figure 4.6A**). Studies have observed an increase in THC AUC after inhalation of THC in chronic versus casual users (Toennes et al., 2008; Desrosiers et al., 2014). Increase in F_{inh} could explain this difference. Indeed, the average optimum F_{inh} for casual and chronic users was 0.19 and 0.35, respectively (**Figure 4.3C**). The overall volume of cannabis that is smoked depends on the puff volume, breathhold duration, interval between puffs, and puff velocity (Azorlosa et al., 1995). History of regular cannabis use is correlated with average volume inhaled per puff and puff volumes (McClure et al., 2012). Furthermore, chronic users develop a tolerance to the psychoactive effects of cannabis and require higher levels of THC to achieve the desired effect (Lee et al., 2013). Therefore, the different smoking topography and tolerance between chronic and casual users leads to the observed difference in F_{inh}.

A linked THC/11-OH-THC PBPK model was built and verified for IV and inhalation of THC in a nonpregnant healthy population. This model is the necessary (mechanistic) foundation that can be used to extrapolate THC/11-OH-THC exposure in special populations (i.e. pregnancy, disease, genetic polymorphism) or predict drug-drug interactions. For example, the final model can be extrapolated to pregnancy by accounting for gestational age dependent changes. Of the relevant DME's to THC and 11-OH-THC metabolism, the activity of CYP2C9, CYP2D6, and CYP3A4 increases up to two-fold during pregnancy while the activity of UGT2B7 and UGT1A9 does not (Anderson, 2005; Ke et al., 2014b). Based off the findings shown in this **Chapter**, these physiological changes are not expected to impact THC clearance but increase 11-OH-THC elimination clearance. Additional information on extrahepatic metabolism (i.e. lung and intestine) is necessary for advancing the PBPK model to inhalation and oral administration of THC. The final THC/11-OH-THC model can also be used to predict drug-drug interactions or impact of genetic polymorphism.

4.6. SUPPLEMENTARY INFORMATION

Supplementary Table 4.1. Description of collected clinical datasets after intravenous administration of THC or 11-OH-THC

				THC					11-OH-THC				
Compound	Dose (mg)	Analytical	Sampling time (hr)	CL (L/hr)	V_{ss} (L/kg)	C_{max} (ng/ml)	AUC (ng/ml*hr)	$t_{1/2}$ (hr)	C_{max} (ng/ml)	AUC (ng/ml*hr)	$t_{1/2}$ (hr)	Use of dataset	Reference
THC	0.5	TLC	72	—	9.4±2.5[a]	—	—	57±4	—	—	—	Removed	(Lemberger et al., 1970)
THC	0.5	TLC	72	—	8.5±1.1[a]	—	—	28±1	—	—	—	Removed	(Lemberger et al., 1971)
THC	0.5	TLC	30	—	—	—	—	—	—	—	—	Removed	(Lemberger et al., 1972b)
THC	2	HPLC-UV	24	36±8.9	8.9±4.2	105±10		20±4	—	—	—	THC verification	(Hunt and Jones, 1980)
THC	5	GC/MS	4	—	—	219	72±7.0	1.4±0.4	—	—	—	THC verification	(Ohlsson et al., 1980)
THC	5	GC/MS	4	—	—	288±119	72±28	—	—	—	—	THC verification	(Lindgren et al., 1981)
THC	5	GC/MS	4	—	—	302±95	101±37	—	—	—	—	THC verification	(Lindgren et al., 1981)
THC	4-5	TLC	72	—	—	62±3.0	—		3.4±0.6	—	—	Removed	(Wall and Perez-Reyes, 1981)
THC	5	GC/MS	48	59±9.0	—	61±5.4	86±14	20	—	—	—	THC Training	(Ohlsson et al., 1982)
THC	5	GC/MS	48	57±12	—	72±9.0	91±20	—	—	—	—	THC Training	(Ohlsson et al., 1982)
THC	4	TLC	48	15±3.7	10±6.3[b]	71±34	280±67	36	3.7±2.3	—	15	THC verification	(Wall et al., 1983)
THC	2.2	TLC	48	12±3.0	7.5±3.1[b]	85±26	202±77	29	3.8±2.8	—	33	THC verification	(Wall et al., 1983)
THC	5	GC/MS	8	46±17	1.1±0.5	386±29	118±38	1.6±0.5	—	—	—	THC verification	(Kelly and Jones, 1992)
THC	5	GC/MS	8	47±41	1.1±0.2	438±36	165±63	2.0±0.3	—	—	—	THC verification	(Kelly and Jones, 1992)
THC	0.053 mg/kg	GC/MS	8	47±24	0.6±0.2	272±61	117±97	1.2	9.1±0.8	25±15	—	11-OH-THC Training	(Naef et al., 2004)
THC	2.5	GC/MS	2	—	—	177±34	34±7.1	—	4.4±2.1	—	—	THC verification	(Morrison et al., 2009)
THC	2.5	GC/MS	2	—	—	151±20	29±7.2	—	—	—	—	THC verification	(Barkus et al., 2011)
11-OH-THC	1	TLC	8	—	—	—	—	—	—	—	22	Removed	(Lemberger et al., 1972a)
11-OH-THC	1	TLC	72	—	—	—	—	—	—	—	—	Removed	(Lemberger et al., 1973)

[a] apparent volume of distribution – V_{ss} not reported. [b] V_{β} – V_{ss} not reported. Data show are mean and standard deviation (where available) of reported parameters from clinical studies in healthy subjects where THC was administered IV. Dashed lines represent parameter was not reported. Studies that used TLC to measure THC and 11-OH-THC concentration were removed (see Methods).

Supplementary Table 4.2. Description of collected clinical datasets after inhalation of THC

Dose (mg)	Analytical	Sampling time (hr)	THC			11-OH-THC			Use of dataset	Reference
			C_{max} (ng/ml)	T_{max} (hr)	AUC (ng/ml*hr)	C_{max} (ng/ml)	T_{max} (hr)	AUC (ng/ml*hr)		
10	TLC	24	—	—	—	—	—	—	Removed	(Lemberger et al., 1972b)
13	GS/MS	3	77 (33-118)	0.05	33±11	—	—	—	Extrapolation	(Ohlsson et al., 1980)
8.94	RIA	2	90±50	0.09	27±7.8	—	—	—	Extrapolation	(Barnett et al., 1982)
13.4	GS/MS	2	67±38	0.05	24±12	—	—	—	Extrapolation	(Lindgren et al., 1981)
12.7	GS/MS	2	98±44	0.05	36±17	—	—	—	Extrapolation	(Lindgren et al., 1981)
10	GS/MS	48	16±5.9	0.17	24±5.7	—	—	—	Extrapolation	(Ohlsson et al., 1982)
10	GS/MS	48	32±6.9	0.17	41±8.8	—	—	—	Extrapolation	(Ohlsson et al., 1982)
9.7	RIA	6	100±10	0.11	68±8.5	—	—	—	Extrapolation	(Perez-Reyes et al., 1982)
12.8	RIA	6	120±11	0.13	71±12	—	—	—	Extrapolation	(Perez-Reyes et al., 1982)
16	RIA	6	162±19	0.13	93±11	—	—	—	Extrapolation	(Perez-Reyes et al., 1982)
	GS/MS	22	85±45	0.08	—	19±12	0.33	—	Extrapolation	(McBurney et al., 1986)
15	GS/MS	360	10	—	—	—	—	—	Extrapolation	(Johansson et al., 1988)
15.8	GS/MS	168	84(50-129)	0.14	—	6.7(3.3-10)	0.25	—	Extrapolation	(Huestis et al., 1992)
33.8	GS/MS	168	162(76-267)	0.14	—	7.5(3.8-16)	0.25	—	Extrapolation	(Huestis et al., 1992)
0.25 mg/kg	GS/MS	6	48±35	0.05	23±13	2.5±1.6	0.18	4.6±2.7	Extrapolation and 11-OH-THC verification	(Kauert et al., 2007)
0.5 mg/kg	GS/MS	6	79±43	0.05	40±21	3.6±2.2	0.13	8.0±4.2	Extrapolation and 11-OH-THC verification	(Kauert et al., 2007)
29.3	LC-MS/MS	8	135±69	0.16	76±38	9.2±7.6	0.42	24±16	Extrapolation and 11-OH-THC verification	(Hunault et al., 2008)
49.1	LC-MS/MS	8	203±112	0.24	113±53	16±15	0.37	37±24	Extrapolation and 11-OH-THC verification	(Hunault et al., 2008)
69.4	LC-MS/MS	8	231±109	0.21	150±73	16±8.8	0.42	40±19	Extrapolation and 11-OH-THC verification	(Hunault et al., 2008)

0.5 mg/kg	GS/MS	8	49±24.9	0.10	35±14	6.7±5.1	0.10	14±7.0	Extrapolation and 11-OH-THC verification	(Toennes et al., 2008)
0.5 mg/kg	GS/MS	8	121±78	0.10	86±54	12±11	0.10	31±23	Extrapolation and 11-OH-THC verification	(Toennes et al., 2008)
70	GS/MS	8	21±17	0.08	—	1.8±1.2	0.17	—	Removed - outlier	(Brenneisen et al., 2010)
54	LC-MS/MS	22	76(1-110)	0.26	110(25-235)	10(4-16)	0.26	19(7.5-42)	Extrapolation and 11-OH-THC verification	(Schwope et al., 2011)
0.4 mg/kg	GS/MS	4	112±48	0.25	88±38	17±9.8	0.50	31±22	Extrapolation and 11-OH-THC verification	(Toennes et al., 2011)
54	LC-MS/MS	30	17(5.4-84)	0.50	29(3.6-107)	5.3(0-15.6)	0.60	11(0.9-36)	Extrapolation and 11-OH-THC verification	(Desrosiers et al., 2014)
54	LC-MS/MS	30	48(26-69)	0.50	178(37-109)	10.5(3.6-26)	0.50	65(20-106)	Extrapolation and 11-OH-THC verification	(Desrosiers et al., 2014)
29.3	LC-MS/MS	8	124±66	0.17	—	—	—	—	Extrapolation	(Hunault et al., 2014)
49.1	LC-MS/MS	8	168±100	0.17	—	—	—	—	Extrapolation	(Hunault et al., 2014)
69.4	LC-MS/MS	8	190±107	0.17	—	—	—	—	Extrapolation	(Hunault et al., 2014)
50.6	LC-MS/MS	3.5	44.4(1.3-174)[a]	0.10	—	1.9(0.5-8.7)[a]	0.19	—	Extrapolation and 11-OH-THC verification	(Newmeyer et al., 2017b)
50.6	LC-MS/MS	3.5	117(53-471)[a]	0.13	—	7.2(1.9-31)[a]	0.20	—	Extrapolation and 11-OH-THC verification	(Newmeyer et al., 2017b)

[a] blood concentration. All other measurements are plasma or serum. RIA – radioimmunoassay, TLC – thin layer chromatography. Data show are mean and standard deviation or range (min-max) of reported parameters from clinical studies in healthy subjects where THC was inhaled. Dashed lines represents parameter was not reported. TLC studies were removed due to analytical issues. For 11-OH-THC verification, only datasets that measured both THC and 11-OH-THC were utilized.

Supplementary Table 4.3. Simulated and observed values for THC inhalation

Study	User type	THC C_{max} (ng/ml)		THC AUC (ng*hr/ml)		
		Sim.	Obs.	Sim.	Obs.	Optimum F_{inh}[a]
McBurney_1986	Casual	33	85	29	67	0.50
Kauert_2007a	Casual	52	48	37	23	0.12
Kauert_2007b	Casual	104	79	75	40	0.12
Toennes_2008a	Casual	94	49	70	35	0.10
Schwope_2011a	Casual	155	76	138	110	0.16
Desrosiers_2014a	Casual	151	48	140	29	0.05
Lindgren_1981a	Casual	37	67	19	24	0.22
Ohlsson_1982a	Casual	28	16	26	24	0.22
Newmeyer_2017a	Casual	105	44	NR	NR	NR
Huestis_1992a	Chronic	45	84	30	79	0.45
Huestis_1992b	Chronic	97	162	65	152	0.45
Hunault_2008a	Chronic	80	135	64	76	0.22
Hunault_2008b	Chronic	135	210	107	113	0.22
Hunault_2008c	Chronic	191	231	152	150	0.22
Toennes_2008b	Chronic	95	121	72	86	0.22
Toennes_2011	Chronic	72	112	46	88	0.38
Desrosiers_2014b	Chronic	157	17	137	178	0.22
1980 Ohlsson	Chronic	37	77	23	33	0.35
1981 Barnett	Chronic	27	90	13	27	0.51
Ohlsson_1980	Chronic	35	98	18	36	0.46
Barnett_1981	Chronic	29	32	27	41	0.38
Perez-Reyes_1982a	Chronic	39	120	26	71	0.65
Perez-Reyes_1982b	Chronic	49	163	33	93	0.68
Perez-Reyes_1982b	Chronic	30	100	20	68	0.82
Johansson_1988	Chronic	41	10	39	36	0.22
Hunault_2014a	Chronic	81	124	65	69	0.22
Hunault_2014b	Chronic	136	168	108	102	0.22
Hunault_2014c	Chronic	192	190	153	135	0.22
Newmeyer_2017b	Chronic	99	117	NR	NR	NR

[a] For studies where the simulated THC $AUC_{0\text{-}t}$ did not fall within the 95% confidence interval of the observed value (confidence intervals not shown), F_{inh} was optimized via manual sensitivity in order to identify the optimum F_{inh} for the simulated value to match the observed value. NR – AUC not reported by authors

Supplementary Table 4.4. THC PK parameters for optimized THC inhalation model

Study	User type	F_{inh}[a]	THC C_{max}				THC AUC_{0-t}			
			Sim.	Obs.	95% CI limits or range[b]		Sim.	Obs.	95% CI limits or range[b]	
McBurney_1986	Casual	0.50	75	85	53	117	66	67	44	90
Huestis_1992a	Chronic	0.45	68	84	50	129	45	79	NC	NC
Huestis_1992b	Chronic	0.45	145	162	76	267	97	152	NC	NC
Kauert_2007a	Casual	0.12	28	48	23	73	20	23	13	32
Kauert_2007b	Casual	0.12	57	79	49	110	41	40	26	55
Hunault_2008a	Chronic	0.22	**80**	135	101	169	64	76	57	95
Hunault_2008b	Chronic	0.22	**135**	203	150	256	107	113	88	138
Hunault_2008c	Chronic	0.22	191	231	180	282	152	150	116	184
Toennes_2008a	Casual	0.10	49	49	33	65	37	35	26	44
Toennes_2008b	Chronic	0.22	110	121	71	171	84	86	52	120
Schwope_2011	Casual	0.16	**113**	76	18	110	100	110	25	135
Toennes_2001	Casual	0.38	**147**	112	89	135	95	88	70	106
Desrosiers_2014a	Casual	0.05	35	17	5	84	31	29	3.6	107
Desrosiers_2014b	Chronic	0.22	**151**	48	26	69	137	178	109	374
Newmeyer_2017a	Casual	0.22	105	44	1	174	67	NR	NR	NR
Newmeyer_2017b	Chronic	0.22	99	117	53	471	65	NR	NR	NR

[a] F_{inh} was individually optimized so simulated THC AUC_{0-t} and C_{max} approximated observed values. This was done to ensure that the THC exposure after inhalation was simulated well in order to verify the 11-OH-THC model. As such, the THC C_{max} and AUC_{0-t} listed are not part of the THC model verification. [b] The range (min – max) of the observed parameter is listed for the following datasets since no standard deviation was reported: Huestis et al., 1992, Schwope et al., 2011, Desrosiers et al., 2014, Newmeyer et al., 2017. NC – 95% confidence interval not calculated since AUC was estimated via trapezoidal rule of the digitized average concentrations. NR – parameter not reported by Newmeyer et al,. 2017. Bolded values are simulated values that did not fall within the 95% confidence interval of the observed value. To note, F_{inh} was optimized primarily on observed THC AUC_{0-t} and not THC C_{max}.

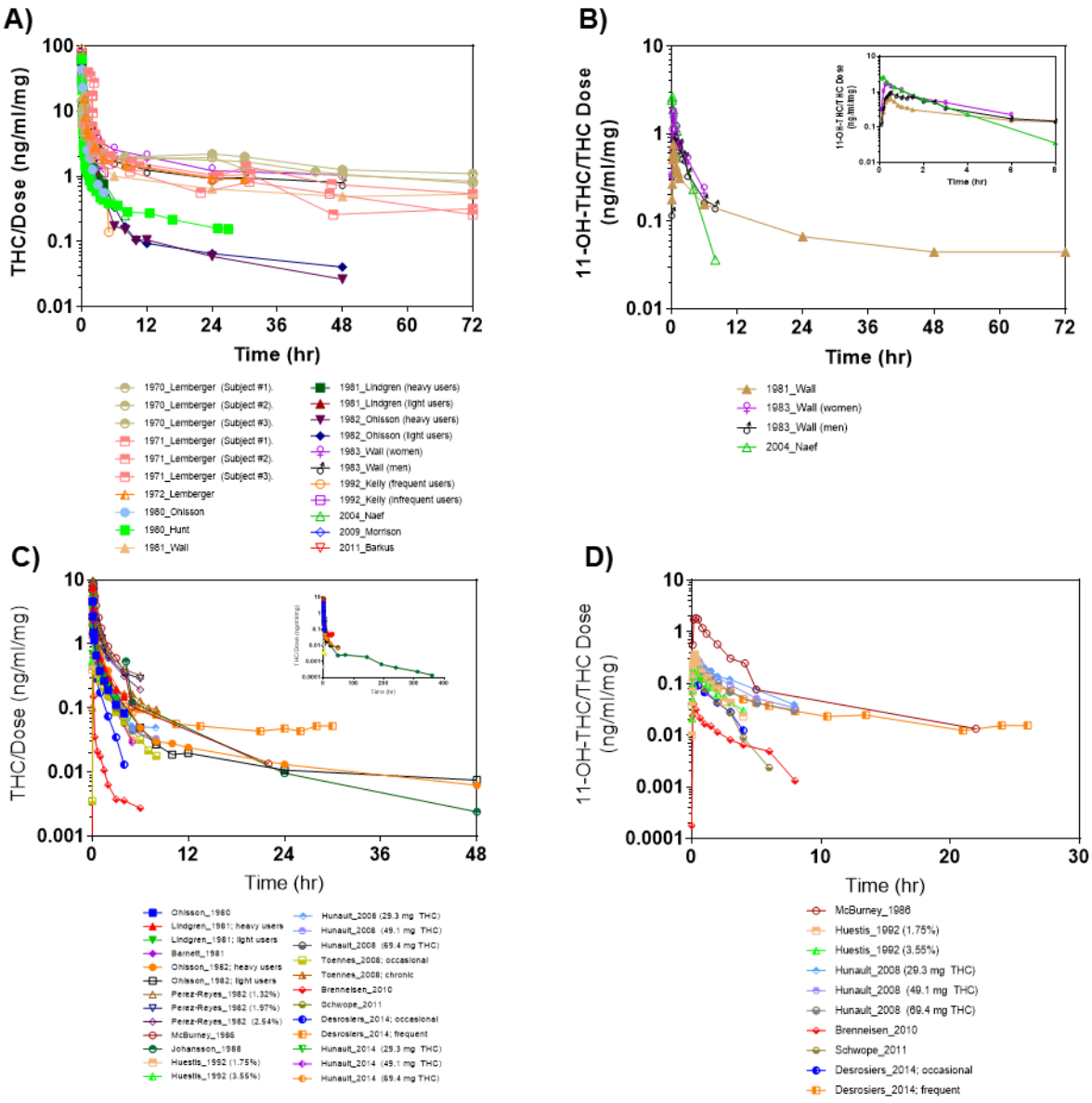

Supplementary Figure 4.1 Dose-normalized IV and inhalation datasets used for THC and 11-OH-THC PBPK model development and verification

Dose-normalized concentration-time profiles of THC (panels A and C) and 11-OH-THC (panels B and D) after IV administration of THC (panels A and B) or inhalation of THC (panels of C and D). The markers represent the mean concentration from each study, except for 1970 and 1971 Lemberger et al where the markers represent individual subjects. 11-OH-THC concentrations are normalized by the administered THC dose. Studies that used TLC (1970, 1971, 1971 Lemberger et al and 1981, 1983 Wall et al) have been removed from PBPK training and verification (panels A-B). Furthermore, Brenneisen et al., 2010 dataset was removed from inhalation verification since the dose-normalized THC and 11-OH-THC concentrations are at least an order of magnitude less than all other studies (panels C-D). Only inhalation studies that measured both THC and 11-OH-THC were used for verification purposes (panel D).

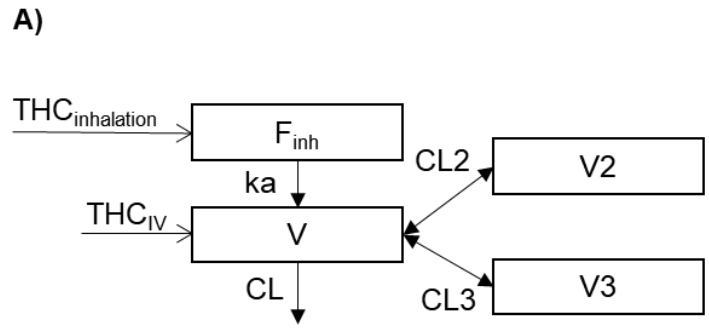

Parameter	Estimate (CV%)
V (L)	22 (19%)
V2 (L)	393 (46%)
V3 (L)	43 (10%)
CL (L/hr)	43 (21%)
CL2 (L/hr)	40 (21%)
CL3 (L/hr)	128 (12%)
Ka (hr^{-1})	12 (11%)
F_{inh}	0.22 (33%)
V_{ss} (L/kg)[a]	6.5 (39%)
MRT (hr)	11 (56%)
$t_{1/2}$ (hr)	14 (48%)

[a] assuming a 70 kg individual

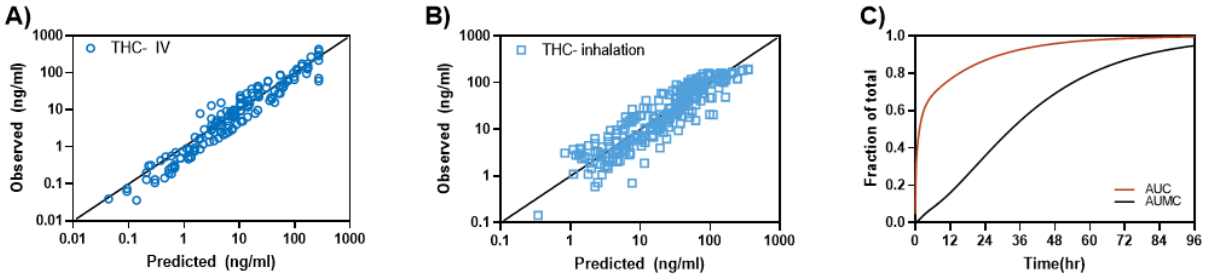

Supplementary Figure 4.2. Non-linear mixed effects (NLME) model for estimating in vivo PK input parameters for THC PBPK model development

A) Three-compartment NLME model with absorption after inhalation was fit to observed THC mean concentrations from IV and inhalation datasets (detailed in **Supplementary Tables 4.1-4.2** and shown in **Supplementary Figure 4.1**). Observed versus predicted THC concentrations for B) IV and C) inhalation datasets. C) Theoretical simulation of the impact of sampling time on AUC and AUMC measurements. Using the final parameter estimates show in panel A, THC concentrations after IV administration were simulated and AUC and AUMC from 0 to t were calculated using the trapezoidal rule. Due to the fast-initial decline in concentrations (α and β half-lives were estimated as 3.5 and 42 minutes, respectively), majority of the THC AUC will be captured within the first 12 hours. However, due to the long terminal half-life of 14 hours, much longer sampling time is necessary to fully capture the THC AUMC. As such, studies that sampled less than 12 and 56 hours will underestimate THC CL and V_{ss}, respectively, since less than 80% of AUC_{inf} and $AUMC_{inf}$ is captured.

Chapter 5. Prospective predictions of maternal and fetal cannabinoid maternal-fetal concentrations throughout pregnancy using PBPK M & S

5.1. ABSTRACT

In order to assess the risk associated with maternal cannabis use, the maternal and fetal cannabinoid (THC and 11-OH-THC) exposure must be known. Here, we extrapolate the linked THC/11-OH-THC PBPK model in healthy nonpregnant subjects from **Chapter 4**. By applying gestational-age dependent physiological changes, which includes increase in P450 activity and decrease in protein binding proteins, the exposure (concentrations and AUC) of THC and 11-OH-THC were simulated during the first, second, and third trimester (T1, T2, T3, respectively). Simulations show that during pregnancy, THC AUC does not change but 11-OH-THC AUC decreased by up to 90%. However, the combined THC and 11-OH-THC exposure decreased by 20%. As such, the exposure to the cannabinoids is similar before and during pregnancy. Using the pregnancy THC/11-OH-THC PBPK model, a preliminary extrapolation was made and compared to observed data of maternal THC concentrations at delivery. Lastly, fetal (F) and maternal (M) THC concentrations were simulated using a maternal-fetal PBPK and compared to observed F/M pairs in the presence and absence of placental active efflux.

5.2. INTRODUCTION

Pregnant women use cannabis at the highest frequency amongst all illicit drugs (SAMHSA, 2017). Furthermore, the concentrations of THC, the psychotropic component in cannabis, have steadily been increasing over the past two decades (ElSohly et al., 2016). It is not known how the increase in frequency of use during pregnancy and potency of THC will ultimately impact maternal and fetal outcomes. Thus, in order to anticipate the risk of maternal cannabis use, it is necessary to quantify or predict maternal and fetal exposure to THC and its active hydroxy metabolite, 11-OH-THC.

Due to the ethical and logistical constraints, clinical studies to assess the maternal and fetal exposure, safety, and toxicity of THC are not possible. PBPK M & S is a non-invasive alternative to make in silico predictions of THC and 11-OH-THC maternal and fetal exposure throughout pregnancy. Our lab has previously demonstrated the validity of using PBPK M & S to predict maternal and fetal exposure to a variety of drugs (Ke et al., 2012; Ke et al., 2014a; Zhang and Unadkat, 2017).

The aim of this study was to extrapolate the linked THC/11-OH-THC PBPK model in healthy nonpregnant subjects (**Chapter 4**) by adjusting for gestational-age dependent physiological changes, such as increase in CYP2C9 and CYP3A4 activity and decrease in albumin concentrations. Dynamic predictions of THC and 11-OH-THC concentrations throughout pregnancy were made to see how the gestational-age dependent changes impact the PK of THC and 11-OH-THC. A preliminary extrapolation of THC concentrations was made and compared with observed maternal concentrations at delivery. Using a maternal-fetal PBPK model previously established in our lab (Zhang and Unadkat, 2017), we simulated the maternal and fetal THC concentrations after smoking cannabis in the presence and absence of placental transport and compared with observed values.

5.3. METHODS

5.3.1. Disposition of THC and 11-OH-THC by placental human microsomes (HPM)

Previously prepared HPM (human placental microsomes) samples were utilized to study placental disposition of THC and 11-OH-THC (Anoshchenko et al. – manuscript in preparation). Briefly, preterm and term placentae from normal pregnancies were obtained from University of Washington Birth Defect Research Laboratory (Seattle, WA) or were provided by Labor and Delivery Unit at the University of Washington (Seattle, WA), respectively. HPMs (0.25 – 0.5 mg/ml) from T1 (n = 2), T2 (n = 4), or T3 (n = 2) were incubated with 500 nM THC or 50 nM 11-OH-THC in 0.1 M potassium phosphate buffer containing 0.2% BSA in the presence of NADPH regenerating system (CYP metabolism) or UDPGA (UGT metabolism) using experimental conditions as previously described (Patilea-Vrana et al., 2018). In all studies THC, 11-OH-THC, and COOH-THC was monitored via LC-MS/MS as previously described (Patilea-Vrana et al., 2018). Two independent experiments with single or duplicate determinations (depending on sample availability) were performed.

5.3.2. Extrapolating the linked THC/11-OH-THC PBPK model from healthy population to pregnant women

An overview of the THC/11-OH-THC PBPK model development and extrapolation to pregnancy is shown in **Figure 5.1**. Based off phenytoin (a CYP2C9 substrate) data in pregnant and nonpregnant

subjects as well as PBPK modeling in pregnancy previously done in our lab, CYP2C9 activity increases 40%, 50%, and 60% during the first, second, and third trimester (T1-T3), respectively (Ke et al., 2014a). Based off midazolam (CYP3A4 substrates) in pregnant and nonpregnant subject as well as in vitro evidence and PBPK modeling previously done in our lab, CYP3A4 activity increases 100% throughout pregnancy (T1-T3) (Hebert et al., 2008; Ke et al., 2012; Zhang et al., 2015). There is no significant change to zidovudine (a UGT2B7 substrate) during pregnancy, suggesting there is no increase in the UGT2B7 activity during pregnancy (O'Sullivan et al., 1993). There is no current data on the changes to UGT1A9 during pregnancy (Anderson, 2005; Tasnif et al., 2016). The final linked THC/11-OH-THC model shown in **Chapter 4** was used to simulated disposition of THC and 11-OH-THC in a pregnant population (gestational age (GW) = 40 weeks) after THC inhalation using the Simcyp Virtual Pregnancy Population. Within the Virtual Pregnancy Population, CYP2C9 and CYP3A4 expression was increased by 40%, 60%, and 100%, for T1, T2, and T3, respectively. The trial design consisted of 10 trials with 10 subjects per trial of women age 20-45 aged at GW = 12, 26, and 40 weeks to represent T1, T2, and T3, respectively.

5.3.3. Simulating THC maternal and fetal concentrations in the presence and absence of placental active efflux

Only one human clinical studied measured THC serum concentrations in maternal blood and umbilical cord (fetal) blood at delivery (Blackard and Tennes, 1984). The study had ten subjects that reported daily cannabis use during the third trimester. Of the total subjects, five maternal and six fetal THC serum concentrations were below the lower limit of sensitivity (0.2 ng/ml), leaving only three viable fetal-maternal (F/M) concentrations pairs (Subjects A, B, C). Information on the time since last smoking cannabis is provided but the dose is not. The THC dose the subjects may have inhaled was calculated by multiplying the average % THC (w/w) in 1984 (ElSohly et al., 2000) with the average weight of a joint (Mariani et al., 2011). The THC dose was approximated to be 21.8 mg. Simulations were performed using a THC dose of 21.8 mg and inhalation bioavailability of 0.35, which was calculated for chronic cannabis users (see **Chapter 4**). Simulated plasma concentrations are reported since it was assumed serum and plasma THC concentrations are similar.

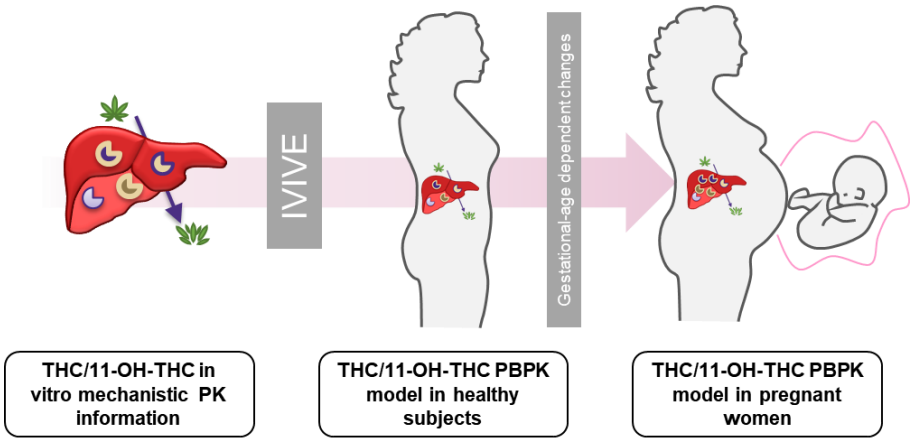

Figure 5.1. Development of the THC/11-OH-THC PBPK model during pregnancy.
The in vitro mechanistic PK information from **Chapters 2** and **3** was extrapolated to in vivo to build a linked THC/11-OH-THC PBPK model in nonpregnant population. The verified THC/11-OH-THC PBPK model for inhalation of THC from **Chapter 4** was extrapolated to pregnancy by accounting for gestational-age physiological changes.

Fetal concentrations of THC in the presence of placental efflux transport were simulated using a maternal-fetal model previously described (Zhang et al., 2017a; Zhang and Unadkat, 2017). Using the observed maternal plasma concentrations from Subjects A-C, adjustments were made to the THC dose in order for the simulated maternal THC plasma concentration to match the observed data. This was done to ensure that the maternal plasma concentrations, which drive fetal concentrations, were well predicted. Since THC is a highly lipophilic drug, a large placental passive diffusion clearance of 500 L/hr was assumed (this is the same passive diffusion clearance as midazolam, which was previously used as a calibrator in the m-f-PBPK model, see Zhang et al., 2017b for more details). Additionally, no placental or fetal THC metabolism was assumed. The simulations were first run with no placental efflux transport. To match the observed fetal concentrations, the fraction (ft) of active placental efflux (expressed as a fraction of active plus passive clearance) was manually adjusted in order for the simulated fetal THC concentration to match observed value.

5.4. RESULTS

5.4.1. Depletion of THC and 11-OH-THC by HPMs

The depletion of 500 nM THC and 50 nM 11-OH-THC (P450 and UGT mediated) was tested in HPMs from T1, T2, and T3 subjects (n = 10 total subjects). As shown in **Figure 5.2**, there was minimal depletion of either THC or 11-OH-THC in the samples tested. This indicates minimal metabolism of THC and 11-OH-THC in the placenta. To note, the HPM metabolic integrity was checked by monitoring the conversion of testosterone to β – estradiol via CYP19, the majorly expressed DME in the placenta (Al-Enazy et al., 2017). β – estradiol concentrations increased with incubation time, showing metabolic activity in the HPMs tested (n=3, two T2 and one T3 HPM) (data not shown).

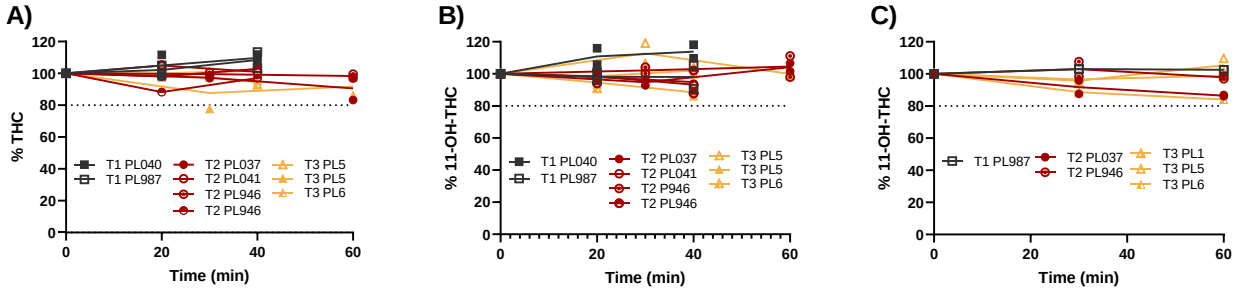

Figure 5.2. Depletion of THC and 11-OH-THC in placental human microsomes
Depletion of A) THC, and 11-OH-THC by B) P450 and C) UGT enzyme in placental microsomes. Showing data from two independent experiments (one with t=40 min and t=60 min) with duplicate determinations for each experiment. T1, T2, T3 designated placental samples was from a subject in the first, second, or third trimester. The ID of each subject is listed after trimester designation. Because of sample availability, subject PL946 and PL5 was tested in both experiments.

5.4.2. Extrapolation of THC and 11-OH-THC concentrations during different stages of pregnancy

Gestational-age dependent changes were applied to the final linked THC/11-OH-THC PBPK model shown in **Chapter 4** and cannabinoid disposition were simulated at the end of T1 (GW = 12), T2 (GW = 26), at T3 (GW = 40). As show in **Figure 5.3**, the overall simulated THC concentration-time profile or AUC did not change during pregnancy. The simulated 11-OH-THC AUC decreased 50%, 70%, and 90% during T1, T2, and T3 respectively. Overall, the simulated combined THC + 11-OH-THC AUC decreased 10-20% during pregnancy.

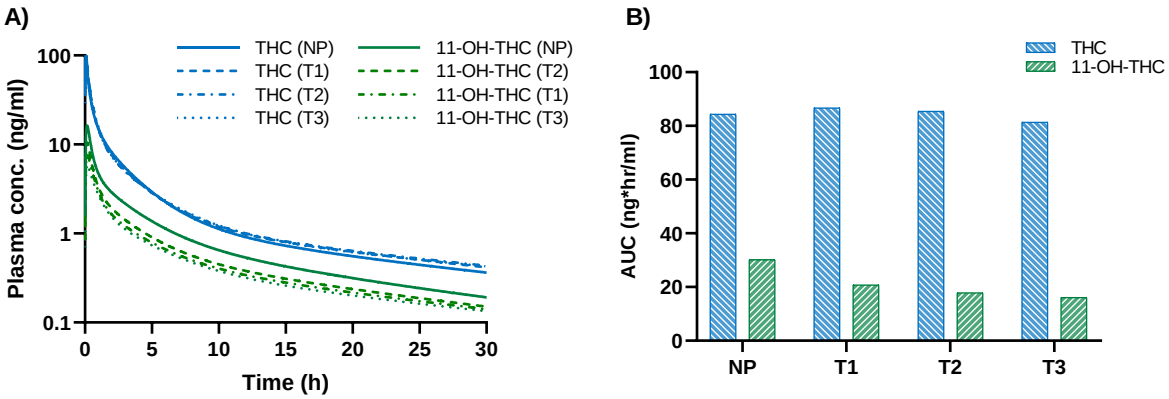

Figure 5.3. Simulation of THC and 11-OH-THC disposition during different stages of pregnancy
Simulation of THC and 11-OH-THC **A)** concentration-time profile and **B)** AUC in nonpregnant (NP) and pregnant (T1: first trimester (GW = 12), T2: second trimester (GW = 26), T3: third trimester (GW = 40)) subjects after inhalation of THC.

To investigate the impact of the gestational-age dependent physiological changes on the observed THC and 11-OH-THC PK changes during pregnancy, a systematic sensitivity analysis was performed. As shown in **Table 5.1**, THC AUC was not sensitive to any of the gestational-age dependent changes. 11-OH-THC AUC was most sensitive to the increase in fu_p (simulated fu_p was 0.0050 and 0.0069 for NP and T3, respectively). The next sensitive parameter to 11-OH-THC AUC was the increase in the overall P450 enzyme depletion clearance (represented by 11-OH-THC CYP3A4 and CYP2C9 V_{max}). Even though 50% increase in CYP2C9 activity led to 50% increase the intrinsic formation clearance of 11-OH-THC (represented by THC CYP2C9 V_{max}), the overall formation fm increased from 0.91 to 0.94. As such, the increase in intrinsic formation clearance was not a sensitive parameter. Pooling the information together, the simulated decrease in 11-OH-THC AUC during pregnancy was due to an increase in unbound elimination clearance of 11-OH-THC.

5.4.3. Simulated maternal-fetal THC concentrations with and without placental efflux

To test if the extrapolation of THC from the nonpregnant to pregnant population, THC plasma concentrations were simulated after inhalation of an average joint with THC concentrations reflective of 1984 versus the observed data from Blackard and Tennes, 1984 is shown in **Figure 5.4**. While dosing information is missing from Blackard and Tennes, 1984, the simulated concentrations after inhalation of

THC dose representative of THC levels in 1984 are comparable to the observed data, indicating partial success.

Table 5.1. Sensitivity analysis of gestational-age dependent physiological changes on THC and 11-OH-THC PK

Percent change: input parameters						Percent change: output parameters			
THC		11-OH-THC				THC		11-OH-THC	
CYP2C9 V_{max}	fu_p	CYP2C9 V_{max1}	CYP2C9 V_{max2}	CYP3A4 V_{max}	fu_p	C_{max}	AUC_{0-t}	C_{max}	AUC_{0-t}
—	—	↑50%	↑50%	—	—	↔	↔	↓10%	↓10%
—	—	—	—	↑100%	—	↔	↔	↓20%	↓20%
↑50%	—	—	—	—	—	↔	↔	↑10%	↔
—	—	—	—	—	↑40%	↔	↔	↓40%	↓40%
—	↑40%	↑50%	—	—	—	↓10%	↓10%	↓10%	↔
—	—	↑50%	↑50%	↑100%	—	↔	↔	↓20%	↓30%
↑50%	—	↑50%	↑50%	↑100%	—	↔	↔	↓10%	↓20%
↑50%	—	↑50%	↑50%	↑100%	↑40%	↔	↔	↓60%	↓70%
↑50%	↑40%	↑50%	↑50%	↑100%	↑40%	↓10%	↓10%	↓80%	↓80%

[a] Sensitivity analysis was run in a nonpregnant population to demonstrate how the physiological changes observed in pregnancy help explain the simulated change in THC and 11-OH-THC during pregnancy (**Figure 5.3**). The input parameters are the fold PK changes caused by gestational-age dependent physiological changes were as follows: 50% and 100% increase in CYP2C9 and CYP3A4 activity, increase in THC and 11-OH-THC fu_p from 0.0022 to 0.0039 and 0.005 to 0.0069 (as predicted by the simulation of THC and 11-OH-THC in a pregnant population by Simcyp at GW = 40 weeks). To note, while there is an increase in CYP2D6 activity during pregnancy (Anderson, 2005; Tasnif et al., 2016), no sensitivity analysis was run since CYP2D6 fm is small (fm = 0.09). Furthermore, no sensitivity analysis was run on UGT-mediated clearance of 11-OH-THC since expression of UGT2B7 or UGT1A9 does not change during pregnancy (Anderson, 2005; Tasnif et al., 2016). Lines means input parameter was not changed.

THC plasma concentrations were simulated using the m-f-PBPK model as shown in **Table 5.2**. The dose for each subject was adjusted in order for the simulated THC maternal plasma concentration to approximate the observe value. This was to ensure that the maternal concentrations that drive fetal THC concentrations are well predicted. The observed THC F/M range 0.17 – 0.38 (mean = 0.26). This suggests that there is placental efflux, placental metabolism, or fetal metabolism that limits fetal exposure to THC. Indeed, simulations were run in the absence of any placental and fetal metabolism/transport, the simulated F/M overpredicted the observed values (**Table 5.2**). Since the HPM studies showed limited depletion (**Figure 5.2**) and activity in recombinant CYP3A7 was low (**Chapter 2 – Figure 2.1**), we simulated the impact of placental efflux. We manually adjusted the placental efflux ft (representing total active efflux clearance) and observed that a ft of 0.88 – 0.92 (average = 0.91) was necessary to

recapitulate the observed fetal THC concentrations (**Table 5.2**). This analysis suggests that placental efflux clearance is much higher than placental passive diffusion clearance of THC.

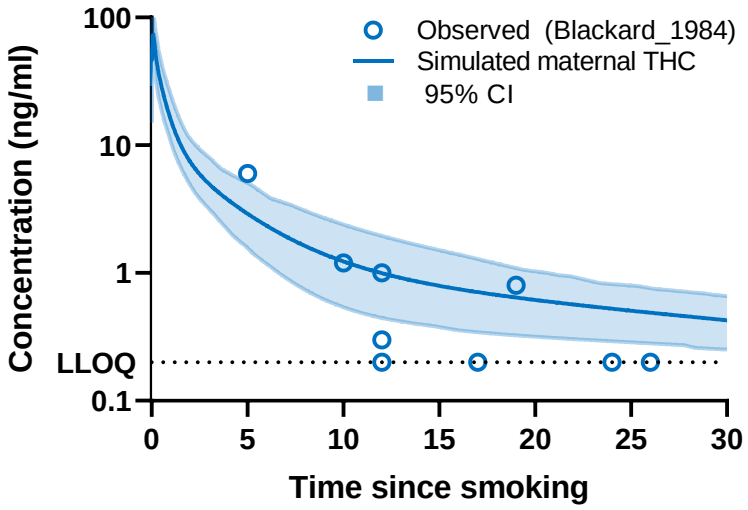

Figure 5.4. Extrapolation of maternal THC plasma concentrations during pregnancy and comparison with observed data.

A) Simulated plasma THC concentrations at term (GW= 40) and observed maternal values at delivery after smoking cannabis. To note, each marker represents observed value from a different subject (ten total subjects, four subjects had THC levels below the lower limit of quantification (LLOQ), and one subject did not have time after smoking information and was not included). The report by Blackard and Tennes, 1984 does not report the dose of THC used by the subjects. As such, simulations were run assuming a dose representative of average THC concentrations in cannabis in 1984 (see **Methods** section).

Table 5.2. Observed and simulated maternal and fetal THC concentrations with and without placental efflux

Observed					Simulated					
Subject[a]	Hours since smoking	Maternal THC (ng/ml)	Fetal THC (ng/ml)	F/M Ratio	Maternal[b] THC (ng/ml)	ft[c]	Fetal THC[c] (ng/ml)	F/M ratio	ft[d]	Fetal THC[d] (ng/ml)
A	5	6	1	0.17	6.0	0	5.3	0.9	0.88	1.0
B	10	1.2	0.3	0.25	1.2	0	2.9	2.4	0.93	0.3
C	19	0.8	0.3	0.38	0.8	0	3.3	4.1	0.92	0.3

[a] Serum maternal and fetal umbilical cord concentration pairs from Blackard and Tennes, 1984. [b] THC dose was adjusted manually in order for the simulated maternal THC plasma concentrations to match observed value. To note, it was assumed THC plasma and serum concentrations were similar. [c] Simulated fetal THC concentrations and F/M are shown when the placental efflux ft, expressed as the fraction of total placental efflux and passive diffusion clearance was set to zero. [d] Placental efflux ft was manually optimized in order for simulated fetal THC concentration (and therefore F/M) to match observed value. Simulations demonstrate that in the absence of placental efflux transport, the fetal concentrations are overestimated.

5.5. DISCUSSION

Previous studies from our lab demonstrated successful prediction of drugs, such as midazolam, indinavir, and glyburide, using PBPK M & S (Ke et al., 2012; Ke et al., 2014a). Using the same approach, exposure of THC and 11-OH-THC after inhalation of THC was simulated throughout pregnancy by extrapolating the THC/11-OH-THC PBPK model from **Chapter 4** by accounting for gestational-age dependent changes. As predicted in **Chapter 4**, increase in CYP2C9 activity during pregnancy did not affect THC AUC. This is because THC clearance is blood flow limited and not sensitive to changes in THC intrinsic clearance (CL_{int}). 11-OH-THC AUC was predicted to decrease 90% by T3 (**Figure 5.3**). The AUC of 11-OH-THC is defined as shown in **Eq. 29**.

$$AUC_{11\text{–}OH\text{–}THC} = \frac{fm \times CL_{THC}}{fuCL\,int_{11\text{–}OH\text{–}THC}} \quad (29)$$

The 50% increase in CYP2C9 caused THC CYP2C9 fm value to change from 0.91 to 0.94. If 11-OH-THC had a smaller fm value, then the impact of CYP2C9 increased activity may be more pronounced. This may be true for subjects with CYP2C9 genetic polymorphism that confer decreased activity (and therefore lower fm). However, it is unknow if polymorphic CYP2C9 activity changes in a similar manner as the wild-type allele. The pregnancy-induced increase in both 11-OH-THC fu (from 0.005 to 0.0069) combined with the increase in 11-OH-THC CL_{int} due to increased activity of CYP2C9 and CYP3A4 caused the overall 11-OH-THC AUC to decrease up to 90% during pregnancy. While this is a significant decrease in 11-OH-THC exposure during pregnancy, the combined THC and 11-OH-THC AUC decreased 20%. Therefore, the overall cannabinoid (THC and 11-OH-THC) AUC is predicted to be similar before and during pregnancy.

The study by Blackard and Tennes, 1984 is the only available dataset of paired maternal and fetal concentrations in humans. While lacking in dosing information, the preliminary extrapolation for THC shown in **Figure 5.4** is promising. Unfortunately, 11-OH-THC concentrations were not measured in Blackard and Tennes, 1984 study and no other datasets exist. Further verification using observed THC and 11-OH-THC concentrations in maternal plasma and umbilical blood is necessary.

The observed THC F/M concentrations ratios in humans ranged from 0.17 – 0.38 (mean = 0.26) (Blackard and Tennes, 1984). Initial simulations assuming no placental and fetal metabolism or transport overestimated the THC F/M concentration ratio (**Table 5.2**). Since the observed THC F/M is less than one, placental and fetal metabolism or placental efflux may limit exposure of THC to the fetus. Based off recombinant enzyme studies in **Chapter 2**, CYP1A1, UGT1A9, and UGT2B7, enzymes that are expressed in the placenta (assessed via protein expression) (Al-Enazy et al., 2017), turned over THC and 11-OH-THC (UGTs only). However, there was minimal depletion in the HPMs tested (**Figure 5.2**). To note, there is wide interindividual variability in the activity of placental CYP1A1 and UGT2B7 (Collier et al., 2002), and the small sample size in this study may be insufficient in detecting the turnover of THC and 11-OH-THC by HPMs. Furthermore, fetal metabolism is unlikely to be a big contributor to fetal exposure because the fetal liver is small and the clearance of CYP3A7 observed in **Chapter 2, Figure 2.1** was also small. Another possibility for the THC F/M is active placental efflux. Indeed, THC is a substrate of P-gp and BCRP (Bonhomme-Faivre et al., 2008; Spiro et al., 2012a). In *Abcb1a/b(-/-)* (P-gp) and *Abcg2 (-/-)* (BCRP) mice, THC had up to 4.2- and 6.1-fold increase in the brain/blood ratio compared to wild-type mice, respectively (Spiro et al., 2012a). Based off the increase in the THC brain/blood ratio in the knock-out versus wild-type mice, the THC P-gp and BCRP ft is as high as 0.76 and 0.83, respectively (Prasad and Unadkat, 2015). In order to recapitulate the observed F/M ratios, we estimated the average placental efflux ft was 0.91. While the ft via P-gp and BCRP may not be large, the ft of the combined clearances of P-gp and BCRP may become significant (Kusuhara and Sugiyama, 2009). For example, if both the ft of P-gp and BCRP at the placenta was 0.45 each, then the combined placental efflux ft would be 0.90. It should be noted that the magnitude of placental diffusion clearance can also impact the F/M ratio (Zhang et al., 2017a). However, the psychoactive effects of THC are within minutes after inhalation, thus demonstrating good permeability across the blood-brain barrier. Alternatively, if there is significant placental metabolism, then the placental efflux ft would be smaller than what was estimated. Due to the small sample size of HPMs in this study, further studies are needed to confirm placental metabolism of THC as well as efflux via P-gp and BCRP. The latter can be addressed with P-gp/BCRP single and double knock-out animals and with the perfused human placenta with and without inhibitors of P-gp and/or BCRP.

Overall, THC and 11-OH-THC disposition was extrapolated from healthy subjects (**Chapter 4**) to pregnancy. Simulations show that during pregnancy, THC AUC does not change, 11-OH-THC AUC decreases up to 90%, but the combined THC and 11-OH-THC exposure did not decrease by a large amount. Simulated THC pal concentrations after smoking a THC dose representative of THC doses in 1984 were comparable to observed values from Blackard and Tennes, 1984. However, this is not enough to verify the THC pregnancy extrapolation. Lastly, we simulated THC fetal concentrations and estimated the placental efflux ft necessary to recapitulate observed values.

Chapter 6. General conclusions and future directions

6.1. GENERAL CONCLUSIONS

Subtle but persistent neurodevelopmental effects and lower birth weight are associated with maternal cannabis use. However, confounding factors, such as reliance on self-reporting, concurrent tobacco and alcohol use, diverse socioeconomic background, changing composition of cannabis, and varying cannabis administration routes make it difficult to establish the independent risk factors of maternal cannabis use using observational studies. Prospective studies to study the safety and toxicity of cannabis in pregnant women are not possible due to ethical considerations Preclinical studies have identified THC, the psychoactive component in cannabis, and its active hydroxy metabolite, 11-OH-THC can dysregulate the endocannabinoid system and lead to toxicity during early pregnancy advancement, placentation, and fetal neurodevelopment. It is difficult to translate the magnitude of toxicity observed in preclinical studies to humans since it is unknown how the doses/concentrations of THC used in preclinical studies relate to those observed in-utero in humans. Measuring maternal and fetal concentrations throughout pregnancy is not logistically or ethically possible. An alternative is to make in silico predictions using PBPK M & S. PBPK models incorporates physiological data, such as tissue composition and blood flows, with mechanistic drug PK parameters, such as metabolism and transport, to mechanistically predict in vivo disposition of a xenobiotic. Utilizing PBPK M & S, the objective of this dissertation project was to prospectively predict cannabinoid (THC and its active metabolite, 11-OH-THC) exposure in pregnant women and the fetus. By bridging THC and 11-OH-THC mechanistic PK data with PBPK modeling, this project provides the mechanistic foundation to dynamically predict clinically relevant predictions of maternal and fetal THC exposure following cannabis consumption.

In the first half of project, we identified and quantified the enzyme kinetics of DMEs important in THC and 11-OH-THC disposition. In **Chapter 2**, we conducted reaction phenotyping studies using recombinant P450 and UGT enzymes to identify which DMEs deplete THC and 11-OH-THC and form 11-OH-THC. While similar in vitro studies have been previously done, they focused on only the formation of 11-OH-THC (Bornheim et al., 1992; Watanabe et al., 2007; Mazur et al., 2009b). We confirmed previous observations and in addition found that CYP1A1, CYP3A7, UGT1A9, and UGT2B7 metabolize THC and 11-OH-THC. These DMEs are of particular importance since they are present in the placenta and fetal

liver (CYP3A7 only). We then quantified the fractional contribution of each DME in human liver microsomes using selective chemical inhibitors and adjusting for enzyme cross-inhibition. Importantly, we did these studies using pharmacologically relevant concentrations of THC and 11-OH-THC after smoking cannabis (500 nM THC and 50 nM 11-OH-THC). We found CYP2C9 is the major DME responsible for THC depletion and 11-OH-THC formation while 11-OH-THC depletion is split between UGT enzymes, CYP3A4, and CYP2C9. Unlike previous studies, we found CYP3A4 contribution was negligible to THC depletion. However, the THC concentrations used in those studies ranged from 64 – 130 μM (Bornheim et al., 1992; Watanabe et al., 2007) and likely saturated CYP2C9. Indeed, in **Chapter 3** we quantified the kinetics (CL_{int}, V_{max}, K_m) of individual enzyme pathways using in vitro modeling and found CYP2C9 becomes saturated at low μM range. In addition, we quantified the kinetics for THC depletion via CYP2C9 and CYP2D6, and 11-OH-THC depletion via CYP2C9, CYP3A, and UGT enzymes. The enzyme fractional contributions estimated using in vitro modeling approach were comparable with our results using chemical inhibitors shown in **Chapter 2**.

In **Chapter 4**, the mechanistic PK information provided in **Chapters 2** and **3** was extrapolated to in vivo via IVIVE and used to build and verify a PBPK model of THC and 11-OH-THC disposition in nonpregnant population. Based off our optimization (only had to change fu_p), success criteria, and model performance, we conclude the IVIVE was successful. Furthermore, we recognized that while 11-OH-THC formation is much greater than its elimination (based of CL_{int}), and thus would be expected to be elimination rate-limited, it is not. This is because the apparent formation of 11-OH-THC in plasma is driven by the blood-flow limited THC plasma clearance. This helps explain why the 11-OH-THC to THC AUC plasma ratios are less than one and the cannabinoids have similar half-lives. We found that the difference in THC AUCs after inhalation were different between chronic and casual cannabis users was because of difference in inhalation bioavailability (F_{inh}) and not differences in THC clearance. We estimated F_{inh} of 0.35 and 0.19 for chronic and casual users, respectively. The difference is likely due to user experience (e.g. chronic users have longer puff volume and duration compared to casual users) and tolerance to THC. Overall, in this **Chapter** we verified a linked THC/11-OH-THC model for inhalation of THC in a healthy nonpregnant population.

In **Chapter 5,** we extrapolated the verified THC/11-OH-THC PBPK model in nonpregnant population by adjusting for gestational-age dependent changes. This included an increase in CYP2C9, CYP3A4, and CYP2D6 and no change to UGT expression at various stages during pregnancy. Our simulations show that THC AUC does not change during pregnancy but 11-OH-THC AUC decreased up to 90% by the third trimester. However, the combined cannabinoid exposure (THC + 11-OH-THC AUC) decreased by up to 20%. While the pregnancy THC/11-OH-THC PBPK model could not be verified, a preliminary extrapolation was made and compared to observed data of maternal THC concentrations at delivery. Because the preliminary extrapolation was promising, THC and 11-OH-THC concentrations were simulated for inhalation of a contemporary THC dose in chronic and casual users. Furthermore, fetal THC concentrations in these simulations were calculated based on the observed fetal to maternal (F/M) THC concentration ratios. The results from these simulations will inform in vitro and animal studies on the pharmacologically relevant cannabinoid concentrations to be used when assessing the effects of fetal cannabinoid (THC and 11-OH-THC) exposure, and thus ultimately help further knowledge on the safety and toxicity of cannabis use during pregnancy.

6.2. FUTURE DIRECTIONS

The simulations of maternal and fetal THC and 11-OH-THC concentrations need to be verified in humans. Ideally, verification should be done in a similar fashion as for the linked THC/11-OH-THC nonpregnant model in **Chapter 3**. However, it is logistically difficult to obtain maternal samples, particularly in this instance where cannabis is considered a controlled substance I. Furthermore, it is only possible to obtain fetal concentrations at delivery and not any time prior. Nevertheless, opportunistic studies could identify subjects that already use cannabis during pregnancy.

The mean observed THC F/M in humans was 0.26 (Blackard and Tennes, 1984). This suggests that there may be placental efflux, metabolism, or fetal metabolism that limits THC fetal exposure. Our studies in placental microsomes from first through third trimester showed minimal metabolism of THC and 11-OH-THC (**Chapter 5**) even though these cannabinoids are turned over by CYP1A1, UGT1A9, and UGT2B7 (**Chapter 2**). THC is transported by P-gp and BCRP (Bonhomme-Faivre et al., 2008; Spiro et al., 2012a), and the activity of these placental efflux transporters may be the reason for the observed F/M

ratio. Therefore, the efflux of THC and 11-OH-THC by these two transporters needs to be verified in animal studies usual dual P-gp/BCRP knock-outs and perfused placenta studies.

To dynamically predict THC and 11-OH-THC fetal concentrations via m-f-PBPK modeling (Zhang and Unadkat, 2017), the placental metabolism of the cannabinoids needs to be verified as well as placental efflux and passive diffusion clearance needs to be elucidated. Our previous m-f-PBPK model calculates placental passive diffusion based off the xenobiotic's in vitro measured permeability (P_{app}) to that of midazolam's (the model's reference point). There is no measurement of THC or 11-OH-THC P_{app} in established epithelial cell lines (i.e., Madin-Darby canine kidney and Caco-2). This is an important parameter to establish since the placental passive diffusion impacts fetal but not maternal concentration-time profiles, and thus the F/M ratio at a given sampling time (Zhang et al., 2017a).

The nonpregnant THC/11-OH-THC PBPK model can be extended to include oral (PO) administration of THC as well. For this, mechanistic information on intestinal metabolism is necessary. Based of our previous results, there may be intestinal metabolism due to CYP2C9 and UGT2B7. Furthermore, a PO PBPK model is necessary to verify hepatic THC CL_{int} values. As demonstrated in **Chapter 4**, THC CL_{int} is not a sensitive parameter to THC plasma clearance due to blood flow limitations. However, during oral administration, the apparent plasma clearance is a function of hepatic clearance and bioavailability. As such, changes in CL_{int} should be reflective in changes to THC AUC. Indeed, when given THC orally, CYP2C9 deficient carriers (*CYP2C9*3/*3*) have a three-fold higher THC plasma $AUC_{0\text{-}inf}$ (Sachse-Seeboth et al., 2009). Lastly, 11-OH-THC AUC is approximately twice as large as THC AUC after oral administration of THC, and therefore will contribute more to the combined effect, and therefore toxicity, when compared to inhalation.

REFERENCES

Achour B, Rostami-Hodjegan A, and Barber J (2014) Protein expression of various hepatic uridine 5'-diphosphate glucuronosyltransferase (UGT) enzymes and their inter-correlations: a meta-analysis. *Biopharm Drug Dispos* **35:**353-361.

Agurell S, Carlsson S, Lindgren JE, Ohlsson A, Gillespie H, and Hollister L (1981) Interactions of delta 1-tetrahydrocannabinol with cannabinol and cannabidiol following oral administration in man. Assay of cannabinol and cannabidiol by mass fragmentography. *Experientia* **37:**1090-1092.

Agurell S, Halldin M, Lindgren JE, Ohlsson A, Widman M, Gillespie H, and Hollister L (1986) Pharmacokinetics and metabolism of delta 1-tetrahydrocannabinol and other cannabinoids with emphasis on man. *Pharmacol Rev* **38:**21-43.

Al-Enazy S, Ali S, Albekairi N, El-Tawil M, and Rytting E (2017) Placental control of drug delivery. *Adv Drug Deliv Rev* **116:**63-72.

Alaniz VI, Liss J, Metz TD, and Stickrath E (2015) Cannabinoid hyperemesis syndrome: a cause of refractory nausea and vomiting in pregnancy. *Obstet Gynecol* **125:**1484-1486.

Alpár A, Di Marzo V, and Harkany T (2016) At the Tip of an Iceberg: Prenatal Marijuana and Its Possible Relation to Neuropsychiatric Outcome in the Offspring. *Biol Psychiatry* **79:**e33-45.

Anderson GD (2005) Pregnancy-induced changes in pharmacokinetics: a mechanistic-based approach. *Clin Pharmacokinet* **44:**989-1008.

Andrews KH and Bracero LA (2015) Cannabinoid Hyperemesis Syndrome During Pregnancy: A Case Report. *J Reprod Med* **60:**430-432.

Arnold JC, Hone P, Holland ML, and Allen JD (2012) CB2 and TRPV1 receptors mediate cannabinoid actions on MDR1 expression in multidrug resistant cells. *Pharmacol Rep* **64:**751-757.

Awasthi R, An G, Donovan MD, and Boles Ponto LL (2018) Relating Observed Psychoactive Effects to the Plasma Concentrations of Delta-9-Tetrahydrocannabinol and Its Active Metabolite: An Effect-Compartment Modeling Approach. *J Pharm Sci* **107:**745-755.

Azorlosa JL, Greenwald MK, and Stitzer ML (1995) Marijuana smoking: effects of varying puff volume and breathhold duration. *J Pharmacol Exp Ther* **272:**560-569.

Bailey JR, Cunny HC, Paule MG, and Slikker W (1987) Fetal disposition of delta 9-tetrahydrocannabinol (THC) during late pregnancy in the rhesus monkey. *Toxicol Appl Pharmacol* **90:**315-321.

Banderali G, Martelli A, Landi M, Moretti F, Betti F, Radaelli G, Lassandro C, and Verduci E (2015) Short and long term health effects of parental tobacco smoking during pregnancy and lactation: a descriptive review. *J Transl Med* **13:**327.

Barkus E, Morrison PD, Vuletic D, Dickson JC, Ell PJ, Pilowsky LS, Brenneisen R, Holt DW, Powell J, Kapur S, and Murray RM (2011) Does intravenous Δ9-tetrahydrocannabinol increase dopamine release? A SPET study. *J Psychopharmacol* **25:**1462-1468.

Barnett G, Chiang CW, Perez-Reyes M, and Owens SM (1982) Kinetic study of smoking marijuana. *J Pharmacokinet Biopharm* **10:**495-506.

Barrus DG, Capogrossi KL, Cates SC, Gourdet CK, Peiper NC, Novak SP, Lefever TW, and Wiley JL (2016) Tasty THC: Promises and Challenges of Cannabis Edibles. *Methods Rep RTI Press* **2016**.

Bayrampour H, Zahradnik M, Lisonkova S, and Janssen P (2019) Women's perspectives about cannabis use during pregnancy and the postpartum period: An integrative review. *Prev Med* **119:**17-23.

Benito-Gallo P, Marlow M, Zann V, Scholes P, and Gershkovich P (2016) Linking in Vitro Lipolysis and Microsomal Metabolism for the Quantitative Prediction of Oral Bioavailability of BCS II Drugs Administered in Lipidic Formulations. *Mol Pharm* **13:**3526-3540.

Blackard C and Tennes K (1984) Human placental transfer of cannabinoids. *N Engl J Med* **311:**797.

Bland TM, Haining RL, Tracy TS, and Callery PS (2005) CYP2C-catalyzed delta9-tetrahydrocannabinol metabolism: kinetics, pharmacogenetics and interaction with phenytoin. *Biochem Pharmacol* **70:**1096-1103.

Bonhomme-Faivre L, Benyamina A, Reynaud M, Farinotti R, and Abbara C (2008) Disposition of Delta tetrahydrocannabinol in CF1 mice deficient in mdr1a P-glycoprotein. *Addict Biol* **13:**295-300.

Bornheim LM, Lasker JM, and Raucy JL (1992) Human hepatic microsomal metabolism of delta 1-tetrahydrocannabinol. *Drug Metab Dispos* **20:**241-246.

Brenneisen R, Meyer P, Chtioui H, Saugy M, and Kamber M (2010) Plasma and urine profiles of Delta9-tetrahydrocannabinol and its metabolites 11-hydroxy-Delta9-tetrahydrocannabinol and 11-nor-9-carboxy-Delta9-tetrahydrocannabinol after cannabis smoking by male volunteers to estimate recent consumption by athletes. *Anal Bioanal Chem* **396:**2493-2502.

Brockman AH, Oller HR, Moreau B, Kriksciukaite K, and Bilodeau MT (2015) Simple method provides resolution of albumin, lipoprotein, free fraction, and chylomicron to enhance the utility of protein binding assays. *J Med Chem* **58:**1420-1425.

Brown QL, Sarvet AL, Shmulewitz D, Martins SS, Wall MM, and Hasin DS (2017) Trends in Marijuana Use Among Pregnant and Nonpregnant Reproductive-Aged Women, 2002-2014. *JAMA* **317:**207-209.

Brunet B, Doucet C, Venisse N, Hauet T, Hébrard W, Papet Y, Mauco G, and Mura P (2006) Validation of Large White Pig as an animal model for the study of cannabinoids metabolism: application to the study of THC distribution in tissues. *Forensic Sci Int* **161:**169-174.

Brzozowska NI, de Tonnerre EJ, Li KM, Wang XS, Boucher AA, Callaghan PD, Kuligowski M, Wong A, and Arnold JC (2017) The Differential Binding of Antipsychotic Drugs to the ABC Transporter P-Glycoprotein Predicts Cannabinoid-Antipsychotic Drug Interactions. *Neuropsychopharmacology* **42:**2222-2231.

Chanda D, Neumann D, and Glatz JFC (2019) The endocannabinoid system: Overview of an emerging multi-faceted therapeutic target. *Prostaglandins Leukot Essent Fatty Acids* **140:**51-56.

Chang JC, Tarr JA, Holland CL, De Genna NM, Richardson GA, Rodriguez KL, Sheeder J, Kraemer KL, Day NL, Rubio D, Jarlenski M, and Arnold RM (2019) Beliefs and attitudes regarding prenatal marijuana use: Perspectives of pregnant women who report use. *Drug Alcohol Depend* **196:**14-20.

Chiang CW and Barnett G (1984) Marijuana effect and delta-9-tetrahydrocannabinol plasma level. *Clin Pharmacol Ther* **36:**234-238.

Coleman-Cowger VH, Schauer GL, and Peters EN (2017) Marijuana and tobacco co-use among a nationally representative sample of US pregnant and non-pregnant women: 2005-2014 National Survey on Drug Use and Health findings. *Drug Alcohol Depend* **177:**130-135.

Collier AC, Tingle MD, Paxton JW, Mitchell MD, and Keelan JA (2002) Metabolizing enzyme localization and activities in the first trimester human placenta: the effect of maternal and gestational age, smoking and alcohol consumption. *Hum Reprod* **17:**2564-2572.

Conner SN, Bedell V, Lipsey K, Macones GA, Cahill AG, and Tuuli MG (2016) Maternal Marijuana Use and Adverse Neonatal Outcomes: A Systematic Review and Meta-analysis. *Obstet Gynecol* **128:**713-723.

Cook CE, Hawos ML, Amerson EW, Pitt CG, and Williams D (1976) Radiommunoassay of delta9-tetrahydrocannabinol. *NIDA Res Monogr***:**15-27.

Cook JL and Blake JM (2018) Cannabis: Implications for Pregnancy, Fetal Development, and Longer-Term Health Outcomes. *J Obstet Gynaecol Can* **40:**1204-1207.

Correa F, Wolfson ML, Valchi P, Aisemberg J, and Franchi AM (2016) Endocannabinoid system and pregnancy. *Reproduction* **152:**R191-R200.

Costa MA (2016) The endocannabinoid system: A novel player in human placentation. *Reprod Toxicol* **61:**58-67.

Costa MA, Fonseca BM, Marques F, Teixeira NA, and Correia-da-Silva G (2015) The psychoactive compound of Cannabis sativa, Δ(9)-tetrahydrocannabinol (THC) inhibits the human trophoblast cell turnover. *Toxicology* **334:**94-103.

Day NL, Richardson GA, Goldschmidt L, Robles N, Taylor PM, Stoffer DS, Cornelius MD, and Geva D (1994) Effect of prenatal marijuana exposure on the cognitive development of offspring at age three. *Neurotoxicol Teratol* **16:**169-175.

de Oliveira RW, Oliveira CL, Guimarães FS, and Campos AC (2019) Cannabinoid signalling in embryonic and adult neurogenesis: possible implications for psychiatric and neurological disorders. *Acta Neuropsychiatr* **31:**1-16.

Desrosiers NA, Himes SK, Scheidweiler KB, Concheiro-Guisan M, Gorelick DA, and Huestis MA (2014) Phase I and II cannabinoid disposition in blood and plasma of occasional and frequent smokers following controlled smoked cannabis. *Clin Chem* **60:**631-643.

Dickson B, Mansfield C, Guiahi M, Allshouse AA, Borgelt LM, Sheeder J, Silver RM, and Metz TD (2018) Recommendations From Cannabis Dispensaries About First-Trimester Cannabis Use. *Obstet Gynecol* **131:**1031-1038.

Dinis-Oliveira RJ (2016) Metabolomics of Δ(9)-tetrahydrocannabinol: implications in toxicity. *Drug Metab Rev* **48:**80-87.

El Marroun H, Hudziak JJ, Tiemeier H, Creemers H, Steegers EA, Jaddoe VW, Hofman A, Verhulst FC, van den Brink W, and Huizink AC (2011) Intrauterine cannabis exposure leads to more aggressive behavior and attention problems in 18-month-old girls. *Drug Alcohol Depend* **118:**470-474.

El Marroun H, Tiemeier H, Steegers EA, Jaddoe VW, Hofman A, Verhulst FC, van den Brink W, and Huizink AC (2009) Intrauterine cannabis exposure affects fetal growth trajectories: the Generation R Study. *J Am Acad Child Adolesc Psychiatry* **48:**1173-1181.

ElSohly MA, Mehmedic Z, Foster S, Gon C, Chandra S, and Church JC (2016) Changes in Cannabis Potency Over the Last 2 Decades (1995-2014): Analysis of Current Data in the United States. *Biol Psychiatry* **79:**613-619.

ElSohly MA, Ross SA, Mehmedic Z, Arafat R, Yi B, and Banahan BF (2000) Potency trends of delta9-THC and other cannabinoids in confiscated marijuana from 1980-1997. *J Forensic Sci* **45:**24-30.

Fanali G, Cao Y, Ascenzi P, Trezza V, Rubino T, Parolaro D, and Fasano M (2011) Binding of δ9-tetrahydrocannabinol and diazepam to human serum albumin. *IUBMB Life* **63:**446-451.

Fisher SE, Atkinson M, and Chang B (1987) Effect of delta-9-tetrahydrocannabinol on the in vitro uptake of alpha-amino isobutyric acid by term human placental slices. *Pediatr Res* **21:**104-107.

Fried PA, Watkinson B, and Gray R (2003) Differential effects on cognitive functioning in 13- to 16-year-olds prenatally exposed to cigarettes and marihuana. *Neurotoxicol Teratol* **25:**427-436.

Fusar-Poli P, Crippa JA, Bhattacharyya S, Borgwardt SJ, Allen P, Martin-Santos R, Seal M, Surguladze SA, O'Carrol C, Atakan Z, Zuardi AW, and McGuire PK (2009) Distinct effects of {delta}9-tetrahydrocannabinol and cannabidiol on neural activation during emotional processing. *Arch Gen Psychiatry* **66:**95-105.

Garrett ER and Hunt CA (1974) Physiochemical properties, solubility, and protein binding of delta9-tetrahydrocannabinol. *J Pharm Sci* **63:**1056-1064.

Giroud C, Ménétrey A, Augsburger M, Buclin T, Sanchez-Mazas P, and Mangin P (2001) Delta(9)-THC, 11-OH-Delta(9)-THC and Delta(9)-THCCOOH plasma or serum to whole blood concentrations distribution ratios in blood samples taken from living and dead people. *Forensic Sci Int* **123:**159-164.

Goldschmidt L, Richardson GA, Willford JA, Severtson SG, and Day NL (2012) School achievement in 14-year-old youths prenatally exposed to marijuana. *Neurotoxicol Teratol* **34:**161-167.

Grant KS, Petroff R, Isoherranen N, Stella N, and Burbacher TM (2017) Cannabis Use during Pregnancy: Pharmacokinetics and Effects on Child Development. *Pharmacol Ther*.

Gronewold A and Skopp G (2011) A preliminary investigation on the distribution of cannabinoids in man. *Forensic Sci Int* **210:**e7-e11.

Grotenhermen F (2003) Pharmacokinetics and pharmacodynamics of cannabinoids. *Clin Pharmacokinet* **42:**327-360.

Gunn JK, Rosales CB, Center KE, Nuñez A, Gibson SJ, Christ C, and Ehiri JE (2016) Prenatal exposure to cannabis and maternal and child health outcomes: a systematic review and meta-analysis. *BMJ Open* **6:**e009986.

Haddad S, Poulin P, and Krishnan K (2000) Relative lipid content as the sole mechanistic determinant of the adipose tissue:blood partition coefficients of highly lipophilic organic chemicals. *Chemosphere* **40:**839-843.

Halldin MM, Isaac H, Widman M, Nilsson E, and Ryrfeldt A (1984) A comparison between the metabolism of delta 1-tetrahydrocannabinol by perfused lung and liver of rat and guinea-pig. *Xenobiotica* **14:**277-282.

Hebert MF, Easterling TR, Kirby B, Carr DB, Buchanan ML, Rutherford T, Thummel KE, Fishbein DP, and Unadkat JD (2008) Effects of pregnancy on CYP3A and P-glycoprotein activities as measured by disposition of midazolam and digoxin: a University of Washington specialized center of research study. *Clin Pharmacol Ther* **84:**248-253.

Heuberger JA, Guan Z, Oyetayo OO, Klumpers L, Morrison PD, Beumer TL, van Gerven JM, Cohen AF, and Freijer J (2015) Population pharmacokinetic model of THC integrates oral, intravenous, and pulmonary dosing and characterizes short- and long-term pharmacokinetics. *Clin Pharmacokinet* **54:**209-219.

Holland CL, Nkumsah MA, Morrison P, Tarr JA, Rubio D, Rodriguez KL, Kraemer KL, Day N, Arnold RM, and Chang JC (2016) "Anything above marijuana takes priority": Obstetric providers' attitudes and counseling strategies regarding perinatal marijuana use. *Patient Educ Couns* **99:**1446-1451.

Holland ML, Allen JD, and Arnold JC (2008) Interaction of plant cannabinoids with the multidrug transporter ABCC1 (MRP1). *Eur J Pharmacol* **591:**128-131.

Holland ML, Lau DT, Allen JD, and Arnold JC (2007) The multidrug transporter ABCG2 (BCRP) is inhibited by plant-derived cannabinoids. *Br J Pharmacol* **152:**815-824.

Holland ML, Panetta JA, Hoskins JM, Bebawy M, Roufogalis BD, Allen JD, and Arnold JC (2006) The effects of cannabinoids on P-glycoprotein transport and expression in multidrug resistant cells. *Biochem Pharmacol* **71:**1146-1154.

Huestis MA (2007) Human cannabinoid pharmacokinetics. *Chem Biodivers* **4:**1770-1804.

Huestis MA, Henningfield JE, and Cone EJ (1992) Blood cannabinoids. I. Absorption of THC and formation of 11-OH-THC and THCCOOH during and after smoking marijuana. *J Anal Toxicol* **16:**276-282.

Huizink AC (2014) Prenatal cannabis exposure and infant outcomes: overview of studies. *Prog Neuropsychopharmacol Biol Psychiatry* **52:**45-52.

Hunault CC, Böcker KB, Stellato RK, Kenemans JL, de Vries I, and Meulenbelt J (2014) Acute subjective effects after smoking joints containing up to 69 mg Δ9-tetrahydrocannabinol in recreational users: a randomized, crossover clinical trial. *Psychopharmacology (Berl)* **231:**4723-4733.

Hunault CC, Mensinga TT, de Vries I, Kelholt-Dijkman HH, Hoek J, Kruidenier M, Leenders ME, and Meulenbelt J (2008) Delta-9-tetrahydrocannabinol (THC) serum concentrations and pharmacological effects in males after smoking a combination of tobacco and cannabis containing up to 69 mg THC. *Psychopharmacology (Berl)* **201:**171-181.

Hunt CA and Jones RT (1980) Tolerance and disposition of tetrahydrocannabinol in man. *J Pharmacol Exp Ther* **215:**35-44.

Ishida K and Unadkat J (2016) Successful prediction of in vivo hepatobiliary clearance and hepatic concentrations of rosuvastatin using sandwich-cultured rat hepatocytes, transporter-expressing cell lines and quantitative proteomics, To be submitted to DMD.

Ishigam M, Uchiyama M, Kondo T, Iwabuchi H, Inoue S, Takasaki W, Ikeda T, Komai T, Ito K, and Sugiyama Y (2001) Inhibition of in vitro metabolism of simvastatin by itraconazole in humans and prediction of in vivo drug-drug interactions. *Pharm Res* **18:**622-631.

Isoherranen N, Kunze KL, Allen KE, Nelson WL, and Thummel KE (2004) Role of itraconazole metabolites in CYP3A4 inhibition. *Drug Metab Dispos* **32:**1121-1131.

Jikomes N and Zoorob M (2018) The Cannabinoid Content of Legal Cannabis in Washington State Varies Systematically Across Testing Facilities and Popular Consumer Products. *Sci Rep* **8:**4519.

Johansson E, Agurell S, Hollister LE, and Halldin MM (1988) Prolonged apparent half-life of delta 1-tetrahydrocannabinol in plasma of chronic marijuana users. *J Pharm Pharmacol* **40:**374-375.

Jones HM and Houston JB (2004) Substrate depletion approach for determining in vitro metabolic clearance: time dependencies in hepatocyte and microsomal incubations. *Drug Metab Dispos* **32:**973-982.

Karschner EL, Darwin WD, Goodwin RS, Wright S, and Huestis MA (2011) Plasma cannabinoid pharmacokinetics following controlled oral delta9-tetrahydrocannabinol and oromucosal cannabis extract administration. *Clin Chem* **57:**66-75.

Karschner EL, Swortwood MJ, Hirvonen J, Goodwin RS, Bosker WM, Ramaekers JG, and Huestis MA (2016) Extended plasma cannabinoid excretion in chronic frequent cannabis smokers during sustained abstinence and correlation with psychomotor performance. *Drug Test Anal* **8:**682-689.

Kauert GF, Ramaekers JG, Schneider E, Moeller MR, and Toennes SW (2007) Pharmacokinetic properties of delta9-tetrahydrocannabinol in serum and oral fluid. *J Anal Toxicol* **31:**288-293.

Ke AB, Nallani SC, Zhao P, Rostami-Hodjegan A, and Unadkat JD (2012) A PBPK Model to Predict Disposition of CYP3A-Metabolized Drugs in Pregnant Women: Verification and Discerning the Site of CYP3A Induction. *CPT Pharmacometrics Syst Pharmacol* **1:**e3.

Ke AB, Nallani SC, Zhao P, Rostami-Hodjegan A, and Unadkat JD (2014a) Expansion of a PBPK model to predict disposition in pregnant women of drugs cleared via multiple CYP enzymes, including CYP2B6, CYP2C9 and CYP2C19. *Br J Clin Pharmacol* **77:**554-570.
Ke AB, Rostami-Hodjegan A, Zhao P, and Unadkat JD (2014b) Pharmacometrics in pregnancy: An unmet need. *Annu Rev Pharmacol Toxicol* **54:**53-69.
Keating E, Gonçalves P, Campos I, Costa F, and Martel F (2009) Folic acid uptake by the human syncytiotrophoblast: interference by pharmacotherapy, drugs of abuse and pathological conditions. *Reprod Toxicol* **28:**511-520.
Kelly P and Jones RT (1992) Metabolism of tetrahydrocannabinol in frequent and infrequent marijuana users. *J Anal Toxicol* **16:**228-235.
Kemp PM, Cardona PS, Chaturvedi AK, and Soper JW (2015) Distribution of ∆(9)-Tetrahydrocannabinol and 11-Nor-9-Carboxy-∆(9)-Tetrahydrocannabinol Acid in Postmortem Biological Fluids and Tissues From Pilots Fatally Injured in Aviation Accidents. *J Forensic Sci* **60:**942-949.
Khare M, Taylor AH, Konje JC, and Bell SC (2006) Delta9-tetrahydrocannabinol inhibits cytotrophoblast cell proliferation and modulates gene transcription. *Mol Hum Reprod* **12:**321-333.
Kim HG, Moon J, Dixon H, and Tullar P (2018) Recurrent Nausea and Vomiting in a Pregnant Woman with Chronic Marijuana Use. *Case Rep Obstet Gynecol* **2018:**9746062.
Klausner HA, Wilcox HG, and Dingell JV (1975) The use of zonal ultracentrifugation in the investigation of the binding of delta9-tetrahydrocannabinol by plasma lipoproteins. *Drug Metab Dispos* **3:**314-319.
Klumpers LE, Beumer TL, van Hasselt JG, Lipplaa A, Karger LB, Kleinloog HD, Freijer JI, de Kam ML, and van Gerven JM (2012) Novel Δ(9) -tetrahydrocannabinol formulation Namisol® has beneficial pharmacokinetics and promising pharmacodynamic effects. *Br J Clin Pharmacol* **74:**42-53.
Ko JY, Farr SL, Tong VT, Creanga AA, and Callaghan WM (2015) Prevalence and patterns of marijuana use among pregnant and nonpregnant women of reproductive age. *Am J Obstet Gynecol* **213:**201.e201-201.e210.
Kreuz DS and Axelrod J (1973) Delta-9-tetrahydrocannabinol: localization in body fat. *Science* **179:**391-393.
Kudo K, Nagata T, Kimura K, Imamura T, and Jitsufuchi N (1995) Sensitive determination of delta 9-tetrahydrocannabinol in human tissues by GC-MS. *J Anal Toxicol* **19:**87-90.
Kuepfer L, Niederalt C, Wendl T, Schlender JF, Willmann S, Lippert J, Block M, Eissing T, and Teutonico D (2016) Applied Concepts in PBPK Modeling: How to Build a PBPK/PD Model. *CPT Pharmacometrics Syst Pharmacol* **5:**516-531.
Kumar V, Nguyen T, Tóth B, Juhasz V, and Unadkat J (2016) Optimization and application of a biotinylation method for quantitative determination of plasma membrane expression of transporters in cells, To be published in DMD.
Kumar V, Prasad B, Patilea G, Gupta A, Salphati L, Evers R, Hop CE, and Unadkat JD (2015) Quantitative transporter proteomics by liquid chromatography with tandem mass spectrometry: addressing methodologic issues of plasma membrane isolation and expression-activity relationship. *Drug Metab Dispos* **43:**284-288.
Kusuhara H and Sugiyama Y (2009) In vitro-in vivo extrapolation of transporter-mediated clearance in the liver and kidney. *Drug Metab Pharmacokinet* **24:**37-52.
Lambert TE EJ, Small M, Brown H (2016) Marijuana in Pregnancy; its Relationship to Nausea, Emesis, and Hyperemesis. *Journal of Addiction Medicine and Therapy* **4**.
Lee D, Vandrey R, Mendu DR, Anizan S, Milman G, Murray JA, Barnes AJ, and Huestis MA (2013) Oral fluid cannabinoids in chronic cannabis smokers during oral δ9-tetrahydrocannabinol therapy and smoked cannabis challenge. *Clin Chem* **59:**1770-1779.
Lemberger L, Crabtree RE, and Rowe HM (1972a) 11-hydroxy- 9 -tetrahydrocannabinol: pharmacology, disposition, and metabolism of a major metabolite of marihuana in man. *Science* **177:**62-64.
Lemberger L, Martz R, Rodda B, Forney R, and Rowe H (1973) Comparative pharmacology of Delta9-tetrahydrocannabinol and its metabolite, 11-OH-Delta9-tetrahydrocannabinol. *J Clin Invest* **52:**2411-2417.
Lemberger L, Silberstein SD, Axelrod J, and Kopin IJ (1970) Marihuana: studies on the disposition and metabolism of delta-9-tetrahydrocannabinol in man. *Science* **170:**1320-1322.
Lemberger L, Tamarkin NR, Axelrod J, and Kopin IJ (1971) Delta-9-tetrahydrocannabinol: metabolism and disposition in long-term marihuana smokers. *Science* **173:**72-74.

Lemberger L, Weiss JL, Watanabe AM, Galanter IM, Wyatt RJ, and Cardon PV (1972b) Delta-9-tetrahydrocannabinol. Temporal correlation of the psychologic effects and blood levels after various routes of administration. *N Engl J Med* **286:**685-688.

Lile JA, Kelly TH, Charnigo RJ, Stinchcomb AL, and Hays LR (2013) Pharmacokinetic and pharmacodynamic profile of supratherapeutic oral doses of Δ(9) -THC in cannabis users. *J Clin Pharmacol* **53:**680-690.

Lindgren JE, Ohlsson A, Agurell S, Hollister L, and Gillespie H (1981) Clinical effects and plasma levels of delta 9-tetrahydrocannabinol (delta 9-THC) in heavy and light users of cannabis. *Psychopharmacology (Berl)* **74:**208-212.

Machado JeB, Chatkin JM, Zimmer AR, Goulart AP, and Thiesen FV (2014) Cotinine and polycyclic aromatic hydrocarbons levels in the amniotic fluid and fetal cord at birth and in the urine from pregnant smokers. *PLoS One* **9:**e116293.

Maia J, Midão L, Cunha SC, Almada M, Fonseca BM, Braga J, Gonçalves D, Teixeira N, and Correia-da-Silva G (2019) Effects of cannabis tetrahydrocannabinol on endocannabinoid homeostasis in human placenta. *Arch Toxicol*.

Mariani JJ, Brooks D, Haney M, and Levin FR (2011) Quantification and comparison of marijuana smoking practices: blunts, joints, and pipes. *Drug Alcohol Depend* **113:**249-251.

Marinol (2017) [package label], AbbVie Inc, North Chicago, IL.

Mark K, Gryczynski J, Axenfeld E, Schwartz RP, and Terplan M (2017) Pregnant Women's Current and Intended Cannabis Use in Relation to Their Views Toward Legalization and Knowledge of Potential Harm. *J Addict Med* **11:**211-216.

Mazur A, Lichti CF, Prather PL, Zielinska AK, Bratton SM, Gallus-Zawada A, Finel M, Miller GP, Radominska-Pandya A, and Moran JH (2009a) Characterization of human hepatic and extrahepatic UDP-glucuronosyltransferase enzymes involved in the metabolism of classic cannabinoids. *Drug metabolism and disposition: the biological fate of chemicals* **37:**1496-1504.

Mazur A, Lichti CF, Prather PL, Zielinska AK, Bratton SM, Gallus-Zawada A, Finel M, Miller GP, Radomińska-Pandya A, and Moran JH (2009b) Characterization of human hepatic and extrahepatic UDP-glucuronosyltransferase enzymes involved in the metabolism of classic cannabinoids. *Drug Metab Dispos* **37:**1496-1504.

McBurney LJ, Bobbie BA, and Sepp LA (1986) GC/MS and EMIT analyses for delta 9-tetrahydrocannabinol metabolites in plasma and urine of human subjects. *J Anal Toxicol* **10:**56-64.

McClure EA, Stitzer ML, and Vandrey R (2012) Characterizing smoking topography of cannabis in heavy users. *Psychopharmacology (Berl)* **220:**309-318.

Metz TD, Allshouse AA, Hogue CJ, Goldenberg RL, Dudley DJ, Varner MW, Conway DL, Saade GR, and Silver RM (2017) Maternal marijuana use, adverse pregnancy outcomes, and neonatal morbidity. *Am J Obstet Gynecol* **217:**478.e471-478.e478.

Morrison PD, Zois V, McKeown DA, Lee TD, Holt DW, Powell JF, Kapur S, and Murray RM (2009) The acute effects of synthetic intravenous Delta9-tetrahydrocannabinol on psychosis, mood and cognitive functioning. *Psychol Med* **39:**1607-1616.

Ménétrey A, Augsburger M, Favrat B, Pin MA, Rothuizen LE, Appenzeller M, Buclin T, Mangin P, and Giroud C (2005) Assessment of driving capability through the use of clinical and psychomotor tests in relation to blood cannabinoids levels following oral administration of 20 mg dronabinol or of a cannabis decoction made with 20 or 60 mg Delta9-THC. *J Anal Toxicol* **29:**327-338.

Nadulski T, Pragst F, Weinberg G, Roser P, Schnelle M, Fronk EM, and Stadelmann AM (2005) Randomized, double-blind, placebo-controlled study about the effects of cannabidiol (CBD) on the pharmacokinetics of Delta9-tetrahydrocannabinol (THC) after oral application of THC verses standardized cannabis extract. *Ther Drug Monit* **27:**799-810.

Naef M, Russmann S, Petersen-Felix S, and Brenneisen R (2004) Development and pharmacokinetic characterization of pulmonal and intravenous delta-9-tetrahydrocannabinol (THC) in humans. *J Pharm Sci* **93:**1176-1184.

Nakazawa K and Costa E (1971) Metabolism of delta 9 -tetrahydrocannabinol by lung and liver homogenates of rats treated with methylcholanthrene. *Nature* **234:**48-49.

Nath A and Atkins WM (2006) A theoretical validation of the substrate depletion approach to determining kinetic parameters. *Drug Metab Dispos* **34:**1433-1435.

National Academies of Sciences Engineering and Medicine (U.S.). Committee on the Health Effects of Marijuana (2017) The health effects of cannabis and cannabinoids : the current state of evidence and recommendations for research, pp 1 online resource (xviii, 468 pages), The National Academies Press,, Washington, DC.
Newmeyer MN, Swortwood MJ, Andersson M, Abulseoud OA, Scheidweiler KB, and Huestis MA (2017a) Cannabis Edibles: Blood and Oral Fluid Cannabinoid Pharmacokinetics and Evaluation of Oral Fluid Screening Devices for Predicting Δ. *Clin Chem* **63:**647-662.
Newmeyer MN, Swortwood MJ, Taylor ME, Abulseoud OA, Woodward TH, and Huestis MA (2017b) Evaluation of divided attention psychophysical task performance and effects on pupil sizes following smoked, vaporized and oral cannabis administration. *J Appl Toxicol* **37:**922-932.
Njuguna NM, Umehara KI, Huth F, Schiller H, Chibale K, and Camenisch G (2016) Improvement of the chemical inhibition phenotyping assay by cross-reactivity correction. *Drug Metab Pers Ther* **31:**221-228.
O'Sullivan MJ, Boyer PJ, Scott GB, Parks WP, Weller S, Blum MR, Balsley J, and Bryson YJ (1993) The pharmacokinetics and safety of zidovudine in the third trimester of pregnancy for women infected with human immunodeficiency virus and their infants: phase I acquired immunodeficiency syndrome clinical trials group study (protocol 082). Zidovudine Collaborative Working Group. *Am J Obstet Gynecol* **168:**1510-1516.
Obach RS (1997) Nonspecific binding to microsomes: impact on scale-up of in vitro intrinsic clearance to hepatic clearance as assessed through examination of warfarin, imipramine, and propranolol. *Drug Metab Dispos* **25:**1359-1369.
Oh DA, Parikh N, Khurana V, Cognata Smith C, and Vetticaden S (2017) Effect of food on the pharmacokinetics of dronabinol oral solution versus dronabinol capsules in healthy volunteers. *Clin Pharmacol* **9:**9-17.
Ohlsson A, Lindgren JE, Wahlen A, Agurell S, Hollister LE, and Gillespie HK (1980) Plasma delta-9 tetrahydrocannabinol concentrations and clinical effects after oral and intravenous administration and smoking. *Clin Pharmacol Ther* **28:**409-416.
Ohlsson A, Lindgren JE, Wahlén A, Agurell S, Hollister LE, and Gillespie HK (1982) Single dose kinetics of deuterium labelled delta 1-tetrahydrocannabinol in heavy and light cannabis users. *Biomed Mass Spectrom* **9:**6-10.
Oudgenoeg-Paz O, Mulder H, Jongmans MJ, van der Ham IJM, and Van der Stigchel S (2017) The link between motor and cognitive development in children born preterm and/or with low birth weight: A review of current evidence. *Neurosci Biobehav Rev* **80:**382-393.
Pang KS, Morris ME, and Sun H (2008) Formed and preformed metabolites: facts and comparisons. *J Pharm Pharmacol* **60:**1247-1275.
Paria BC, Das SK, and Dey SK (1995) The preimplantation mouse embryo is a target for cannabinoid ligand-receptor signaling. *Proc Natl Acad Sci U S A* **92:**9460-9464.
Paria BC, Ma W, Andrenyak DM, Schmid PC, Schmid HH, Moody DE, Deng H, Makriyannis A, and Dey SK (1998) Effects of cannabinoids on preimplantation mouse embryo development and implantation are mediated by brain-type cannabinoid receptors. *Biol Reprod* **58:**1490-1495.
Parikh N, Kramer WG, Khurana V, Cognata Smith C, and Vetticaden S (2016) Bioavailability study of dronabinol oral solution versus dronabinol capsules in healthy volunteers. *Clin Pharmacol* **8:**155-162.
Patilea-Vrana GI, Anoshchenko O, and Unadkat JD (2018) Hepatic enzymes relevant to the disposition of (-)-Δ^9-tetrahydrocannabinol (THC) and its psychoactive metabolite, 11-OH-THC. *Drug Metab Dispos*.
Perez-Reyes M (1990) Marijuana smoking: factors that influence the bioavailability of tetrahydrocannabinol. *NIDA Res Monogr* **99:**42-62.
Perez-Reyes M, Di Guiseppi S, Davis KH, Schindler VH, and Cook CE (1982) Comparison of effects of marihuana cigarettes to three different potencies. *Clin Pharmacol Ther* **31:**617-624.
Perez-Reyes M, Timmons MC, Lipton MA, Davis KH, and Wall ME (1972) Intravenous injection in man of 9 -tetrahydrocannabinol and 11-OH- 9 -tetrahydrocannabinol. *Science* **177:**633-635.
Pergolizzi JJ, LeQuang JA, Bisney JF (2018) Cannabinoid Hyperemesis. *Medical Cannabis and Cannabinoids* **1:**73-95.

Pertwee RG (2008) The diverse CB1 and CB2 receptor pharmacology of three plant cannabinoids: delta9-tetrahydrocannabinol, cannabidiol and delta9-tetrahydrocannabivarin. *Br J Pharmacol* **153:**199-215.
Polanska K, Dettbarn G, Jurewicz J, Sobala W, Magnus P, Seidel A, and Hanke W (2014) Effect of prenatal polycyclic aromatic hydrocarbons exposure on birth outcomes: the Polish mother and child cohort study. *Biomed Res Int* **2014:**408939.
Prasad B and Singh S (2009) In vitro and in vivo investigation of metabolic fate of rifampicin using an optimized sample preparation approach and modern tools of liquid chromatography-mass spectrometry. *J Pharm Biomed Anal* **50:**475-490.
Prasad B and Unadkat JD (2015) The concept of fraction of drug transported (ft) with special emphasis on BBB efflux of CNS and antiretroviral drugs. *Clin Pharmacol Ther* **97:**320-323.
Rodgers T and Rowland M (2007) Mechanistic approaches to volume of distribution predictions: understanding the processes. *Pharm Res* **24:**918-933.
Rostami-Hodjegan A and Tucker GT (2007) Simulation and prediction of in vivo drug metabolism in human populations from in vitro data. *Nat Rev Drug Discov* **6:**140-148.
Roth MD, Marques-Magallanes JA, Yuan M, Sun W, Tashkin DP, and Hankinson O (2001) Induction and regulation of the carcinogen-metabolizing enzyme CYP1A1 by marijuana smoke and delta (9)-tetrahydrocannabinol. *Am J Respir Cell Mol Biol* **24:**339-344.
Sachse-Seeboth C, Pfeil J, Sehrt D, Meineke I, Tzvetkov M, Bruns E, Poser W, Vormfelde SV, and Brockmöller J (2009) Interindividual variation in the pharmacokinetics of Delta9-tetrahydrocannabinol as related to genetic polymorphisms in CYP2C9. *Clin Pharmacol Ther* **85:**273-276.
Saenz SR, Lewis RJ, Angier MK, and Wagner JR (2017) Postmortem Fluid and Tissue Concentrations of THC, 11-OH-THC and THC-COOH. *J Anal Toxicol* **41:**508-516.
SAMHSA (2017) National Survey on Drug Use and Health, Substance Abuse and Mental Health Services Administration.
Schauer GL, King BA, Bunnell RE, Promoff G, and McAfee TA (2016) Toking, Vaping, and Eating for Health or Fun: Marijuana Use Patterns in Adults, U.S., 2014. *Am J Prev Med* **50:**1-8.
Schuhmacher J, Bühner K, and Witt-Laido A (2000) Determination of the free fraction and relative free fraction of drugs strongly bound to plasma proteins. *J Pharm Sci* **89:**1008-1021.
Schwilke EW, Karschner EL, Lowe RH, Gordon AM, Cadet JL, Herning RI, and Huestis MA (2009) Intra- and intersubject whole blood/plasma cannabinoid ratios determined by 2-dimensional, electron impact GC-MS with cryofocusing. *Clin Chem* **55:**1188-1195.
Schwope DM, Karschner EL, Gorelick DA, and Huestis MA (2011) Identification of recent cannabis use: whole-blood and plasma free and glucuronidated cannabinoid pharmacokinetics following controlled smoked cannabis administration. *Clin Chem* **57:**1406-1414.
Sheiner LB and Beal SL (1981) Some suggestions for measuring predictive performance. *J Pharmacokinet Biopharm* **9:**503-512.
Spiro AS, Wong A, Boucher AA, and Arnold JC (2012a) Enhanced brain disposition and effects of Delta9-tetrahydrocannabinol in P-glycoprotein and breast cancer resistance protein knockout mice. *PLoS One* **7:**e35937.
Spiro AS, Wong A, Boucher AA, and Arnold JC (2012b) Enhanced brain disposition and effects of Δ9-tetrahydrocannabinol in P-glycoprotein and breast cancer resistance protein knockout mice. *PLoS One* **7:**e35937.
Stickrath E (2019) Marijuana Use in Pregnancy: An Updated Look at Marijuana Use and Its Impact on Pregnancy. *Clin Obstet Gynecol* **62:**185-190.
Stott C, White L, Wright S, Wilbraham D, and Guy G (2013) A Phase I, open-label, randomized, crossover study in three parallel groups to evaluate the effect of Rifampicin, Ketoconazole, and Omeprazole on the pharmacokinetics of THC/CBD oromucosal spray in healthy volunteers. *Springerplus* **2:**236.
Stout SM and Cimino NM (2014) Exogenous cannabinoids as substrates, inhibitors, and inducers of human drug metabolizing enzymes: a systematic review. *Drug Metab Rev* **46:**86-95.
Strougo A, Zuurman L, Roy C, Pinquier JL, van Gerven JM, Cohen AF, and Schoemaker RC (2008) Modelling of the concentration--effect relationship of THC on central nervous system parameters

and heart rate -- insight into its mechanisms of action and a tool for clinical research and development of cannabinoids. *J Psychopharmacol* **22:**717-726.
Sun X and Dey SK (2012) Endocannabinoid signaling in female reproduction. *ACS Chem Neurosci* **3:**349-355.
Tasnif Y, Morado J, and Hebert MF (2016) Pregnancy-related pharmacokinetic changes. *Clin Pharmacol Ther* **100:**53-62.
Thomas BF, Compton DR, and Martin BR (1990) Characterization of the lipophilicity of natural and synthetic analogs of delta 9-tetrahydrocannabinol and its relationship to pharmacological potency. *J Pharmacol Exp Ther* **255:**624-630.
Toennes SW, Ramaekers JG, Theunissen EL, Moeller MR, and Kauert GF (2008) Comparison of cannabinoid pharmacokinetic properties in occasional and heavy users smoking a marijuana or placebo joint. *J Anal Toxicol* **32:**470-477.
Toennes SW, Schneider K, Kauert GF, Wunder C, Moeller MR, Theunissen EL, and Ramaekers JG (2011) Influence of ethanol on cannabinoid pharmacokinetic parameters in chronic users. *Anal Bioanal Chem* **400:**145-152.
Tortoriello G, Morris CV, Alpar A, Fuzik J, Shirran SL, Calvigioni D, Keimpema E, Botting CH, Reinecke K, Herdegen T, Courtney M, Hurd YL, and Harkany T (2014) Miswiring the brain: Delta9-tetrahydrocannabinol disrupts cortical development by inducing an SCG10/stathmin-2 degradation pathway. *EMBO J* **33:**668-685.
Tournier N, Chevillard L, Megarbane B, Pirnay S, Scherrmann JM, and Declèves X (2010) Interaction of drugs of abuse and maintenance treatments with human P-glycoprotein (ABCB1) and breast cancer resistance protein (ABCG2). *Int J Neuropsychopharmacol* **13:**905-915.
Vandrey R, Herrmann ES, Mitchell JM, Bigelow GE, Flegel R, LoDico C, and Cone EJ (2017) Pharmacokinetic Profile of Oral Cannabis in Humans: Blood and Oral Fluid Disposition and Relation to Pharmacodynamic Outcomes. *J Anal Toxicol* **41:**83-99.
Vandrey R, Raber JC, Raber ME, Douglass B, Miller C, and Bonn-Miller MO (2015) Cannabinoid Dose and Label Accuracy in Edible Medical Cannabis Products. *JAMA* **313:**2491-2493.
Volkow ND, Han B, Compton WM, and Blanco C (2017) Marijuana Use During Stages of Pregnancy in the United States. *Ann Intern Med* **166:**763-764.
Wahlqvist M, Nilsson IM, Sandberg F, and Agurell S (1970) Binding of delta-1-tetrahydrocannabinol to human plasma proteins. *Biochem Pharmacol* **19:**2579-2584.
Wall ME and Perez-Reyes M (1981) The metabolism of delta 9-tetrahydrocannabinol and related cannabinoids in man. *J Clin Pharmacol* **21:**178S-189S.
Wall ME, Sadler BM, Brine D, Taylor H, and Perez-Reyes M (1983) Metabolism, disposition, and kinetics of delta-9-tetrahydrocannabinol in men and women. *Clin Pharmacol Ther* **34:**352-363.
Wang H, Xie H, Guo Y, Zhang H, Takahashi T, Kingsley PJ, Marnett LJ, Das SK, Cravatt BF, and Dey SK (2006) Fatty acid amide hydrolase deficiency limits early pregnancy events. *J Clin Invest* **116:**2122-2131.
Watanabe K, Matsunaga T, Yamamoto I, Funae Y, and Yoshimura H (1995) Involvement of CYP2C in the metabolism of cannabinoids by human hepatic microsomes from an old woman. *Biol Pharm Bull* **18:**1138-1141.
Watanabe K, Yamaori S, Funahashi T, Kimura T, and Yamamoto I (2007) Cytochrome P450 enzymes involved in the metabolism of tetrahydrocannabinols and cannabinol by human hepatic microsomes. *Life Sci* **80:**1415-1419.
Widman M, Agurell S, Ehrnebo M, and Jones G (1974) Binding of (+)- and (minus)-delta-1-tetrahydrocannabinols and (minus)-7-hydroxy-delta-1-tetrahydrocannabinol to blood cells and plasma proteins in man. *J Pharm Pharmacol* **26:**914-916.
Widman M, Nordqvist M, Dollery CT, and Briant RH (1975) Metabolism of delta1-tetrahydrocannabinol by the isolated perfused dog lung. Comparison with in vitro liver metabolism. *J Pharm Pharmacol* **27:**842-848.
Wiznitzer A, Mayer A, Novack V, Sheiner E, Gilutz H, Malhotra A, and Novack L (2009) Association of lipid levels during gestation with preeclampsia and gestational diabetes mellitus: a population-based study. *Am J Obstet Gynecol* **201:**482.e481-488.

Young-Wolff KC, Sarovar V, Tucker LY, Avalos LA, Conway A, Armstrong MA, and Goler N (2018) Association of Nausea and Vomiting in Pregnancy With Prenatal Marijuana Use. *JAMA Intern Med* **178:**1423-1424.

Young-Wolff KC, Tucker LY, Alexeeff S, Armstrong MA, Conway A, Weisner C, and Goler N (2017) Trends in Self-reported and Biochemically Tested Marijuana Use Among Pregnant Females in California From 2009-2016. *JAMA* **318:**2490-2491.

Zhang JY, Wang Y, and Prakash C (2006) Xenobiotic-metabolizing enzymes in human lung. *Curr Drug Metab* **7:**939-948.

Zhang Z, Farooq M, Prasad B, Grepper S, and Unadkat JD (2015) Prediction of gestational age-dependent induction of in vivo hepatic CYP3A activity based on HepaRG cells and human hepatocytes. *Drug Metab Dispos* **43:**836-842.

Zhang Z, Imperial M, Wedagedera J, Gaohua L, Patilea-Vrana G, and Unadkat J (2016) Development of a Maternal-Fetal Physiologically Based Pharmacokinetic Model I:b Factors that Determine Fetal Drug Exposure, Accepted to CPT:PSP with major revisions.

Zhang Z, Imperial MZ, Patilea-Vrana GI, Wedagedera J, Gaohua L, and Unadkat JD (2017a) Development of a Novel Maternal-Fetal Physiologically Based Pharmacokinetic Model I: Insights into Factors that Determine Fetal Drug Exposure through Simulations and Sensitivity Analyses. *Drug Metab Dispos* **45:**920-938.

Zhang Z, Imperial MZ, Patilea-Vrana GI, Wedagedera J, Gaohua L, and Unadkat JD (2017b) Development of a Novel Maternal-Fetal Physiologically Based Pharmacokinetic Model I: Insights into Factors that Determine Fetal Drug Exposure through Simulations and Sensitivity Analyses. *Drug Metab Dispos*.

Zhang Z and Unadkat JD (2017) Development of a Novel Maternal-Fetal Physiologically Based Pharmacokinetic Model II: Verification of the model for passive placental permeability drugs. *Drug Metab Dispos* **45:**939-946.